Nanostructure and mechanical properties of the elastic fibres in the inter-lamellar matrix of the annulus fibrosus: A multi-scale analysis of intervertebral disc integrity

by

Javad Tavakoli

Thesis
Submitted to Flinders University
for the degree of

Doctor of Philosophy

College of Science and Engineering

November, 2018

Table of contents

List of Figures

List of Tables

Abbreviations

AF	annulus fibrosus
3D	three dimensional
AN	anterior
C	circumferential
CB	cross-bridges
CS	cross section
DOAF	deep outer annulus fibrosus
ECM	extra-cellular matrix
FSU	functional lamellae unit
IAF	inner annulus fibrosus
ILM	inter-lamellar matrix
ILM-int-L	inter-lamellar matrix _ lamella interface
IP	in plane
M	molar
NP	nucleus pulposus
NSD	no significant difference
O.C.T	optimal cutting temperature compoud
OAF	outer annulus fibrosus
PB	partition boundary
PL	posterolateral
R	radial
SEM	scanning electron microscopy
Sig	significant
TCD	tangential to circumferential

Abstract

Among the problems with spinal discs, herniation is the most frequent cause of back pain (in people aged 25-45 years) and can lead to serious disability. Defects such as circumferential tears, delamination of annular layers and loss of structural integrity of the disc increase the risk of herniation. While the role of the nucleus pulposus, annular layers (lamellae) of the annulus fibrosus (AF) and endplates on initiation and propagation of herniation have been the focus of intensive studies, the inter-lamellar matrix (ILM), as a likely site for disc defects, has been poorly studied.

The ILM has an average thickness of less than 30 μm and lies between adjacent lamellae in the AF. The microstructure and composition of the ILM have been studied in various anatomic regions of the disc and it was suggested that the ILM components, mainly elastic fibres, play a role in providing integrity of the AF. However, their contribution to AF mechanical properties and structural integrity is unknown. The overall aim of this thesis was to improve the understanding of role of the ILM in structural integrity and mechanical properties of the AF and its clinical relevance in the progression of herniation for recommending a safe level of lifting load.

The first approach in this thesis was an extensive literature review that summarised the ILM composition, microstructure, and tissue level mechanical properties, which identified the potential role of the ILM in the progression of disc degeneration and herniation, and suggested areas for future investigations. This review revealed that the impact of the ILM and its structural components (mainly elastic fibres) on AF mechanical properties have been the subject of only a few studies and many questions remain. Therefore, a series of studies were undertaken to improve understanding of the structure-function relationships of the ILM.

The first study explained an optimized rapid digestion method for ultrastructural analysis of the disc elastic fibres, while preserving their structural integrity and organization. This study developed a new method for fundamental visualization of elastic fibres and their architecture in the disc. Through ultra-structural analysis, the relationship between structure and function, as well as the role of elastic fibres on the AF mechanical properties can be studied. Based on this study two important findings were revealed. First, while the rapid digestion and subsequent gradual and indirect heat treatment techniques significantly changed the overall structural organization of fibres, these changes were small and would likely have minimal impact on ultra-structural alteration of elastic fibres. Second, elastic fibres comprised of a network structure across the AF, whose size and density varied in different regions.

The second and third studies employed the technique developed from the first study to undertake ultrastructural analysis of elastic fibres in different regions of the AF, including the intra-lamellar region (lamella), ILM and the partition boundary (PB). For all three regions, it was found that the majority of fibres were oriented near 0° with respect to the circumferential direction of the lamellae, with less fibres symmetrically orientated at approximately ±45°. Visualization of the ILM under high magnification revealed a dense network of elastic fibres that has not been previously described. Within the ILM, elastic fibres formed a complex network, which were of different size and shape, and differed to those located in the intra-lamellar region. A loose network of elastic fibres was observed in the intra-lamellar region, which were comprised of almost parallel large fibres (0.5-1.5 μm diameter) and very fine interconnecting fibres of less than 0.2 μm diameter. The density of the elastic fibre network in PBs was lower, and fibre orientation was similar to both the intra-lamellar region and inter-lamellar matrix.

The fourth study aimed, for the first time, to measure the viscoelastic and failure properties of the intact ILM in both tension (radial) and shear (circumferential) directions of loading. The findings from this study identified that the stiffness of the ILM was significantly larger at faster strain rates and the viscoelastic and failure properties were not significantly different under tension and shear loading. A strain-rate dependent response of the ILM was found during dynamic loading, particularly at the fastest rate. The ILM demonstrated a significantly higher capability for energy absorption at slow strain rates compared to medium and fast strain rates. A significant increase in modulus was found in both loading directions and all strain rates, having a trend of larger modulus in tension and at faster strain rates. The finding of no significant difference in failure properties in both loading directions, was consistent with our previous ultra-structural studies that revealed a well-organized elastic fibre orientation in the ILM.

The fifth study identified the role of elastic fibres in the mechanical properties of the ILM by removing the matrix using the digestion technique developed in the first study and repeating the testing on the same samples used in the fourth study. The results of this study confirmed the mechanical contribution of the elastic fibre network to the ILM, and likely structural integrity of the AF. A strain-rate dependent response for the elastic fibres in the ILM was found during dynamic loading, particularly for phase angle and stiffness. The elastic fibres in the ILM demonstrated a significantly higher capability for energy absorption at slow compared to medium and fast strain rates as well as in shear compared to tension loading. Also, when tested to failure, a significantly higher normalized failure force was found in tension compared to the shear direction of loading. In fact, the well-organized elastic fibres that create a highly crosslinked and

orthotropic network, provide both significant viscoelastic and failure mechanical properties to the ILM.

The abovementioned studies have clarified that the ILM plays a key role in structural integrity of the AF and that the elastic fibre network contributes to the viscoelastic and failure properties of the ILM. However, the clinical relevance of the ILM is not very well known. Based on a multi-scale failure analysis of the ILM and the lamella in an ovine model, **the sixth study** explored the biomechanical properties of the ILM and the lamellae before, during (pre-herniation) and after lumbar disc herniation. Compared to the lamella, the ILM was the weaker structure during the progression of herniation in the outer posterolateral region of the disc. The finding of no differences between ILM failure stress during pre-herniation and herniation suggested that there is a loading threshold above which the ILM loses its structural integrity, which has clinical relevance for recommending safe levels of lifting loads.

Declaration

I certify that this thesis does not incorporate without acknowledgement any material previously submitted for a degree or diploma in any university; and that to the best of my knowledge and belief it does not contain any material previously published or written by another person except where due reference is made in the text.

Javad Tavakoli

June, 2018

Acknowledgements

After an intensive period of three years, today is the day: writing the note of thanks to reflect on those who have supported and helped me so much throughout this period.

First and foremost, I would like to express my special thanks and sincere gratitude to my principle PhD supervisor Associate Professor John J. Costi for his continuous support during my research. John, I owe it all to you. I will definitely miss our interesting meetings where your patience, motivation, enthusiasm, and immense knowledge and expertise provided me with a unique opportunity to share and discuss my ideas. Thanks for the useful discussions and brainstorming sessions, especially during the difficult conceptual development stage. I also appreciate your financial support during my research to attend different conferences and meetings. I could not have imagined having a better supervisor and mentor for my PhD research. Many thanks!

My sincere thanks also goes to Professor Mark Taylor for his encouragement. Mark, I can't forget your comments to help me deal with research challenges and building a competitive research record for my future.

I would also like to take this opportunity to thank Professor Dawn M. Elliott for her very helpful comments and suggestions. Dawn, I won't forget your participation on shaping this research.

A very special gratitude goes out to Professor Brian J.C. Freeman and Dhara B. Amin for helping and providing new insights into my research. Dhara and Brian, you are amazing. Can't forget your critical input and insights during our research meetings. What a cracking team!

And finally, last but by no means least, to my life-coach Mina and my beautiful daughter Helena, to whom I dedicate this thesis. Mina, thanks for providing me through moral and emotional support in my life and during my PhD. Having both of you makes me brave enough to chase my dreams. Helena you were always keen to know what I was doing and when I am going to finish my study to buy you a puppy. Seems it's time to think about that, darling!

Publications

A number of publications and conference presentations have or will arise from the work presented in this thesis and are listed below. Publications are noted individually at the beginning of each relevant chapter.

Published research articles in peer-reviewed journals

1. **Tavakoli J,** Elliott DM, Costi JJ. Structure and mechanical function of the inter-lamellar matrix of the annulus fibrosus in the disc, Journal of Orthopedic Research (I.F. = 3.414), 34(8), 1307-1315, 2016.
2. **Tavakoli J,** Costi JJ. Development of a rapid matrix digestion technique for ultrastructural analysis of elastic fibres in the intervertebral disc, Journal of Mechanical Behaviour of Biomedical Materials (I.F. = 3.239), 71, 175-183, 2017.
3. **Tavakoli J,** Elliott DM, Costi JJ. The ultra-structural organization of the elastic network in the intra-and inter-lamellar matrix of the intervertebral disc, Acta Biomaterialia (I.F. = 6.383), 58, 269-277, 2017.
4. **Tavakoli J,** Costi JJ. Ultrastructural organization of elastic fibres in the partition boundaries of the annulus fibrosus within the intervertebral disc, Acta Biomaterialia (I.F. = 6.383), 68, 67-77, 2018.
5. **Tavakoli J,** Costi JJ. New findings confirm the viscoelastic behaviour of the inter-lamellar matrix of the disc annulus fibrosus in radial and circumferential directions of loading, Acta Biomaterialia (I.F. = 6.383), 71, 411-419, 2018.
6. **Tavakoli J,** Costi JJ. New insights into the viscoelastic and failure mechanical properties of the elastic fibre network of the inter-lamellar matrix in the annulus fibrosus of the disc Acta Biomaterialia (I.F. = 6.383), 77, 292-300, 2018.
7. **Tavakoli J,** Amin DB, Freeman BJC, Costi JJ. The Biomechanics of the Inter-Lamellar Matrix and the Lamellae during Progression to Lumbar Disc Herniation: Which is the Weakest Structure? Annals of Biomedical Engineering (I.F. =3.405), 46(9), 1280-1291, 2018.
8. **Tavakoli J,** Costi JJ. A method for visualization and isolation of elastic fibres in annulus fibrosus of the disc, Mater. Sci. Eng. C, 93, 299-304, 2018.

National and International Conferences

1. **J. Tavakoli**, DB. Amin, Brian JC. Freeman, JJ. Costi. The biomechanical role of lamellae and the inter-lamellar matrix in lumbar disc herniation. Which is the weakest link? Proceedings of the 44th Annual Meeting of the International Society for Study of the Lumbar Spine (ISSLS), Canada, May 2018.
2. **J. Tavakoli**, DB. Amin, Brian JC. Freeman, JJ. Costi. The biomechanical role of lamellae and the inter-lamellar matrix in lumbar disc herniation. Which is the weakest link? 29th Annual Scientific Meeting of Spine Society of Australia (SSA), Australia, Adelaide, April 2018.

3. **Tavakoli J,** Costi JJ. New insights reveal the mechanical role of the Inter-lamellar matrix and the elastic fibre network in the annulus fibrosus of the intervertebral disc (Poster), The 64th Annual Meeting of the Orthopaedic Research Society (ORS), New Orleans, USA, March 2018.
4. **Tavakoli J,** Costi JJ. Ultrastructural analysis of annulus fibrosus elastic fibres using a rapid matrix digestion technique (Poster). Proceedings of the 44th Annual Meeting of the International Society for Study of the Lumbar Spine (ISSLS), Greece, May 2017.
5. **Tavakoli J,** Costi JJ. Ultrastructural and orientation of the elastic network within the disc annulus fibrosus (Poster). Proceedings of the 28th Annual Meeting of the Spine Society of Australia (SSA), Hobart, Australia, April 2017.
6. **Tavakoli J,** Costi JJ. Ultrastructural organization of the elastic network within the disc annulus fibrosus. Proceedings of the 29th Annual Meeting of the International Society of Biomechanics (ISB), Brisbane, Australia, July 2017.
7. **Tavakoli J,** Elliott DM, Costi JJ. Visualization of the Elastic Network of the Annulus Fibrosus , Proceedings of the 63rd Annual Meeting of the Orthopaedic Research Society (ORS), San Diego, USA, March 2017.
8. **Tavakoli J,** Elliott DM, Costi JJ. Elastic network in the inter-lamellar matrix of the intervertebral disc. Proceedings of the 22nd Annual Meeting of the Australian and New Zealand Orthopaedic Research Society (ANZORS), Melbourne, Australia, October 2016.
9. **Tavakoli J,** Elliott DM, Costi JJ. Investigation into the structural organisation of elastic fibres in the inter-lamellar matrix and intra-lamellar region of the disc. 14th Adelaide Centre for Spinal Research (ACSR) Spinal Research Symposium, Adelaide, Australia, August 2016.

Awards and Prizes

1. **Clayton Adam Award for Best ECR Scientific Paper Presentation** at the 29th Annual Scientific Meeting of the Spine Society of Australia for "**Tavakoli J**, Amin DB, Freeman BJC, Costi JJ. The biomechanics of the inter-lamellar matrix and the lamella during disc herniation: Which is the weakest link?" April 2018, Australia.
2. **Vice-Chancellor Award for the Best Higher Degree Research Student Publication**, Flinders University, for "**Tavakoli J**, Elliott DM, Costi JJ. The ultra-structural organization of the elastic network in the intra- and inter-lamellar matrix of the intervertebral disc" published at Acta Biomaterialia, December 2017.
3. **International Conference Travel Grant**, Flinders University, May 2018 to attend the 44th Annual Meeting of the International Society for Study of the Lumbar Spine (ISSLS), Canada.
4. **Flinders University Student Association (FUSA) Development Grant**, March 2018 to attend the 44th Annual Meeting of the International Society for Study of the Lumbar Spine (ISSLS), Canada
5. **Travel grant** to attend 22nd Annual Meeting of the Australian and New Zealand Orthopaedic Research Society (ANZORS), Melbourne, Australia, October 2016.

Data Base

1- Database for SEM images of elastic fibre network in the disc
https://researchdata.ands.org.au/ultra-structural-organization-intervertebral-disc/1306246

http://doi.org/10.4226/86/5a680f212c4f1

2- Database for the mechanical properties of the ILM and elastic fibre network in the disc
http://researchdata.ands.org.au/view/?key=http%3A%2F%2Fhdl.handle.net%2F2328.1%2F1209
http://dx.doi.org/10.4226/86/5a79395794c45

1 Chapter 1

1.1 Introduction

1.1.1 Motivation

Back problem and disc disorders, as the third most common long-term health condition reported by people aged 25-45 years, affecting approximately 70% of the adult population with 2.8 million people affected in Australia in 2007-2008 [1]. In 2007, back pain was identified as the most common problem occurring through daily repetitive activities or handling objects among people aged 25-64 years [2]. With the highest number of back problem claims in construction and manufacturing industries and health and community services, the direct expenditures for back problems in 2009 was $925 million, while the indirect costs were ten times more [2]. There is an urgent need for further research and clinical translation into back problems since the socioeconomic burden is not isolated to Australia and causes more global disabilities than any other condition. Not surprisingly, this burden will continue to increase with our aging society. From the clinical point of view, defects and failure of the disc leading to herniation, for various reasons, are the most frequent causes of back pain. Since herniation and its progression are not yet fully understood, neither a proper clinical method nor an appropriate medical device have been introduced to cure herniation and prevent re-herniation.

Disruption of the annulus fibrosus (AF) is manifested as circumferential and radial tears, and rim lesions [3]. These tears are present after cumulative [4] or sudden overloading [5, 6] events that lead to herniation. Circumferential tears are common and were observed in cadaver discs from the teenage years [7]. It is thought that delamination of adjacent lamellae are the first steps towards the development of circumferential tears, which can lead to early disc degeneration [8]. Delamination is a known failure

mechanism of composite, laminate structures, suggesting that the region at highest risk of failure initiation is at the boundary between lamellae, which is also referred to as the inter-lamellar matrix (ILM) [9]. The ILM has an average thickness of less than 30 µm and lies between adjacent lamellae in the AF. The microstructure and composition of the ILM have been studied in various anatomic regions of the disc [10-14]; however, their contribution to AF mechanical properties and structural integrity is unknown [9]. It was suggested that the ILM components, mainly elastic fibres and translamellar cross-bridges, play a role in providing mechanical integrity of the AF [15, 16]. Therefore, the way they respond to different loadings and stabilize adjacent lamellae structures will influence AF tear formation and subsequent herniation.

1.1.2 Aims and significance of research

The overall aims of the research conducted in this thesis were to understand the role that the ILM plays in providing structural integrity and mechanical stability and strength to the AF. More specifically, the aims were:

Aim 1: To develop a technique for ultrastructural analysis of the disc elastic fibres, while preserving their structural integrity and organization.

Aim 2: To present an ultrastructural analysis of the elastic fibre network in the AF to compare the ultra-structural organization of elastic fibres in different regions of the AF and more specifically in the ILM.

Aim 3: To assess the contribution of the ILM in the structural integrity of the AF by measuring its viscoelastic and failure properties in both tension and shear directions of loading.

Aim 4: To evaluate the contribution of the elastic fibre network to the structural integrity of the AF by measuring their viscoelastic and failure properties in both tension and shear directions of loading.

Aim 5: To clarify the clinical relevance of the elastic fibre network by measuring the biomechanical properties of the ILM and the lamellae before, during and after lumbar disc herniation.

While previous studies have focused on microstructural analysis of the ILM and biomechanical properties of the lamellae, the results presented in this thesis, based on well-organized multiscale studies, are novel and present new insight into the ultrastructure and biomechanics of elastic fibre network of the disc. Moreover, the outcome of this thesis will contribute to identifying the clinical relevance of the ILM and elastic fibre network and their biomechanical role during progression to herniation that has not been reported before.

1.1.3 Outline of the thesis

The thesis is structured as follows:

Chapter 1 is an introduction highlighting the motivation, specific aims and the outline of this thesis.

Chapter 2 presents a critical review of the published scientific literatures describing the structure and mechanical function of the ILM in the disc annulus fibrosus.

Chapter 3 presents Study 1 in which a novel method developed for ultrastructural analysis of the elastic fibre network in the disc (**Aim 1**).

Chapter 4 presents Study 2, where based on the technique developed in Chapter 3, the ultrastructural analysis of the elastic fibre network in the ILM and intra-lamellar region were explored (**Aim 2**).

Chapter 5 presents Study 3, where the ultrastructural analysis of the elastic fibre network in the partition boundaries of the AF was explored (**Aim 2**).

Chapter 6 presents Study 4, in which the contribution of the ILM to the structural integrity of the AF was identified in intact samples by measuring its viscoelastic and failure properties in both the tension and shear directions of loading (**Aim 3**).

Chapter 7 presents Study 5 that examined the role of the elastic fibre network in providing structural integrity to the ILM. In this chapter, the viscoelastic and failure properties of elastic fibres of the ILM were measured in both tension and shear directions of loading using digested samples (**Aim 4**).

Chapter 8 presents Study 6, which explores the biomechanical properties of the ILM and the lamellae before, during and after lumbar disc herniation. (**Aim 5**).

Chapter 9 includes the conclusion and future recommendation.

2 Chapter 2 – Literature review on the structure and mechanical function of the Inter-lamellar matrix (ILM)

The study presented in this chapter has been published as:

Tavakoli J, Elliott DM, Costi JJ. Structure and mechanical function of the inter-lamellar matrix of the annulus fibrosus in the disc, Journal of Orthopedic Research, 34(8), 1307-1315, 2016.

2.1 Abstract:

The inter-lamellar matrix (ILM) has an average thickness of less than 30 µm and lies between adjacent lamellae in the annulus fibrosus (AF). The microstructure and composition of the ILM have been studied in various anatomic regions of the disc; however, their contribution to AF mechanical properties and structural integrity is unknown. It was suggested that the ILM components, mainly elastic fibres and cross-bridges, play a role in providing mechanical integrity of the AF. Therefore, the manner in which they respond to different loadings and stabilize adjacent lamellae structure will influence AF tear formation and subsequent herniation. This review paper summarizes the composition, microstructure and potential role of the ILM in the progression of disc herniation, clarifies the micromechanical properties of the ILM, and proposes critical areas for future studies. There are a number of unknown characteristics of the ILM, such as its mechanical role, impact on AF integrity, and ultrastructure of elastic fibres at the ILM-lamella boundary. Determining these characteristics will provide important information for tissue engineering, repair strategies and the development of more-physiological computational models to study the initiation and propagation of AF tears that lead to herniation and degeneration.

2.2 Introduction

The inter-lamellar matrix (ILM) lies between the lamellae of the annulus fibrosus (AF) of the intervertebral disc, and has a thickness of less than 30 µm. The ILM is comprised of four main components: matrix, cross-bridges (collagen), elastic fibres and cells; however, those components are not restricted to the ILM alone (i.e. cross-bridges are present in the ILM space and cross radially through multiple AF layers) [10-14]. ILM failure results in delamination (separation of lamellae) and may be one of the initial stages of herniation and degeneration [8, 17, 18]. Knowledge of the ILM structure and mechanical function is important to determining the loading conditions under which the AF is at risk of delamination and subsequent disc disruption and herniation. This understanding of the ILM may lead to the development of improved clinical strategies for disc treatment of herniation and painful degenerative disc disorders.

AF delamination and tears, and the associated disc degeneration, are directly related to the structural integrity of the ILM [19-22]. Migration of the NP usually propagates circumferentially, increasing ILM localized stress and risk of delamination in deep (i.e. inner) AF layers [18]. ILM failure and associated delamination alters ovine spine segment mechanics and causes increased lamellar thickness and vertebral bone volume fraction [8]. On the other hand, delamination may also lead to increased tensile loading within the collagenous AF lamellae components. Therefore the role of the ILM on the AF microstructural integrity [23] and strength is evident, as mechanical properties of multi-lamellae are different from single lamellae [24].

Herniation, extrusion of the NP through the AF, requires an AF disruption and is likely related to ILM micro-damage and local failure. It is likely that after herniation, increased mechanical stresses and/or strains may accelerate disc degeneration by affecting disc microstructure integrity [25]. The effect of NP pressurization on disrupting the AF

lamellae showed that intra- and inter-lamellar disruption occurred at the outer and mid posterior AF, respectively [17]. The pattern of herniation demonstrated that the outer posterior part of the AF is more vulnerable to structural failure due to weak ILM cohesion [17]. Also, annular wall micro damage was induced by NP pressurization varied systematically from the inner to the outer AF. Severe disruption was observed in the inner AF; however, mild disruption occurred in the outer regions [26]. These patterns of disruption were consistent with the finding of higher AF peel strength (33%) in the outer AF compare to inner AF.[18] Investigating the ILM cohesion under radial stretching revealed a complex hierarchy of interconnecting relationships in ILM-lamella boundary [27]. The AF delamination was reported to be a result of the ILM shear stress that may contribute to AF failure by propagation of circumferential tears [28].

Therefore, because of its important role in overall disc mechanical function and potential impact on disc degeneration and herniation, a fundamental understanding of ILM structure-function behaviour is important. The objectives of this review are: to summarise the ILM composition, microstructure, and tissue level mechanical properties, to identify the potential role of the ILM in the progression of disc degeneration and herniation, and to suggest areas for future investigation.

2.3 Review methodology

This study was undertaken by a thorough search through Web of Science Core, PubMed (NLM) and Science Direct online databases, including English written and published in peer-reviewed journals. The keyword search terms used were based on ILM properties as follows: “annulus fibrosus” AND/OR “inter-lamellar matrix” keywords covering the period from the early 1980s to 2016. The bibliographies of these papers were also used to identify additional relevant papers that did not appear in the keyword search.

During this review, it became apparent that a range of terminologies were used to describe the same features as follows: cross-bridges —a multi-lamellar structure that lies partially in the ILM and not restricted to that region only— ("bridging element", "cross-bridges", "translamellar bridging network", "localized buckling", "crease", "local creased region", "crosslinking"); and elastic fibres (elastin fibres", "elastic fibres", "microfibril", "filamentous network"). For this review, we will be using cross-bridges and elastic fibres.

2.4 Inter-lamellar matrix composition

The ILM is composed of a non-fibrillar matrix, elastic fibres, and cells, with cross-bridges traversing radially through the ILM and AF lamellae. The non-fibrillar matrix, an amorphous proteoglycan-rich gel, mainly consists of water, proteoglycans, lipids and elastic fibres (Table 2.1) [29, 30].

Table 2-1 Composition of the ILM's subcomponents.

ILM Component	Composition	Reference
Matrix (Proteoglycan-rich gel)	water, proteoglycan (lubricin, aggrecan, GAGs, decorine, biglycan, perlecan and versican) and lipids	[12, 13, 29-31]
Elastic fibres	elastin, fibrillin	[32-34]
Cross-bridges	aggrecan, versican, GAGs and collagen type I and VI	[12]
Cells	connective tissue cells	[10]

Several glycoproteins such as lubricin, aggrecan, GAGs, decorine, biglycan, perlecan and versican are the main constituents of the proteoglycan-rich region [35], which are responsible for lubricating the ILM [31] and lamella interface and providing sustainable hydration to the tissue [36, 37]. Elastic fibres are another of the main components of the ILM, having a low weight fraction (less than 2%) compared to other fibrous

constituents,[32, 38] with an overall occupied area of approximately 10% [34]. Elastic fibres in adults consist of a core of the protein elastin that is integrated within a scaffold of microfibrillar glycoproteins (mainly fibrilin) [32, 39].

The cross-bridges, which traverse and interconnect several annular lamellae, are a complex, heterogeneous network having a length of between 0.8 – 1.4 mm [40]. The morphology [23, 41] and composition [12] of cross-bridges change as a function of age, with localisation of aggrecan, versican, GAGs and collagen type I and VI [12]. It is assumed that the change of cross-bridge composition—including a progressive increase in collagen type VI and GAG content—as a function of age, is a sign of adaptation to mechanical loading [12]. The spatial variation of ILM composition from the inner to outer AF has not been identified. One exception is the presence of lubricin in the deep outer ILM layer of the caprine AF [31]. In addition, the ILM's elastic fibres density is significantly higher in the outer AF than in those closer to the NP [16].

2.5 Inter-lamellar matrix microstructure

Many techniques have been employed to investigate the ILM connectivity and structure. These techniques include confocal microscopy with biaxial loading [42], light microscopy [43], a layer by layer peeling method using stereo microscopy [44], and histological and immuno-histochemical detection [45]. An alternative imaging technique using Nomarski differential interference contrast (DIC) optical microscopy, combined with simultaneous micromechanical manipulation, allowed a detailed study of hydrated tissue structure [27]. The following sections describe the multiscale hierarchical structure of the ILM, followed by specific details for elastic fibres, cell morphology, and cross-bridges.

2.5.1 Multiscale hierarchical structure

The ILM has a thickness of approximately one-eighth of a single lamella [27] and has a highly complex and interconnected structure [14]. In order to analyse the ILM structure, different magnifications in the range of 20x to 2,000x, resulting in scale bars ranging from 20 µm to 500 µm, have been used [12, 14, 27, 40, 41, 46]. The younger the tissue source, the greater the magnification needed [41, 47]. In addition, higher magnifications, with scale bars below 20 µm, are used to study the elastic fibres and cells, which will be described in more detail in later sections.

At high magnification (scale bars in the range of up to 50 µm), the integrity and merging of cross-bridging elements with the lamellae, as well as their anchoring mechanism (J1, J2 and J3 junctions) were observed. (Figure 2.1) [27, 48]. Figures 2.1 to 2.3 illustrate how magnification has allowed a detailed multi-scale examination of cross-bridges and ILM structural analysis (under radial extension) over a scale bar range up to 50 µm (high magnification), 50-250 µm (moderate magnification), and 250-500 µm (low magnification).

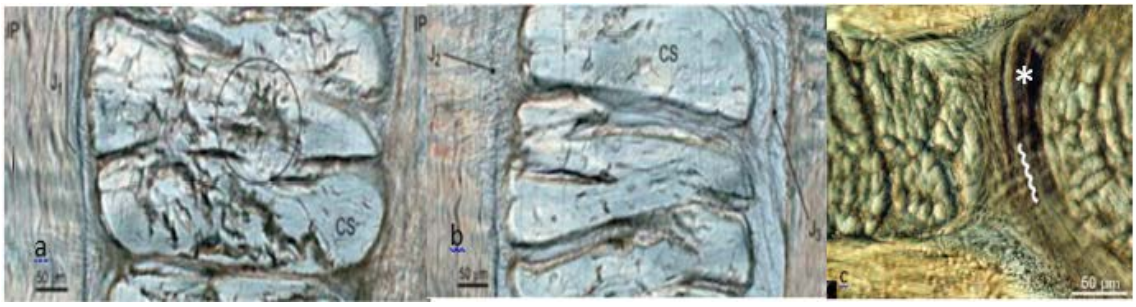

*Figure 2.1 Cross-bridge and the ILM structure in 100% radially fixed-while-stretched AF tissue under high magnification, (a and b): showing significant junction separation (J) between in-plane (IP) and cross-section arrays (CS) (Modified from Pezowicz et al., 2006) [27].The variable junction separation suggests localized inter-lamellar connectivity with discrete anchoring, rather than homogenous interconnectivity. (c): Cross-bridges (denoted by *) appear to stream into the collagen fibres and integration of two structures occur (Modified from Schollum et al., 2009) [48].*

. At moderate magnification (Figure 2.2 - scale bars in the range of 100 to 250 µm), analysis of partial junction separation within the lamellae [47], collagen bundle cohesion [27] and the intra-lamellar relationship [14] within the collagen architecture are shown.

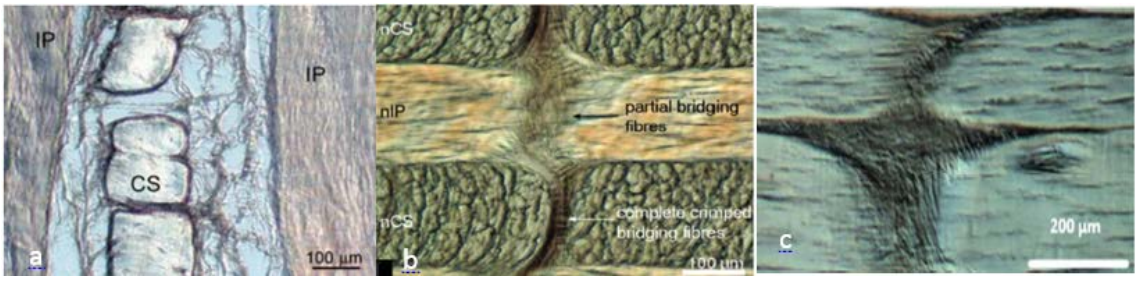

Figure 2.2 Structure of cross-bridge and the ILM under moderate magnification, including in-plane (IP) and cross-section arrays (CS). More extensive junction separation of the ILM occurs with increased radial stretch to 100% (Modified from Pezowicz et al., 2006) [27]. (b): Continuous fibrous nature of cross-bridges is apparent between adjacent lamellae [48]. (c): cross bridging view in a transverse section slice that fragments its fibrous structure (b and c Modified from Schollum et al., 2009) [48].

Finally, at low magnification (Figure 2.3 - scale bars greater than 250 µm), a structural overview of a running cross-bridge as well as a 3-D volumetric image of cross-bridges at the anterior AF, which connected lamellae radially are observed. The intersection of cross-bridges and lamellae, as well as the AF lamellae and cross-bridges' morphological change under varying strain has been studied in the 100-500 µm range [40].

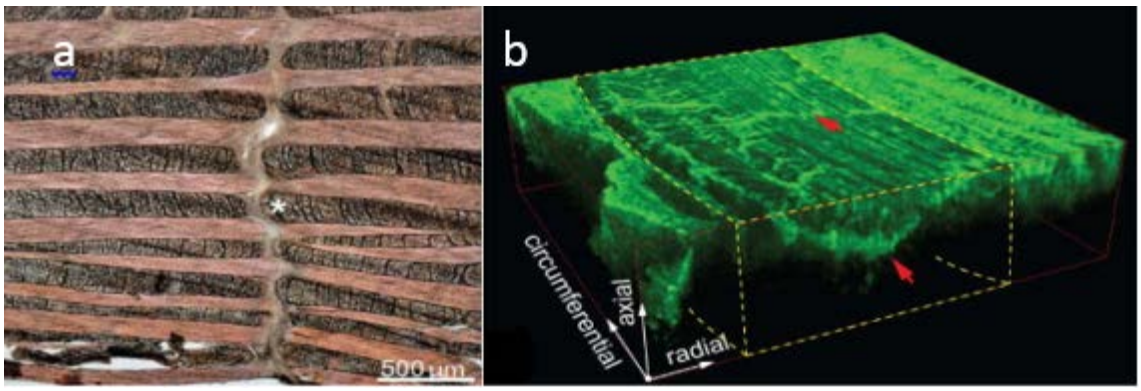

*Figure 2.3 The cross-bridge structure under low magnification. (a): Cross-bridges (denoted by * refer to Figure 1C, for micrograph with higher magnification) as trans-lamellar connecting elements may connect multiple lamellae (Modified from Schollum et al., 2009) [48]. (b): A 3-D network of heterogeneously distributed cross bridges —prepared by optical coherence tomography (red arrows)— that crisscrosses multiple lamellae (Modified from Han et al., 2015) [40].*

2.5.2 Elastic fibre structure

Elastic fibre networks in the ILM have a central elastin core and surrounding micro-fibrils (fibrillin) [13]. These fibres have a circular, longitudinal and oblique orientation. In the ILM, elastic fibres have a complex three dimensional mesh pattern that formed a network (Figure 2.4) [13, 16]. In contrast, within the AF lamella, the elastic fibres are aligned predominantly parallel to the collagen fibres, and a significant number are directly anchored into adjacent vertebral bodies [33]. The elastic fibres within the ILM may permit the AF tissue to return to their original shape after deformation, however their mechanical role remains unknown [15, 49, 50].

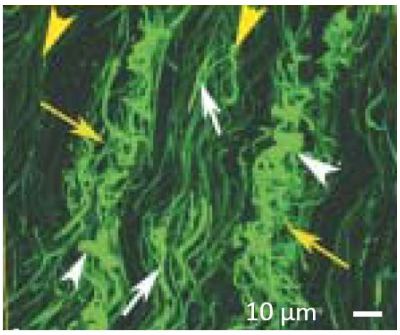

Figure 2.4 The intra- and inter-lamellar space showing elastic fibres structure in the outer AF of a human L3/L4 disc. Yellow arrows and white arrowheads: show the ILM space including thicker elastin fibres in a coil-like structure. Yellow arrowheads and white arrows: present the intra-lamellar space with thicker elastin fibres (Modified from Yu et al., 2007) [13].

Elastic fibres within the ILM form a complex interwoven network branching out from the collagen bundles that are in the adjacent lamellae, and with physical entanglement at their point of branching [16]. Elastic fibres integration, with collagen fibres, brings greater structural complexity in their arrangement in the ILM, compared to those at a single lamella [10, 14]. A comparison between human disc and bovine tail disc on the basis of micro-fibril distribution showed that they were very similar [13]. Micro-fibrils (fibrillin protein) and elastin fibres —as two components of elastic fibres — are more densely organized in the ILM space with a high degree of co-localization. Complexity of

the elastic fibres in the ILM including their thickness and coil-like structures with high degree of elastin-fibrillin co-localization have been suggested to play a mechanical role; however, their impact on AF mechanical properties and integrity is unknown. Therefore using lamellae that were concentric and physically isolated when developing computational models of the AF, may not be an appropriate representation [23, 24, 51]. The pattern of the elastic fibres distribution differs with spatial location in the radial direction. They appeared to be organized radially in the NP, in criss-cross form in the region between the NP and the inner AF, and parallel with collagen fibres in the outer AF (Figure 2.5) [45]. Elastic fibres organization also differs between AF regions and changes with the age. Elastic fibres are not evenly distributed and their concentration appears relatively high within the ILM [45]. Table 2.2 summarizes the characteristics of the elastic v and cells in different regions of the disc.

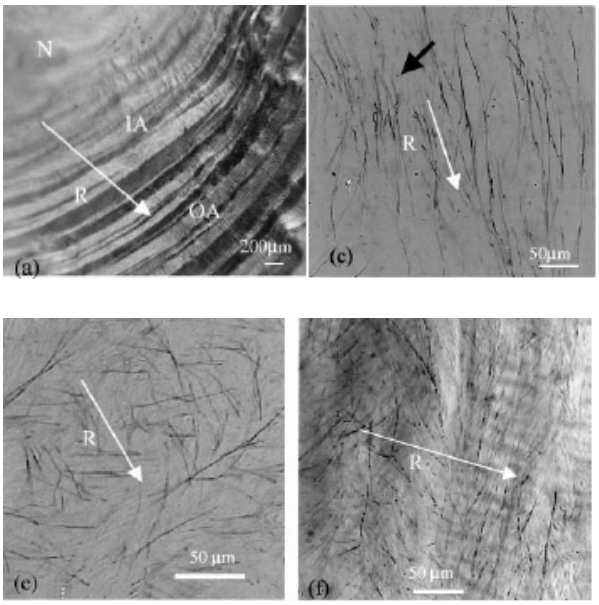

Figure 2.5 Orientation and ultrastructure of the elastic fibres in the inner and outer layer of the AF as well as the NP. Elastic fibres organized radially in the NP(c), in form of criss-cross in the region between the NP and inner AF (e) and parallel with collagen orientation in outer AF (f) [45] (Modified from Yu et al, 2002).

Table 2-2 Organization and arrangement of cells and elastic fibres in the disc.

Compartments	Organization and arrangement	Reference
Elastic fibres		
NP	organized radially	
IAF	in form of criss-cross, low density	[13, 45]
OAF	parallel with collagen fibres, high density	
ILM	forms a criss-cross 3-D coil-like network	[13, 33]
ILS	aligned predominantly parallel to the collagen fibres	
ILM-int-L	form a complex interwoven network branching out from collagen bundles	[16]
CB	streams into the collagen fibres of the lamellae in the same plane, indicating integration of the two structures	[12, 13, 27, 45]
Cells		
DOAF	rarely formed a network, appears like a series of spherical cells that crossed the lamella perpendicular to the collagen fibres	[10, 52]
OAF	cord-like, create inter-connective network	
IAF	flattened and disc-shape	

Inner AF (IAF), Outer AF (OAF), Deep outer AF (DOAF), Cross-bridges (CB), Intra-lamellar space (ILS) and the ILM lamella interface (ILM-int-L).

2.5.3 Inter-lamellar matrix cell morphology

The ILM cells' morphology and population are related to the elastic fibres 'structure in the ILM. The shape of the ILM's cells are cord-like and form an inter-connective network at the outer AF [52], however in the deep outer AF they rarely form a network and appear as a series of spherical cells that cross the lamella perpendicular to the collagen fibres [10]. In contrast, the ILM's cells at the inner AF layers are flattened and disc-shaped [10]. Moving from the ILM centre to its interface with the collagenous wall of the lamella, the cells' shape changes from spherical to fusiform, which is perhaps a consequence of both the collagen fibre's direction within the lamella,[33] and their orientation related to loading direction [10, 42]. Regional variations in cell structure and morphology might be a reflection of different mechanical loads experienced by the AF

[52]. Differences between the AF biochemical properties suggest that the ILM cells might have a different phenotype compared to cells within the lamella [10].

2.5.4 Cross-bridge structure

Cross-bridges, which connect two or more non-consecutive lamellae in the radial direction are another part of the ILM [23, 48]. The existence of this structure in the human AF, at different anatomic regions, was demonstrated by histological observation. It was reported that there was no increase in the number or penetration depth of cross-bridges subsequent to vascular regression [41]. Microscopic investigations of the trans-lamellar bridging network revealed that the organization of the elastic fibre network merged into the lamellae, possibly indicating integration of the two structures that may influence the disc's mechanical properties. (Figure 2.6) [45]. To our knowledge, there are no reports of the presence of collagen in the ILM, apart from within cross-bridges.

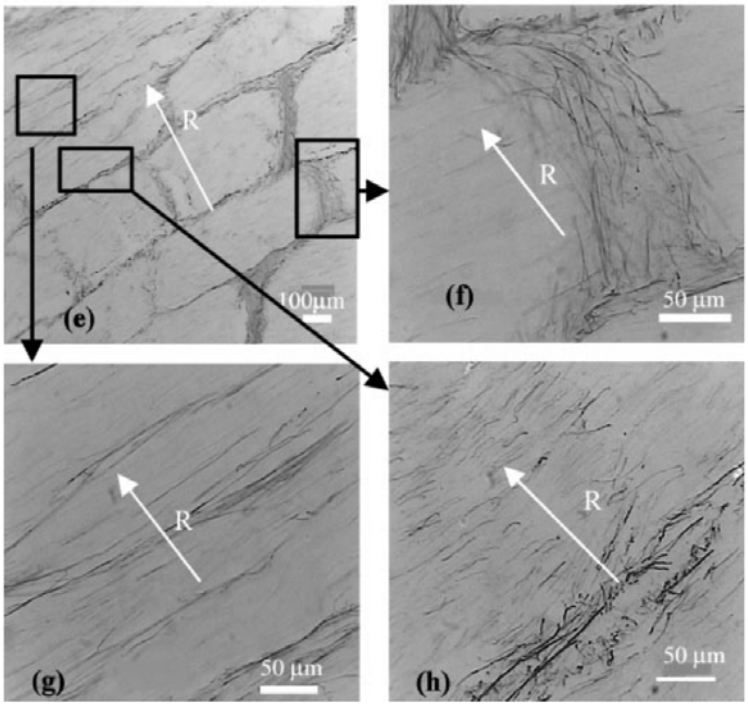

Figure 2.6 Transverse sections of the outer layer of the AF (bovine tail) showing the elastic fibre organization in the outer AF (e), in the intra-lamellar region (g) and within the ILM, as well as a cross-bridge that spans two adjacent lamellae (h). White arrow indicates the NP location in radial direction [45] (Modified from Yu et al., 2002).

2.6 Inter-lamellar matrix micromechanical properties

The ILM's mechanical role in the AF is less known. Some of the experiments that have been used that indirectly assessed the ILM are radial tensile tests of intact tissue and with enzymatic digestion [53] or crosslinking [54], shear testing [55], NP pressurization of the intact disc [17, 26], and peel testing [18]. One recent study, however, has directly assessed ILM mechanical properties [24]. In this study, the stiffness of the ILM under radial loading was consistently higher than the corresponding lamellar values, and was measured to be greater at the outer (43%-75% higher) relative to the inner AF. This higher stiffness reflects the role of the ILM connectivity in contributing to the AF mechanical properties [24].

The presence of extensible elastic fibres in the ILM seems to be important to aid the AF tissue in returning to its original shape after deformation. Studies indicated that only significant changes of elastic fibre quantity (positive or negative) would have associated mechanical consequences; however, there is an absence of evidence that reports the mechanics of the ILM as a function of elastic fibre content, or their physicochemical and mechanical properties [56-58]. The impact of elastic fibre organization [15, 59, 60] on maintaining AF mechanical properties has been demonstrated by measuring the mechanical properties of elastic fibres in isolation [11, 61-63], using targeted enzymatic treatment [15, 53, 55] cell-elastic fibre arrangements [10, 13, 33] or fibre crosslinking [54].

The radial mechanical integrity of the AF may be provided by the ILM's elastic fibres. The widespread fibrilin co-distribution with elastin fibres might reflect their relatively important reinforcement role in the ILM's mechanical function [11, 26]. Also elastin's parallel alignment to the AF lamellar collagen v suggests that separate connection points (cross-collagen connectivity) between adjacent collagen fibres may play an important

role in limiting AF deformation in the radial direction [13, 16]. This enhanced radial integrity stabilizes adjacent lamellae and inhibits tear formation and subsequent herniation [15, 56]. Therefore, it's possible that one role of the elastic fibre network is to restore the lamellae organization after deformation [23]. Removing elastic fibres from the ILM results in a significant decrease in toe and linear region modulus (0.07 to 0.004 MPa and 0.21 to 0.02 MPa, respectively), accompanied by an increase in the extensibility from 0.16 to 0.93 mm/mm [11, 15], and reduction of the AF radial tension. ILM crosslinking by genipin effectively increased inter-lamellar de-bonding resistance, as well as force to yield (59%) and peak force (70%) during shear loading. It is possible that there would be a dependency between adjacent lamellae fibrous network and inter-lamellar shear properties [54].

Some studies use mechanical deformation or loading to investigate ILM structure and connectivity with adjacent lamellae [14, 17, 27]. Although these studies don't directly quantify ILM mechanics, they provide important inferences about ILM function. For example, in intact vertebra-disc-vertebra samples, increasing internal hydrostatic pressure to 20 MPa showed that the ILM junctions have a level of interconnectivity to offer a substantial structural resistance to radial and circumferential internal pressurization [26]. Also it was shown that elastic fibres passing through the ILM were anchored into the in-plane collagenous arrays and tended to create transversal clefts, possibly indicating that they penetrated to an unknown depth within the collagen [27]. In order to provide a substantial resistance to disruption, a sufficient level of intra- and inter-lamellae structural interconnectivity are required [14, 17, 26, 27].

The mechanical properties of the ILM have been measured using a peeling test [18, 57]. Superficial lamella in the outer AF have a 30% higher peel strength than those of deeper lamellae of the outer AF regions, and progression of delamination in the inner layers of

the AF occurred more readily [18]. In addition, the ILM peel strength in rabbit samples associated with degeneration (induced by AF puncture leading to NP dehydration and reduced AF height) was 30% lower than normal discs [57]. The effect of axial vibration (5 Hz, 6000 cycles, flexion-extension under 1200-1500 N static load) on the initiation and propagation of herniation, and influence on the ILM mechanical properties in pig discs, has been studied in-vitro. This study found that axial vibration did not result in significant changes of the ILM sliding modulus, displacement and shear stress at the end of toe region, or failure shear stress; however, extension to failure was increased by 50% [18]. Cross-bridges appeared to maintain the structure of the ILM and adjacent lamellae and its interface with the lamella under radial tensile strain, however, their positive role in ILM mechanics appear to be coincidental [41]. It was suggested that cross-bridges are capable of extending and recovering from tensile strain because of their collagen composition [23]. Although the mechanical properties of cross-bridges haven't been directly measured, they may enhance ILM mechanical properties by creating a trans-lamellar bridging network, where their association has been suggested to be effective in stabilizing incomplete lamellae [23]. By including cross-bridges as an architectural addition to for the simplified AF concentric ring model, an effective mechanism may exist to limit slippage between adjacent lamellae.

In spite of the lack of knowledge about the mechanical properties of the ILM, theoretical models have been developed to attempt to describe the ILM function [24, 28] and the role of ILM properties in AF macroscopic mechanics [61]. It was indicated that using a fibre -reinforced composite model —that has been widely used for the mechanical study of the AF— is not able to explain interactions between the two alternative fibre populations in the ILM, a phenomenon shown to be important for the function of engineered biologic laminates [64]. Therefore extending the existing theoretical

framework would be helpful to describe the ILM shearing interaction [64-66]. Structural damage to the lamellae, mainly as a consequence of degeneration, might increase ILM shear stress and damage propagation. Mechanical studies to quantify the ILM function are challenging due to its small size and close connections to the AF lamella. Some studies are limited in that the applied strains exceed those physiologically feasible in situ. Even so, such studies are useful for demonstrating connectivity and basic mechanical structure-function. Radial tensile tests that apply strains greater than 10% strain are not physiological. Other experimental studies also may not be physiological, however they are all useful to some extent.

2.7 Conclusion- The critical areas

Understanding of the ILM structure-function behaviour is important for determining the complex loading conditions under which the AF is at risk of delamination and subsequent disruption, which may contribute to the pathogenesis of degeneration and herniation. Each component substructure's composition and microstructure of the ILM seems to play an important role in maintaining the AF integrity through preserving sustainable hydration, interface lubrication, and integration between AF lamellae. The complexity of the elastic fibre and cross-bridge arrangements in the ILM suggest a mechanical role. However, their role in the AF mechanical properties and structural integrity is unknown. Indeed, the impact of the ILM and its structural components (elastic fibres and cross-bridges) on AF mechanical properties have been the subject of only a few studies and many questions remain. Therefore further study is required to better understand the structure-function relationships of the ILM. This requires the multiscale measurement of: the mechanical properties of the ILM and its subcomponents; the contributions to adjacent lamella behaviour, and the radial,

circumferential and axial properties of the AF and ILM interface in both normal and degenerated tissue. This new knowledge would provide important data for tissue engineering and repair strategies, as well as the development of more physiological computational models to study the initiation and propagation of AF tears that lead to herniation and degeneration.

3 Chapter 3 - Study 1: Development of a rapid matrix digestion technique for ultrastructural analysis of elastic fibres in the intervertebral disc

The previous chapter (Chapter 2, the literature review) identified the composition and microstructure of the ILM and revealed that the role of the ILM and its main structural component (elastic fibres) on the AF mechanical properties is unknown. While the complexity of the elastic fibres in the ILM at the micro-scale suggests a mechanical role, lack of knowledge about their ultrastructural organization has led to their unknown function. For a better understanding of the relationship between structure and function, as well as the role of elastic fibres on AF mechanical properties, ultrastructural analysis of elastic fibres is required. Since elastic fibres are intermingled with other fibrous components of the disc and mostly obscured by the extracellular matrix, it is difficult to demonstrate their ultrastructural organization and mechanical properties. Therefore, development of a technique for visualization of elastic fibres is crucial for their ultrastructural analysis. In this chapter, the development of a rapid matrix digestion technique for ultrastructural analysis of the elastic fibres in the disc, while preserving their structural integrity and organization is explained.

The study presented in this chapter has been published as:

Tavakoli J, Costi JJ. Development of a rapid matrix digestion technique for ultrastructural analysis of elastic fibres in the intervertebral disc, Journal of Mechanical Behaviour of Biomedical Materials, 71, 175-183, 2017.

3.1 Abstract:

Collagen and elastic fibres are two major fibrous constituents of the annulus fibrosus (AF) in the disc that contribute to its mechanical and viscoelastic properties. It was thought that elastic fibres play no substantial role in the function and properties of the disc as these fibres were irregularly distributed. Studies that have revealed highly organized elastic fibres with different regional orientation and distribution, while being strongly crosslinked with matrix, suggesting their contribution to disc structure-function properties. These studies that were performed by light microscopic analysis of histologically prepared samples, have not been able to reveal the fine-scale architectural details of the elastic fibre network. Since elastic fibres are intermingled with other fibrous components of the disc and mostly obscured by the extracellular matrix, it is difficult to demonstrate their ultra-structural organization using scanning electron microscopy (SEM).

Therefore the aim of this study was to develop a rapid matrix digestion technique for ultrastructural analysis of the disc elastic fibres. This study provides a new method for fundamental visualization of elastic fibres and their architecture in the disc. Through the ultra-structural analysis, the relationship between structure and function, as well as the role of elastic fibres on AF mechanical properties can be studied. This method may be used to develop a three-dimensional map of elastic fibres distribution within the disc, which would provide valuable information for designing tissue engineered scaffolds for AF repair and replacement.

3.2 Introduction

The major functional role of the intervertebral disc is to transfer loads in six degrees of freedom, while providing flexibility to the spinal column [67]. To perform this dynamic behaviour, the annulus fibrosus (AF) of the disc deforms with load application and then recovers to its original shape and size after load removal [68]. The AF, with its multi-lamellar structure, is comprised of three fibrous elements; collagen, elastic fibres and micro-fibrils. Collagen fibres present as tape- or cord-shape that run a wavy course with a width of 1-20µm, approximately. Micro-fibrils of diameter 30-100 nm are usually observed as a delicate meshwork. Elastic fibres are about 0.2-1.5 µm in diameter, and are generally twisted or straight strands that sometimes branch to form a course network [69].

Previously, elastic fibres have been suggested to play no substantial role in the mechanical properties and function of the AF, due to their irregular distribution [70]. However, studies have reported that elastic fibres are highly organized in the AF and their distribution and orientation vary in different regions [11, 16]. Also biochemical studies suggest that elastic fibres may be strongly cross-linked to the matrix and some other components of the AF [71]. Therefore, it appears that the elastic fibres found in the AF play an important role in contributing to its structure-function properties [15].

According to the above studies it was found that the abundant elastic fibres, exposed by histological staining, are distributed throughout all AF regions with higher density between the lamellae [9]. Furthermore, the manner by which elastic fibres are anchored into the disc's endplate (perpendicular or oblique), have provided new insights into their function [72]. Also, the distinction between the organizational appearance of elastic fibres most likely hinges on the functional requirement of elastic tissues, supporting the

hypothesis that a high degree of organization of elastic fibres in different regions of the AF may indicate their contribution to mechanical properties [73].

Recent studies have revealed that two distinct organizations of elastic fibres are present in the AF. In the lamella, elastic fibres align parallel to the collagen fibres, and are tightly packed within the surrounding matrix [13]. The architecture of the network between two adjacent lamellae was reported to be dense, more complex and anisotropic compared to within lamellae [9]. These observations were acquired by light microscopy analysis of histologically prepared samples. While some of the techniques are advanced, none are able to provide the fine-scale architectural details of the elastic fibre network. On the other hand, since elastic fibres are intermingled with other fibrous components of the disc and mostly obscured by the extracellular matrix, it is difficult to demonstrate their ultra-structural organization using scanning electron microscopy (SEM). Therefore partial digestion of the matrix has been shown to be an effective technique for visualizing their architecture and ultra-structural organization at the ultra-scale [74, 75]. It was previously described that some methods, including hot alkali and formic acid digestion that selectively remove non-elastin components (i.e. microfibrils, collagen, cellular elements and matrix), are effective for observing the architecture of elastin components in tissues by SEM [69]. The SEM imaging of digested tissues for structural analysis is a well-described method that has been used to interpret vascular elastic fibre structure; however [76], its application to the disc has not been studied.

Therefore the aim of this study was to develop a rapid matrix digestion technique for ultrastructural analysis of the disc elastic fibres, while preserving their structural integrity and organization. As the method will be employed for ultra-structural organization assessment of elastic fibres in the AF, three critical research key questions

were addressed: 1) the effectiveness of the method on allowing visualization of elastic fibres, 2) the repeatability of the method and 3) its impact on structural alteration.

This study provides a new method for fundamental visualization of elastic fibres and their architecture. Through the ultra-structural analysis, the relationship between structure and function, as well as the role of elastic fibres on AF mechanical properties can be studied. This method may be used to develop a three-dimensional map of elastic fibres distribution within the disc, which would provide valuable information for designing tissue engineered scaffolds for AF repair and replacement.

3.3 Materials and methods

3.3.1 Sample preparation

Four lumbar sheep spines (18-26 months old) were obtained from a local abattoir, separated into bone-disc-bone segments with level L1/2 and stored at -30°C until used for analyses. Segments were then thawed overnight at room temperature while wrapped in saline soaked gauze. Each disc was dissected from the vertebral bodies. A 10 mm length of the anterior AF was separated from each disc (Figure 3.1a, 1b) and was mounted with optimal cutting temperature compound (O.C.T, Tissue-Tek®) at an angle of approximately 30° to the transverse plane to identify the cutting plane (Figure 3.1c) and stored at -30° C until used. As used previously, a cutting plane with an angle of about 30° was used to cut almost orthogonal to some lamellae and almost parallel to the others [48]. Four samples from adjacent sections (thickness 30 µm) were cut using a cryostat microtome (Leica Biosystems, CM3050) from each of four discs (Figure 3.1d) and were mounted on poly-L-lysine coated microscope slides and stored at -30°C for further analysis. The first sample was not digested or treated (control sample). The second sample was used for histology and stained with orcein to visualize elastic fibres (orcein treated sample). The final two samples were digested in 0.5 M NaOH solution

and sonicated for 15 min at 37°C (digested sample). One of these two samples was then soaked in water at 70 °C for 5 min to remove collagen fibres, leaving the elastic network (digested + heat treated sample). All three treated samples were then dried in a vacuum oven overnight (37°C and -80 kPa) and sputter coated with platinum at 2 nm thickness for SEM imaging.

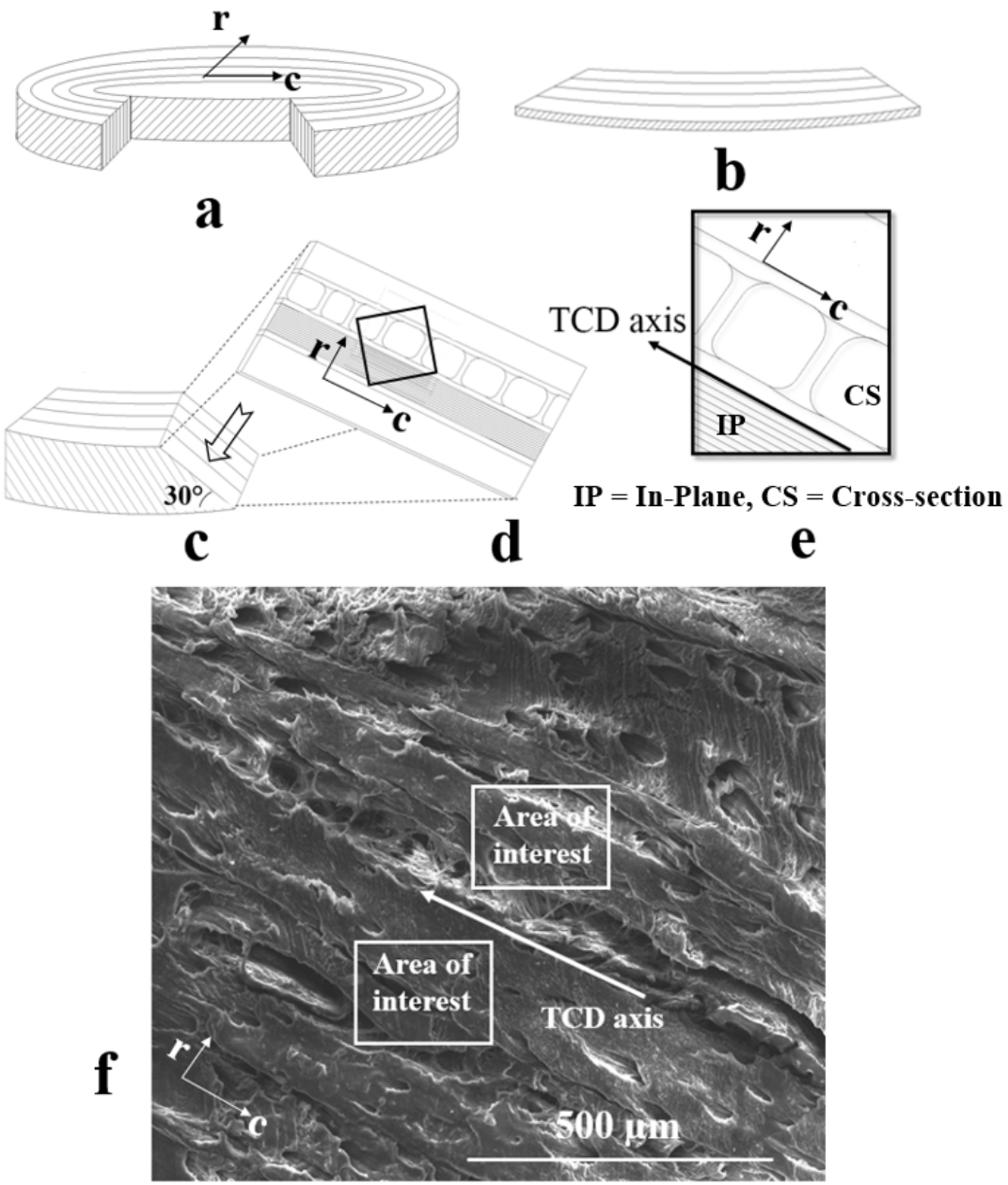

Figure 3.1 Schematic drawing of sample preparation by frozen cutting of 30 µm thickness samples. (a) Anterior AF strips (10 mm in length) were separated from the disc, (b) Samples were cut by microtome to a thickness of 30µm along the cutting plane (approximately 30°), (c, d) Anterior AF strip and frozen section preparation at an angle of approximately 30° to the transverse plane. Scanning electron microscopy images were captured perpendicular to the samples' surface (z plane), as shown in (c), along the direction

indicated by the arrow, (e) Schematic of two adjacent lamellae and their reference axis being tangential to the circumferential direction (TCD) for measuring fibre orientation, and (f) SEM images of a partially digested sample indicating the areas of interest and the TCD axis. "r and c" represent radial and circumferential directions respectively.

3.3.2 Orcein staining

Orcein staining was used to visualize the elastic fibres using a conventional histologic method [45]. Briefly, the sample was soaked in orcein solution for 40 min after having been kept in ethanol (70%) for 5 min at room temperature. It was then soaked in tap water for 5 min. The dehydration process was accomplished by passing the sample through a series of increasing ethanol concentrations. The sample was soaked sequentially twice in 70%, and once each in 90% and 100% ethanol for approximately two minutes. The sample was then placed in a second 100% ethanol solution for 30 seconds to ensure that all water was removed. Finally, the sample was washed in xylene twice and mounted with DPX (mountant for histology). The presence and location of elastic fibres were visualized in the histologically prepared samples using light microscopy analysis (Brightfield BX50, Olympus, Japan).

3.3.3 Sample digestion and heat treatment

Partial NaOH digestion was performed in accordance with the method used on arteries to prepare the samples for SEM [76]. Briefly, dissected samples were placed in 0.5 M NaOH solution and sonicated (SONIC-950WT, MRC, Germany) for 25 min at 37 °C. The ultrasonic frequency was 25 KHz with a probe diameter of 3 mm. The samples became translucent after digestion and maintained their shape during sonication. Instead of heat treatment in an autoclave as per the suggestion of Crissman and Pakulski, indirect and gradual heat treatment of samples was applied by placing them into the water bath. The digested samples were removed from the NaOH solution and placed in distilled water (500 ml). Then the container including samples and distilled water was placed in a water bath whose temperature was set at 70 °C.

When the water bath temperature reached the set point, the samples were kept there for 5 min. Since elastic fibres are resistant to high temperatures (> 200 °C), the gradual temperature increment removed collagen fibres slowly via the process of gelatinization, leaving the elastic fibres intact [77, 78]. All digested and heat treated samples were moved into distilled water using two small forceps to be rinsed for 5 min at room temperature, and partially dried in ethanol (70%; 1 min).

3.3.4 Digestion optimization

Optimization of the digestion process, for effective visualization of elastic fibres, can be influenced by sample thickness, digestion time, digestion media concentration and ultrasonic frequency. In this study, the AF matrix digestion was characterized as a function of digestion time during exposure to the sonication. The sample thickness, concentration of digestion media (NaOH) and intensity of sonication were kept constant during the digestion process. To observe the effect of digestion time, samples were digested at 5, 10, 15, 20 and 25 min, with the resulting SEM images prepared using the method described in scanning electron microscopy section.

3.3.5 Scanning electron microscopy

The samples were dried before SEM imaging (Inspect F50, FEI Company, USA) in a vacuum oven (VO3, LABEC, Australia) overnight at 37°C and -80 kPa. Dried specimens were mounted on aluminium stubs with double adhesive tape, then sputter coated with platinum at 2 nm thickness. SEM images were captured perpendicular to the specimens' surface (z plane) and in the direction of the "arrow" as shown in Figure 3.1-c. High voltage was set at 5 kV and the distance from the sample to the beam source was kept constant for all performed tests. For effective visualization of elastic fibres, a linear horizontal and vertical scan (at steps of approximately 50 µm) at high magnification was

performed over the sample's surface. Once elastic fibres in the digested region were identified, a low magnification (<200 µm) was used as a starting point from which sequential images were acquired at the region of interest in progressively increasing magnifications (Figure 3.2). Elastic fibres were not visible at low magnifications.

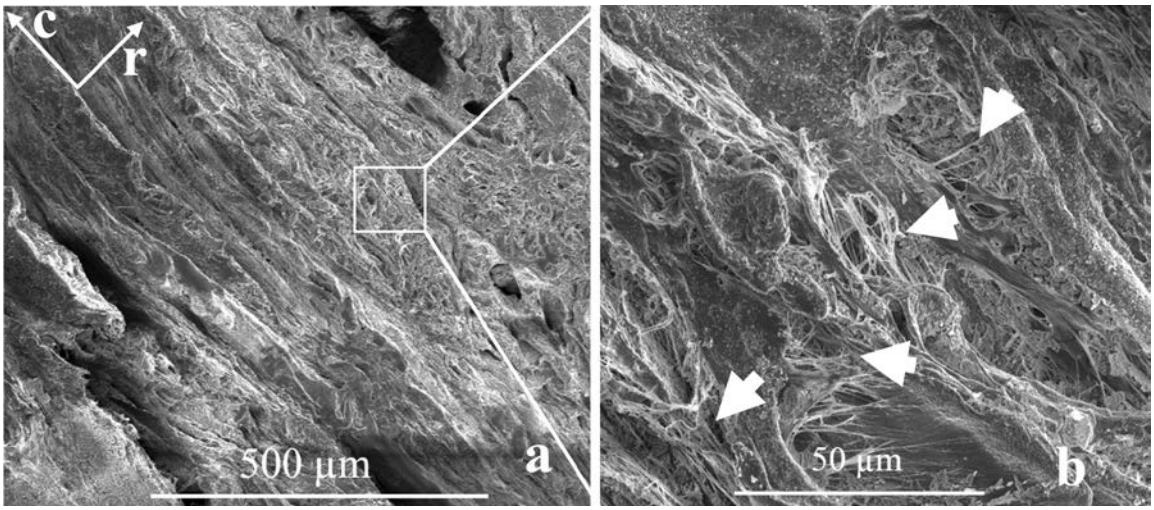

Figure 3.2 SEM images of one sample at different magnifications. Elastic fibres can't be observed under low magnification (a), while using high magnification (b) results in their clear visualization. Elastic fibres in treated areas are shown by arrows and (b) indicates higher magnification of the area that is denoted by the white box in (a).

3.3.6 Quantitative analysis

To quantify fibre orientation as well as their distribution, an open source software (ImageJ) was used [79]. Fibre orientation and their distribution were measured for the adjacent groups of control, digested and heat treated samples at two magnifications (high: SEM level and low: light microscopic level). The orientation and its distribution were measured relative to the tangent to the circumferential direction (TCD) axis (Figure 3.1d). The OrientationJ plugin was used to measure the orientation of structures in the input binary (8-bit) images, with Cubic Spline Gradient selected as the structural tensor for fitting the data. The results of orientation distribution were presented as orientation (°) versus distribution of orientation (count). Figure 3.3 shows examples of the software conversion of TIFF into binary images. During this conversion it was assumed that fibres were black and background was white.

A univariate ANOVA was conducted (IBM SPSS Statistics for Windows, Version 22.0. Armonk, NY: IBM Corp.), having a dependent variable of orientation and a fixed factor of sample preparation (control, digested, digested + heat treatment) using an alpha of 0.05, with post-hoc multiple comparisons conducted using a Bonferroni adjustment on alpha.

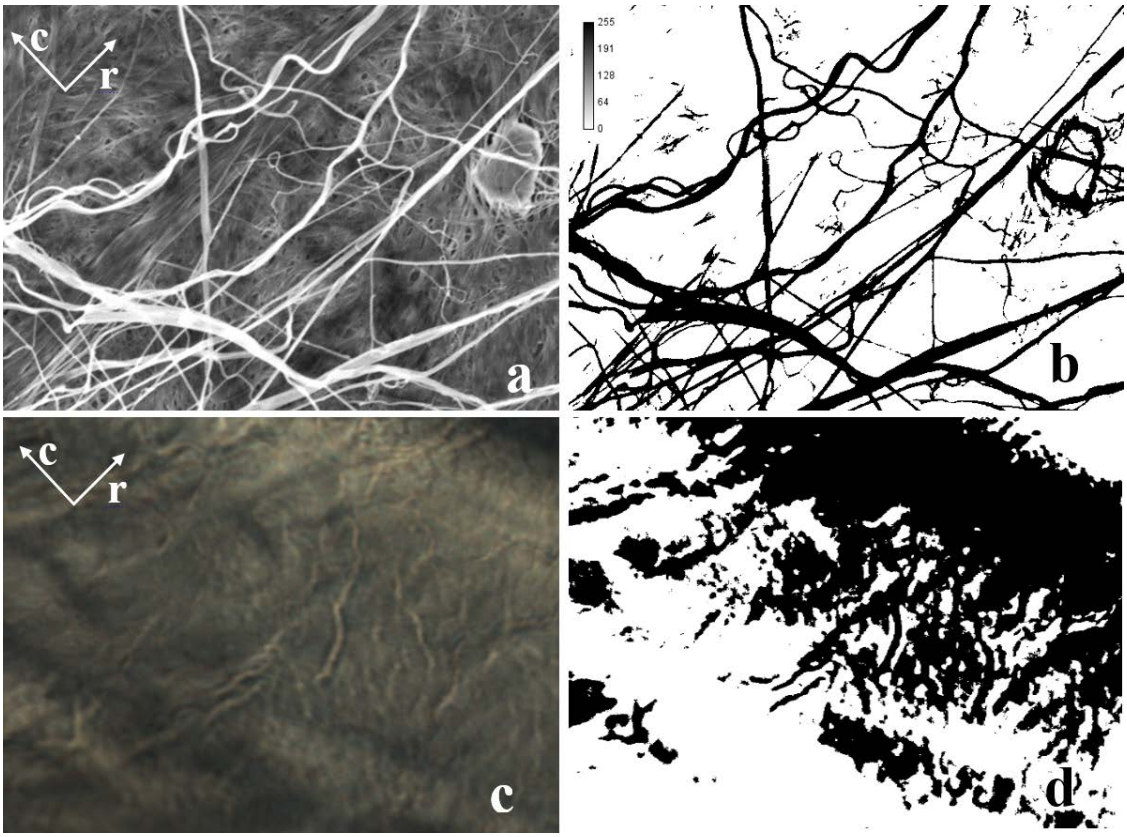

Figure 3.3 Conversion of a high magnification (SEM) image (a) to binary mode (b), and low magnification (light microscopic) image (c, d). Limitations in elastic fibre visualization occurred at the light microscopic level.

3.4 Results

Visualization of elastic fibres were accomplished at two different magnifications; low (light microscopy level) and high (SEM). Figure 3.4 presents images of adjacent control (Figure 3.4a), digested (Figure 3.4b) and orcein treated samples (Figure 3.4c), all visualized by light microscopy at the same magnification. At the light microscopy level, both control and digested samples did not reveal any structural organization of elastic fibres, as they are surrounded by other components. Histology and orcein stained

samples indicate that elastic fibres, were distributed throughout the AF; however, their concentration was higher in the region between two adjacent lamellae than within the lamellar region. Figure 3.4d shows an orecin treated sample after digestion. Although a significant decrease in the masking effect of the matrix leads to a better visualization of elastic fibres when compared with the orcein treated (Figure 3.4c) sample, further analysis of the ultra-structure was required. More clearly, the density of elastic fibres generally increased from the lamellar region to the region between lamellae.

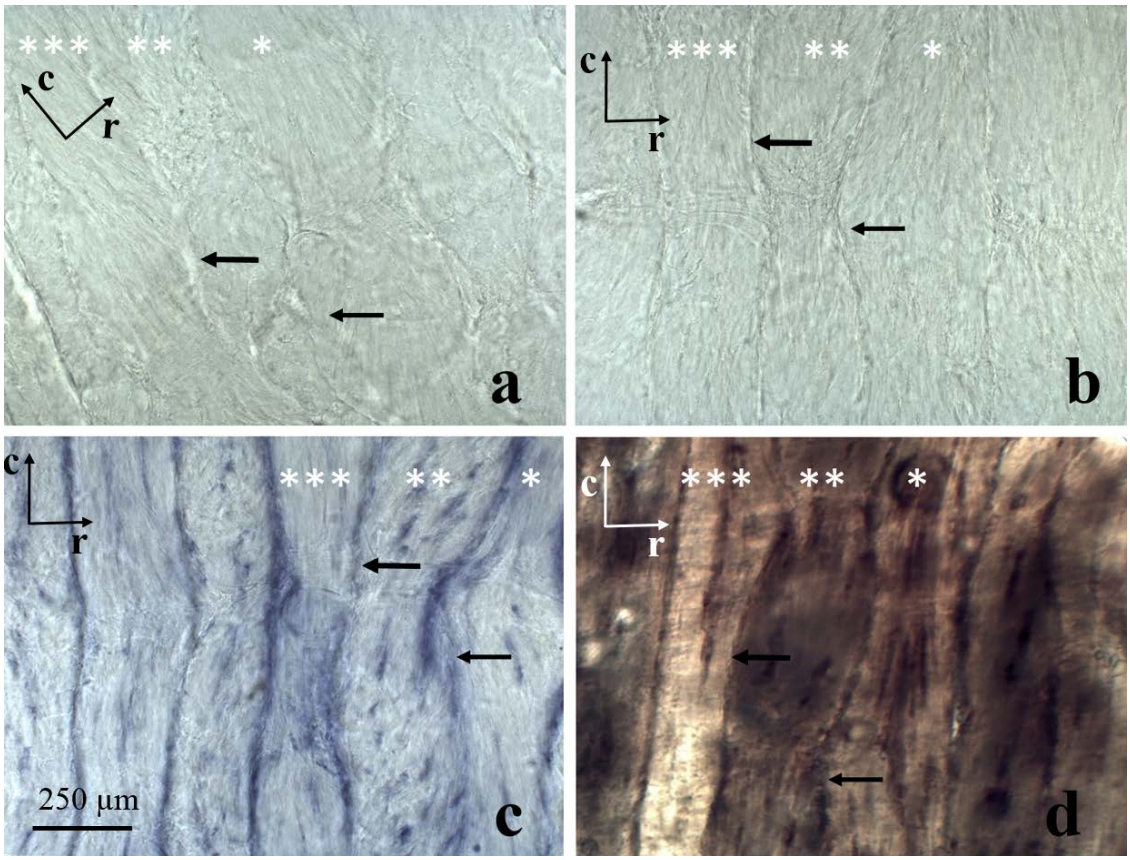

Figure 3.4 Light microscopy images of the ILM at the same magnification of (a) control and the adjacent digested (b) and orcein treated (c) samples. Figure (d) indicates the adjacent sample histologically stained with orcein after digestion. White stars represent corresponding lamellae in all samples. Arrows indicate the regions between lamellae.

Figure 3.5 shows the same region as Figure 3.4d under different magnifications of a sample that was stained with orcein after digestion. The structural organization of elastic fibres could be observed rarely because of the limitation of the light microscopy

scale, and the level the complexity of the elastic structure was not clearly visualized even for a digested sample.

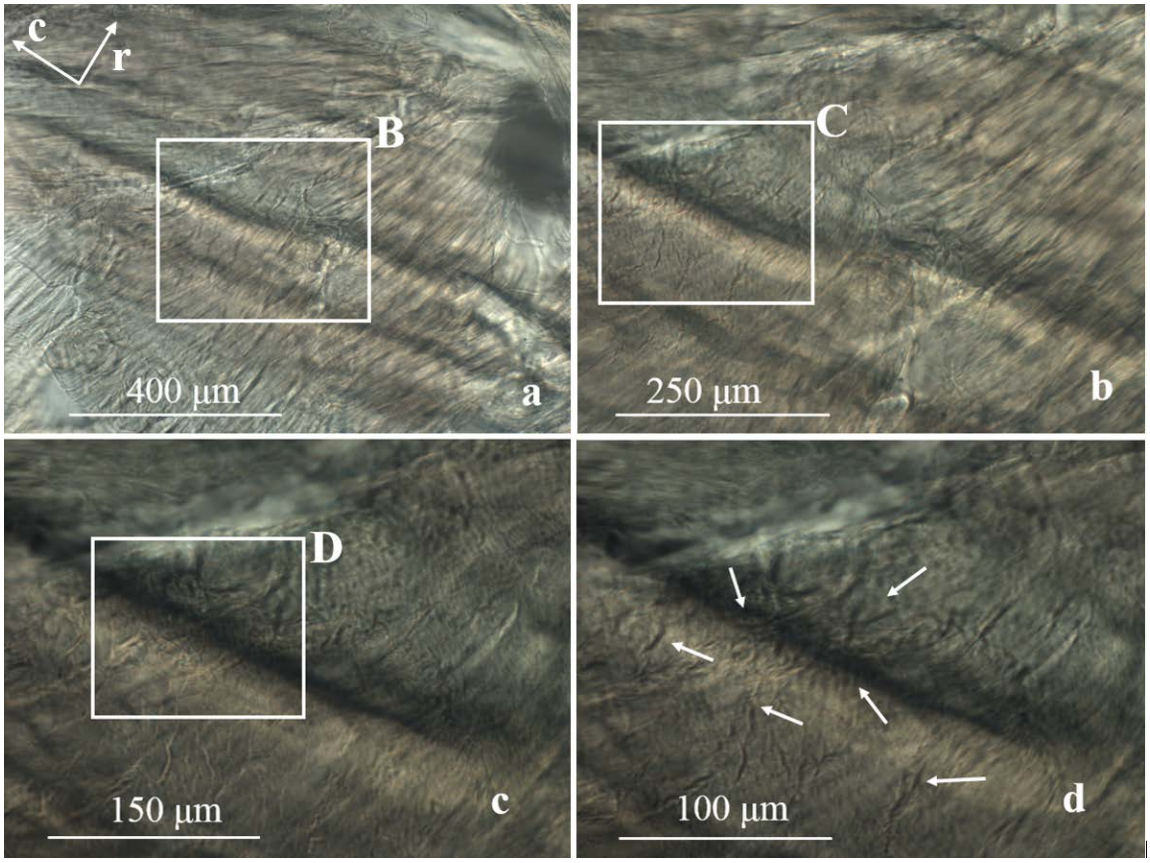

Figure 3.5 Light microscopy images of a digested-orcein stained sample under different magnifications at the same region. At the lower magnifications (a, b) the overall structure of the AF is apparent. Increased magnification (c, d) revealed improved visualization of elastic fibres (denoted by white arrows in figure d) but without clear structural organization. Images shown as b, c and d correspond to the boxes denoted by B, C and D, respectively.

The optimization of the NaOH digestion with the sonication technique was performed as a function of time of sonication, while NaOH concentration, intensity of ultrasound and sample thickness were kept constant. . Since the fibrous constituents of the AF are intermingled with the matrix, it was difficult to observe its fibrous structure in the control sample (Figure 3.6a). Gradual removal of matrix occurred as the sonication time was increased to reveal a progressive improvement in visualization of different fibres within the AF structure (Figures 3.6b-f).

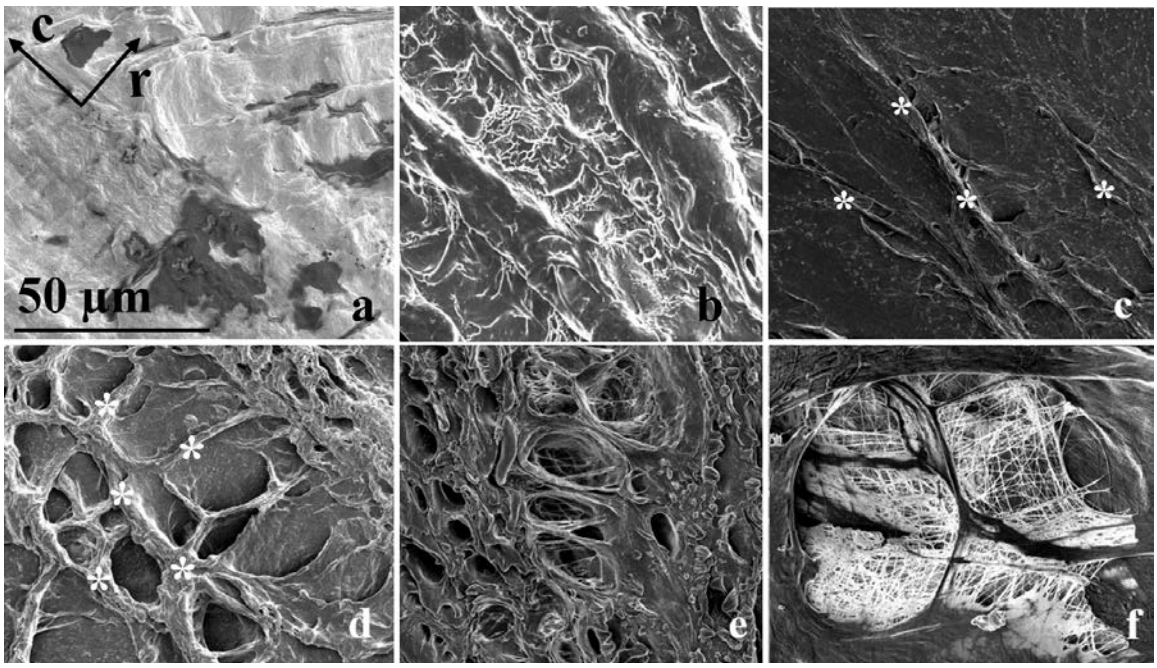

*Figure 3.6 Optimization of NaOH digestion as a function of sonication time in comparison with a control sample, visualized by SEM at the same magnification in all images. SEM images after sonication are shown at 5 min intervals. The structural organization of fibrous elements of the AF lamellae was not revealed in control samples at t=0 min (a). SEM investigations revealed that during the first 5 min (b) to 10 min (c) of digestion, the surface of the samples were affected. After 15 min (d) a change of surface to bulk digestion was observed, revealing the commencement of the fenestration. After 20 min (e), deeper empty oval spaces appeared that revealed some elastic fibres, and at the end of digestion after 25 min (f), the fibrous structure of the AF were more distinguished as matrix was removed from the partially digested regions of the AF. Large bundles (denoted by * in c and d) may represent the inter-lamellar region (boundaries between adjacent lamellae) or partition boundaries (regions that separate collagen bundles in the cross-section plane), where the concentration of intact elastic fibres is high.*

The NaOH digested and sonicated samples revealed a complex network of collagen and elastic fibres that formed different structural organizations throughout the AF when observed at the SEM level. Since AF is heterogeneous, it was found that digestion removed the matrix from separate areas revealing a fenestrated structure. Therefore in the partially digested AF (after 25 min), the regions between fenestrations were preserved intact (Figure 3.7a, as denoted by arrow heads).

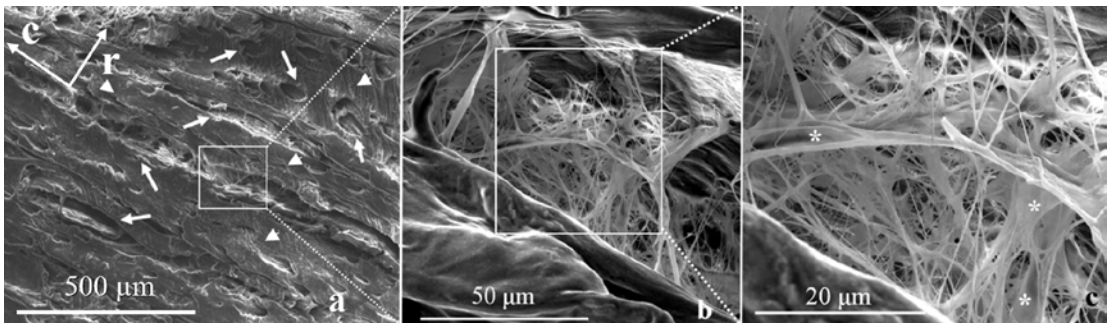

Figure 3.7 SEM images of a partially digested AF sample (after 25 mins of sonication time) under three magnifications. (a) NaOH digestion and sonication removed the matrix to form a fenestrae (white arrows). (b, c) The delicate fibres spanning the fenestrae were preserved intact. The remaining matrix in a digested fenestration are denoted by stars in (c).

Undigested matrix remnants (denoted by star in Figure 3.7c), were observed within the exposed fibre network. Within the digested regions the individual fibres could be easily distinguished by their size that varied between 0.1 to 3 µm. The large fibres branch and anastomose to each other, while very fine fibres interconnect the larger ones; however, making a clear distinction between collagen and elastic fibres after digestion was difficult. Thus, for effective visualization of elastic fibres, selective gelatinization and removal of non-elastin components including micro-fibrils and collagen fibres were extracted by indirect heating in a water bath after digestion (Figure 3.8).

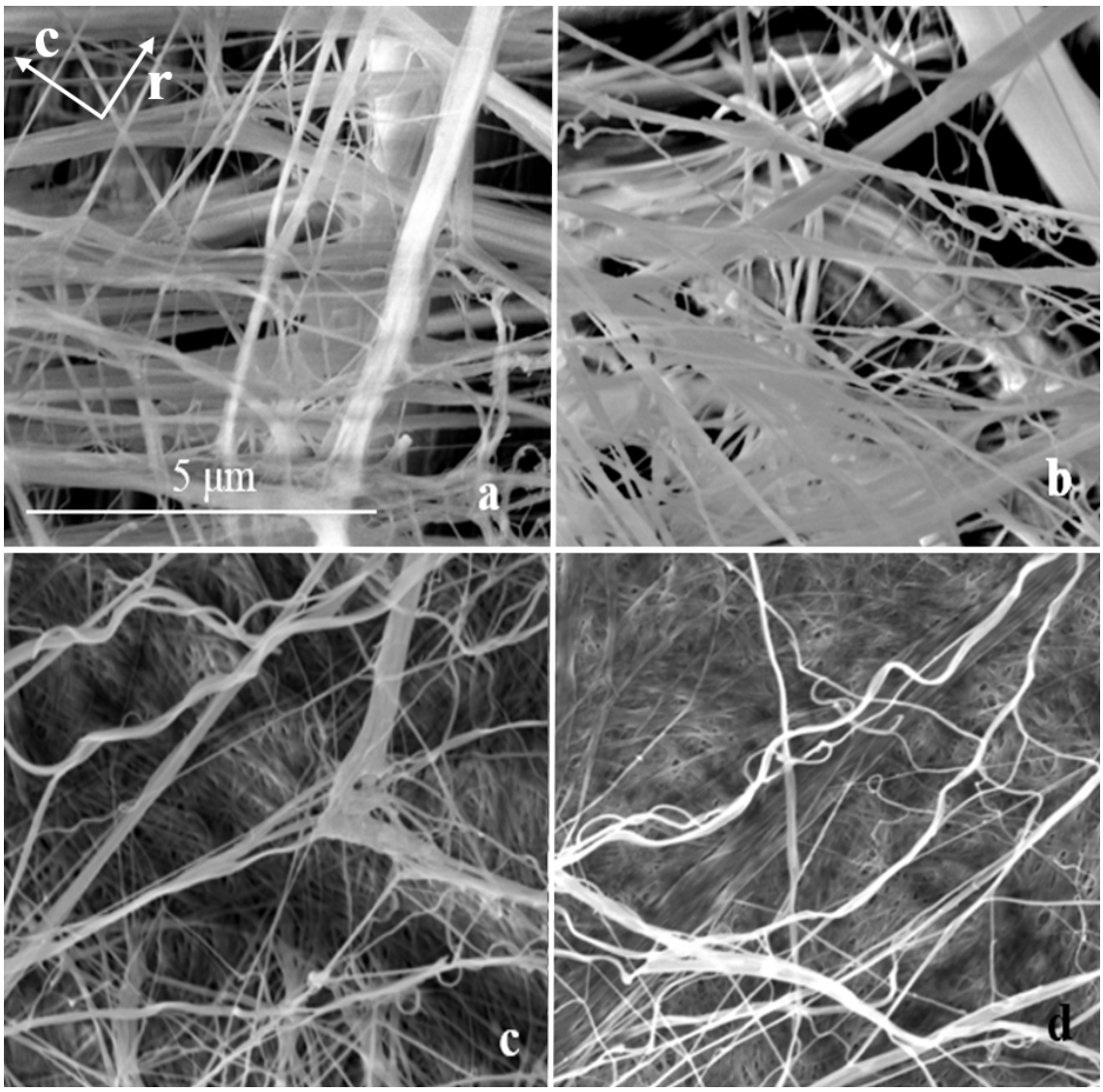

Figure 3.8 Effect of heat treatment after digestion to remove collagen from the intra-lamellar region of the AF. (a, b) Samples that underwent digestion only, revealing both collagen and elastic fibres. (c, d) samples that underwent heat treatment after digestion, which removed collagen and revealed the ultrastructure of the elastic fibres.

In digested samples, both collagen and elastic fibres can be observed as digestion without heat treatment only removed matrix and micro-fibrils. The collagen fibres are larger in size and appear as strands, while smaller, wavy fibres are elastic fibres. In heat treated samples it was possible to observe elastic fibres (Figure 3.8); however, remnants of non-digested matrix and other components (i.e. collagen) still obscured the underlying elastic fibres. A loose network of elastic fibres could be observed in heat treated samples, which were comprised of almost parallel large fibres (0.5-1.5 µm diameter) and very fine interconnecting fibres of less than 0.2 µm diameter. This loose

network of parallel large and fine interconnecting fibres, as a key structural feature, was observed across all heat treated samples (Figure 3.9).

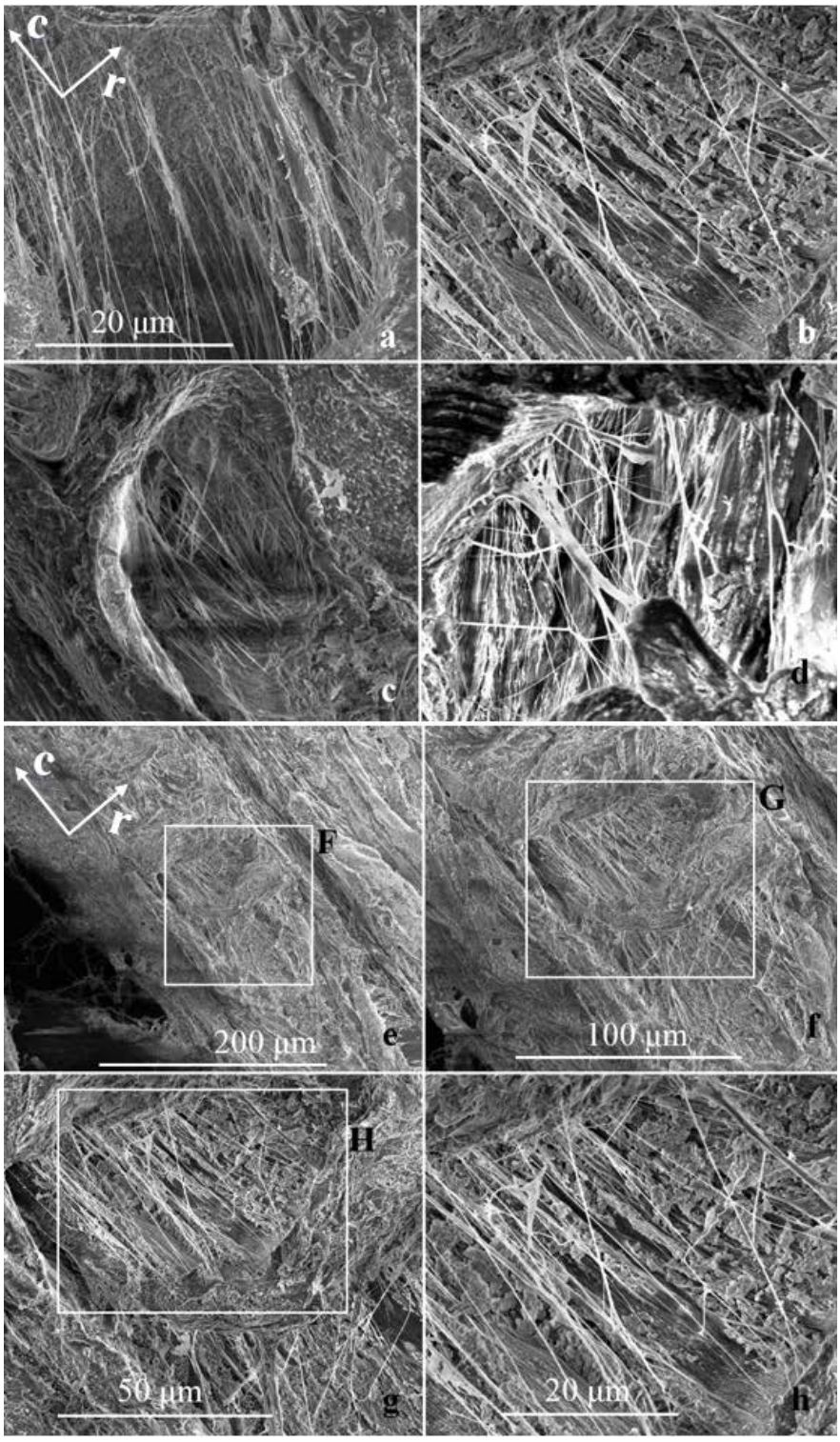

Figure 3.9 Frequency of occurrence of observing the loose elastic fibre network in the AF lamella in different heat treated samples (after 25 min) at the same magnification (a-d). (e–f) ultra-structural organization of elastic fibres of sample 'b' at lower magnifications. The white boxes denoted by F, G and H correspond to higher magnified f, g and h images, respectively.

Figure 3.10 shows the distribution and orientation of fibres in control, digested and heat treated samples for two adjacent samples at high and low magnifications.

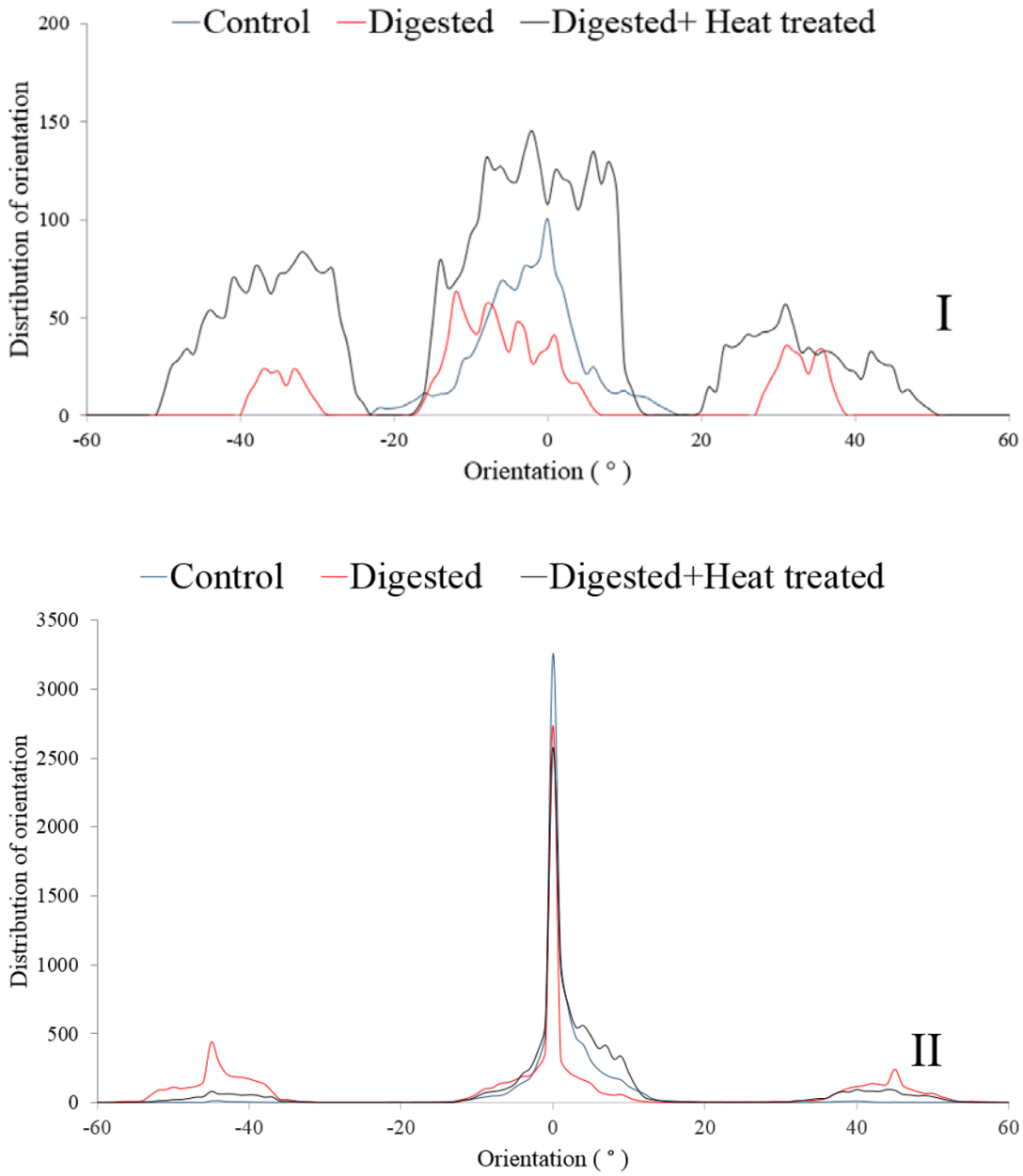

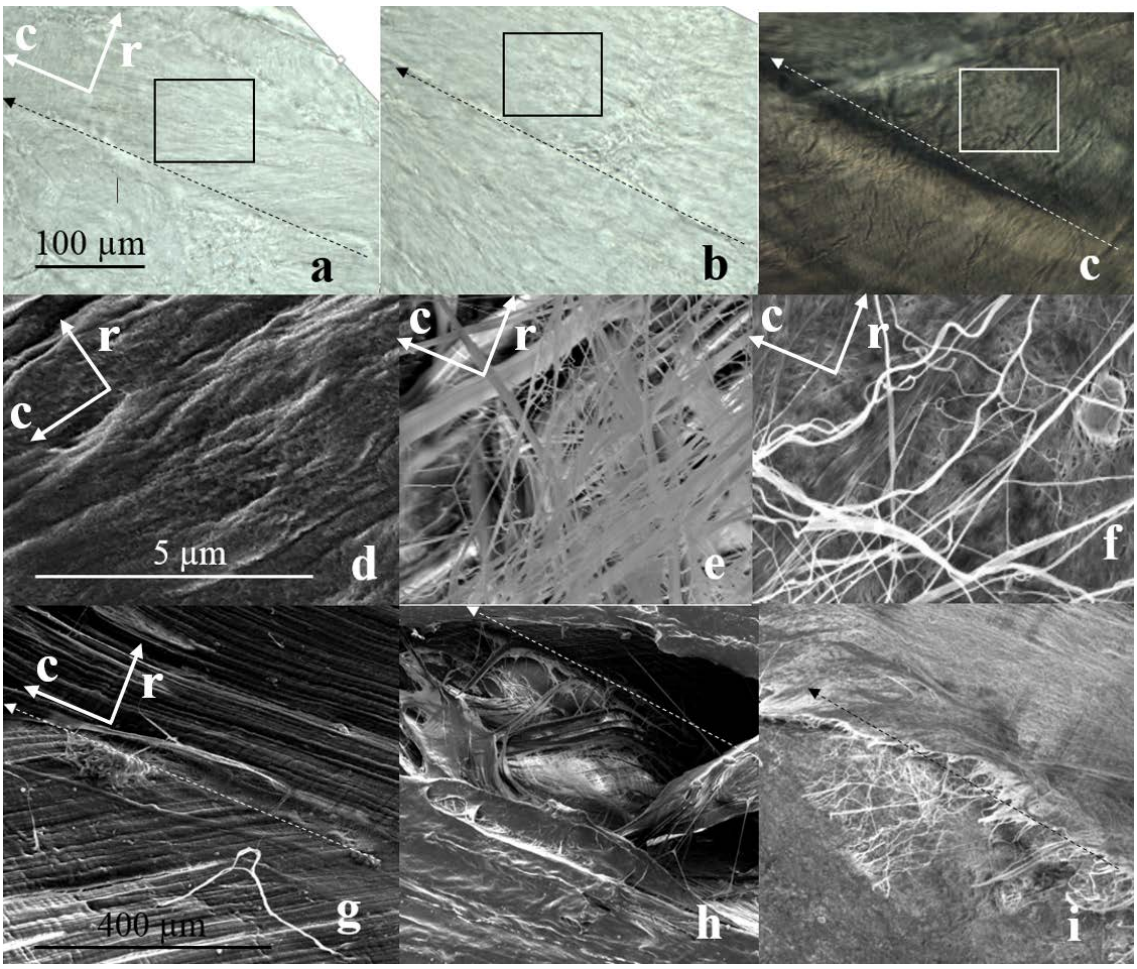

Figure 3.10 Comparison of AF fibre orientation between control, digested and heat treated samples under light microscopy (I) and SEM (II). (a, b, c) Light microscopic level at the same magnification, and (d, e, f) at the SEM magnification for control, digested and heat treated samples respectively. (a, b, c) Arrows show the TCD axis and boxes identify areas that were selected for measurement of orientation. (g, h, i) show images at lower magnification (400 µm) of images d, e and f, respectively.

The AF fibres were found to be orientated at an angle of approximately 4° relative to the TCD axis in control samples. According to the ultra-structure of the fibres, three different symmetrically organized angle of orientations (approximately measured as 45°, 0° and -45°) were detected; however, the principle angle of rotation remained unchanged (0°) when compared to control samples, except for the light microscopy images. Table 3.1 shows the results corresponding to characterization of orientation at the SEM level for all four samples.

Table 3-1 Frequency of "fibre structural orientation" as a key feature for evaluating the impact of sample preparation (digested, digested + heat treatment) on structural orientation, across adjacent AF samples from four different specimens at the SEM level.

Sample	Control	Digested	Digested + Heat treatment
	Orientation (°)		
Specimen 1	4.1	4.4	6.3
Specimen 2	4.6	5.0	6.9
Specimen 3	3.9	4.2	6.0
Specimen 4	3.2	3.9	5.3
Mean (SD)	**3.91 (0.67)**	**4.40 (0.46)**	**5.93 (0.46)**

The overall effect of sample preparation was significant ($p \leq 0.01$), with post-hoc comparisons revealing that the control orientation was not significantly different to the digested orientation ($p=0.673$), with significant differences between the control and digested + heat treatment orientations ($p=0.001$), and between the digested and digested + heat treatment orientations ($p=0.009$).

3.5 Discussion

The viscoelastic and mechanical properties of the AF in the disc are affected by the structural associations of its constituents, which can be obtained from precise ultrastructure observation [55]. The role of elastic fibres on the disc's mechanical properties is not clear, since their ultra-structural organization within the AF has not been accurately determined. Previous studies on visualization of elastic fibres of the AF via light microscopy analysis of histologically prepared tissues, found this characterization extremely challenging to accomplish [34, 45, 70]. The first stage towards describing the role of elastic fibres in the AF is to clearly visualize their ultrastructure organization. The present study reports on the development of a method for ultrastructural visualization of elastic fibres across the AF, which may be used to enhance knowledge of their structure-function relationships.

The NaOH digestion and sonication technique permits quick isolation and exposure of the intact elastic fibre network in the AF for SEM observation. This study showed that sonication of the AF samples in NaOH solution followed by heat treatment increased the digestion rate for removal of non-elastin components (collagen, micro-fibrils and matrix), and prepared elastic fibres for visualization using SEM. The ECM of the disc, which exhibits hydrophilic property, is composed of proteoglycans and fibrous proteins. The main fibrous proteins of the ECM are collagen and elastin. The majority of the ECM space is filled by proteoglycans, which are made of glycosaminoglycan chains. The glycosaminoglycan chains are unbranched polysaccharides that can be divided further into chondroitin and keratan sulfates and hyaluronic acid. The majority of the collagen fibres form a triple strand helix and assembled into the supramolecular structures. In contrast, elastin protein is a crosslinked polymer of tropoelastin monomers that forms a highly hydrophobic and elastic network. The lysyl oxidase enzyme controls the extracellular crosslinking of tropoelastin at which the majority of lysine residues covalently crosslinked via oxidation reaction. The contribution of lysyl oxidase into the crosslinking of elastin, results in creation of 15-20 crosslinks per elastin unit, whereas collagen contains two. Once crosslinked, the dissociation of elastic fibre network into tropoelastin monomer is impossible. This high degree of crosslinking is responsible for the elastic properties of elastin, its insolubility, high resistance to the change of temperature, pH and proteolysis. Therefore, while all proteins can be eliminated or extracted from the disc, the isolation and visualization of elastic fibre network can be accomplished by removing other fibrous proteins and proteoglycans from the ECM. The described method for visualization and isolation of elastic fibre network in the disc takes advantage of the hydrolysis process using alkali metal hydroxides with simultaneous sonication (alkali digestion). In general, the chemical bonds of non-elastin components

of the ECM can be broken down into their building blocks during alkaline hydrolysis followed by penetration of water molecules and ions (H+ and OH-). Since condensation of amino acids into the proteins is reversed during the alkali digestion, all proteins can be demolished except elastin. Both sonication and heat treatment accelerate the digestion process. Application of ultrasound may increase Brownian motion of the ECM small fragments and facilitates the diffusion of ions within the tissue. The increase of temperature slightly above 60 °C assists the elimination of remnant collagen fibres via gelatinization process [80].

A small difference in fibre orientation was found after digestion compared to the control (0.49°). The optimum exposure to sonication through the digestion process preserved the organization and ultra-structure arrangement of the elastic network as well as the very delicate elastic fibres usually lost during light microscopy analysis. However, reduction of sonication time, which leads to less matrix extraction from partially digested regions, provides an opportunity for studying the relationship between the elastic fibre frameworks with other non-elastin components.

As a consequence of partial digestion, a fenestration structure of various sizes (digested regions) was randomly scattered across the sample (Figure 3.7a). Therefore, a vigilant and attentive observation at high magnification near the border of digested regions needs to be accomplished. Moving from the centre of digested fenestrae towards its perimeter results in gradual accumulation of matrix and collagen fibres, and provides a possible opportunity to prepare SEM images that show relationships between elastic fibres and other components of the AF.

Lack of prior similar studies on intervertebral disc made the methodology of this study quiet challenging to compare. In spite of the effectiveness of the described method on visualization of the AF elastic fibres, some limitations need to be addressed for

consideration in further studies. The digestion technique, although optimized in this study, needs to be slightly modified for different disc specimens as their material and biological properties vary across different samples. During SEM analysis, the collagen and elastin fibres were identified by comparing their size and morphology, which was challenging. In addition, the digestion method was found to be ineffective for ultrastructural organization analysis at the light microscopy level. To minimize these limitations, digestion times between 25-35 mins were applied before SEM imaging.

With regards to our findings, elastic fibres within the AF lamella displayed an arrangement similar to that observed at the light microscopy level [13, 45]. Also it was previously described that within the AF lamella, elastic fibres assemble in parallel to each other, which was consistent with the findings from the present study. However, the parallel assembly of elastic fibres formed a small part of the whole structural organization of elastic fibres in the AF lamellae regions. By removing the matrix and extracting collagen fibres, it was demonstrated that large parallel fibres were connected to each other by very fine elastic fibres and form a loose network. It is likely that this new interpretation of elastic fibre ultrastructure hasn't been previously reported due to the limitation of conventional staining techniques, light microscopy methods or the masking effect of the matrix. By using an optimized rapid digestion technique, the elastic network of all fibre sizes was able to be clearly visualized; however, small remnants of undigested matrix were occasionally observed within the network. Also heat treatment was shown to be effective at removing collagen fibres from digested areas only, and not from the intact regions between them. In non-digested regions, stabilization of fibres with matrix prevented the removal of non-elastin components by heat treatment. Through this study it was seen that the size, morphology and arrangement of elastic fibres in the AF were comparable to those described in other tissues after using chemical

or enzymatic digestion [38, 81]. Similar to studies on other tissues, elastic fibres in the AF form generally twisted or straight strands, having approximate diameters of 0.2 to 2 µm [34, 69, 82].

As described, large parallel fibres of loose elastic networks, which intermingle with other constituents of the AF lamellae, align with highly packed collagen fibres (Figure 3.8a and b). Measuring the orientation of different fibres and their relative distribution allows for a quantitative assessment of whether there is any AF structural alteration after digestion and heat treatment when compared to control samples. Based on the statistical analysis, heat treatment significantly affected the structural organization of elastic fibres in digested samples. Also, since elastic and collagen fibres were obscured by the extracellular matrix in control samples, it was not possible to directly measure their orientations. The finding of significant difference in fibre orientation between control and digested + heat treatment samples revealed that under high magnification elastic fibres appeared to be parallel to the collagen fibres. The fixed reference for measuring the fibre orientation and their distribution was chosen to be tangential to the circumferential direction (TCD axis) located between two adjacent lamellae (Figure 3.1d). Referring to the distribution of fibre orientations (Figure 10-II), the observed single peak of control samples was most likely identifying the organization of the abundant collagen fibres rather than micro-fibrils or elastic fibres. Therefore a direct comparison of fibre orientation between control and digested + heat treatment is not applicable. In digested and heat treated samples, the observation of three peaks for distribution of orientation with higher amplitude confirms that more fibres were visualized after matrix removal. For heat treated samples, the principle angle of rotation (5.93° (0.46°)) was significantly larger by approximately 1.5° (34 %) compared to the adjacent digested samples. While this difference was statistically significant, the

magnitude was small and it is likely that large elastic fibres align approximately parallel with collagen fibres, particularly when under load. It seems that fine interconnecting elastic fibres were not organized randomly as their angle of rotation was the same as those in digested samples (Figure 3.10-I). This identifies a relationship between fine elastic fibre organization and micro-fibril structural distribution. Considering the hierarchical scale, the trend under high magnification was consistent with the orientation of different fibres at lower magnification. However it appears that there was a limitation under light microscopy structural analysis for the control samples, where the masking effect of the matrix in revealing the fibre orientation was pronounced.

Measuring elastic fibre orientation angle and distribution using image processing revealed two important findings. First, while the rapid digestion and subsequent gradual and indirect heat treatment techniques significantly changed the overall structural organization of fibres, these changes were small and would likely have minimal impact on ultra-structural alteration of elastic fibres. Secondly, within the loose elastic fibre network, the organization of fine fibres seems to be related to micro-fibril arrangement. Further study is required to clarify the arrangement of elastic fibres-microfibrils in the AF. Also it appears that the small alterations in fibre orientation, subsequent to heat treatment, were consistent among samples. The minimal structural alteration could be described and supported by two observations that were found in SEM images: first, partial digestion created small fenestrations, distributed randomly across the AF, where the exposed elastic fibres were mechanically supported by surrounding non-digested tissue. The size of the fenestrations were less than non-digested regions. The second observation was that remnants of partially digested matrix and other components (i.e. collagen compartment) still obscured the underlying elastic fibres after digestion.

3.6 Conclusion

Knowledge of the ultra-structural organization of elastic fibres in different regions of the AF enhances understanding of their mechanical role and serves as a baseline for studying the elastic framework across the disc. This study describes a rapid digestion technique for exposing elastic fibres of the AF to allow SEM observation of their ultra-structure. Using this technique, ultrastructural analysis of elastic fibres in different regions of the AF and different species (Appendix A) could be studied for changes during mechanical loading, injury and disease compared to normal discs.

4 Chapter 4 - Study 2: The ultra-structural organization of the elastic network in the intra- and inter-lamellar matrix of the intervertebral disc

The previous chapter (Chapter 3, Study 1), explored a novel method for visualization of elastic fibres in the different regions of the disc. Utilizing the method, all components except elastic fibres were removed, allowing elastic fibres to be visualized. Based on the method, this chapter revealed the ultrastructural organization of elastic fibres in the ILM and intra-lamellar region of the AF. The ultrastructural analysis of elastic fibres in the ILM is important for describing their contribution to the structural integrity and mechanical properties of the AF in the disc.

The study presented in this chapter has been published in the following journal and conference proceedings:

Tavakoli J, Elliott DM, Costi JJ. The ultra-structural organization of the elastic network in the intra- and inter-lamellar matrix of the intervertebral disc, Acta Biomaterialia, 58, 269-277, 2017.

Tavakoli J, Costi JJ. Ultrastructural analysis of annulus fibrosus elastic fibres using a rapid matrix digestion technique (Poster). Proceedings of the 44th Annual Meeting of the International Society for Study of the Lumbar Spine (ISSLS), Greece, May 2017.

Tavakoli J, Costi JJ. Ultrastructural and orientation of the elastic network within the disc annulus fibrosus (Poster). Proceedings of the 28th Annual Meeting of the Spine Society of Australia (SSA), Hobart, Australia, April 2017.

Tavakoli J, Elliott DM, Costi JJ. Elastic network in the inter-lamellar matrix of the intervertebral disc. Proceedings of the 22nd Annual Meeting of the Australian and New Zealand Orthopaedic Research Society (ANZORS), Melbourne, Australia, October 2016.

Tavakoli J, Elliott DM, Costi JJ. Investigation into the structural organisation of elastic fibres in the inter-lamellar matrix and intra-lamellar region of the disc. 14th Adelaide Centre for Spinal Research (ACSR) Spinal Research Symposium, Adelaide, Australia, August 2016.

4.1 Abstract

The inter-lamellar matrix (ILM) —located between adjacent lamellae of the annulus fibrosus— consists of a complex structure of elastic fibres, while elastic fibres of the intra-lamellar region are aligned predominantly parallel to the collagen fibres. The organization of elastic fibres under low magnification, in both inter- and intra-lamellar regions, was studied by light microscopic analysis of histologically prepared samples; however, little is known about their ultrastructure. An ultrastructural visualization of elastic fibres in the inter-lamellar matrix is crucial for describing their contribution to structural integrity, as well as mechanical properties of the annulus fibrosus. The aims of this study were twofold: first, to present an ultrastructural analysis of the elastic fibre network in the ILM and intra-lamellar region, including cross section (CS) and in-plane (IP) lamellae, of the AF using Scanning Electron Microscopy (SEM) and second, to - compare the elastic fibre orientation between the ILM and intra-lamellar region. Four samples (lumbar sheep discs) from adjacent sections (30 μm thickness) of anterior annulus were partially digested by a developed NaOH-sonication method for visualization of elastic fibres by SEM. Elastic fibre orientation and distribution were quantified relative to the tangential to circumferential reference axis. Visualization of the ILM under high magnification revealed a dense network of elastic fibres that has not been previously described. Within the ILM, elastic fibres form a complex network, consisting of different size and shape fibres, which differed to those located in the intra-lamellar region. For both regions, the majority of fibres were oriented near 0° with respect to tangential to circumferential (TCD) direction and two minor symmetrical orientations of approximately ±45°. Statistically, the orientation of elastic fibres between the ILM and intra-lamellar region was not different (p= 0.171). The present study used extracellular matrix partial digestion to address significant gaps in

understanding of disc microstructure and will contribute to multidisciplinary ultrastructure-function studies.

4.2 Introduction

The intervertebral disc, located between each adjacent vertebrae in the spine, undergoes large mechanical loads and deformations during physiological loading, thus its underlying structural components, including the interconnectivity of the lamellae in the annulus fibrosus (AF), must preserve structural integrity and restrict radial bulging [15, 83]. The impact of fibrous constituents on disc properties had been noticed previously and a review paper published in 1988 by Humzah and Soames, mentioned that structural properties of the disc together with its biochemical characteristics are closely related to the function [84].

In the AF, the orientation of collagen fibres within adjacent lamellae alternate by approximately 90° to each other, hence their intersection with an oblique plane reveals both cross-section (CS) and in-plane (IP) lamellae (Figure 1e, 1f). Insights into the fibrous organization of CS and IP lamellae of this intra-lamellar region have suggested a contribution to AF biomechanics [48]. The inter-lamellar matrix (ILM), with a thickness of approximately 20 µm or less, lies between the lamellae of the AF and its complex elastic fibre network imparts annular structural integrity that may contribute to mechanical properties [9, 85]. Insightful hypotheses correspond to the mechanical role of the ILM have appeared from observations indicating the ILM higher stiffness than adjacent lamellae [24], presence of extensible elastic fibres [15, 16], co-localization of fibrilin and elastin fibres [33], inter-lamellar cohesion [27] and dependency between adjacent lamellae fibrous constituent and the ILM shear properties [28].

Elastic fibres are commonly composed of two distinct components: a central core of amorphous elastin and a meshwork of micro-fibrils that surround the core [38, 81]. The amorphous elastin core appears as both twisted and straight strands (0.2-1.5 µm thickness), and the micro-fibrils are mainly comprised of fibrillins (10-30 nm thickness), which are also abundant within the lamellae of the AF [86, 87].

The presence and organization of the elastic fibre network in the disc has been studied at the light microscopy and SEM scales [11, 16, 34, 45, 82, 88, 89]. In 1976, the presence of elastic fibres of the disc, in both the annulus and nucleus, were reported by Buckwalter et al. using the SEM technique [89]. It was described that the long elastin fibres of the nucleus pulposus (NP) extend radially toward the AF, while some are oriented towards the endplates [45]. In the AF, two distinct organizations of elastic fibres have been reported. In the intra-lamellar space (including CS and IP lamellae), elastin fibres are aligned parallel to the collagen fibres, and are tightly packed within the surrounding matrix. The architecture of the network between two adjacent lamellae, known as the inter-lamellar matrix (ILM), has been reported to be dense and more complex compared to within lamellae [11]. However, the ultrastructural organization of elastic fibres in the ILM and the intra-lamellar region is unknown.

Visualization of the disc's elastic fibre structure has been performed histologically, primarily by staining using haematoxylin-eosin, Weigher's resorcin-fuchsin, Verhoff's iron-haematoxylin, orcein and immune-staining techniques [34, 45, 90, 91]. Using light microscopy, the elastic fibre structure has been examined with polarized light, bright field, laser confocal and Nomarski differential interface contrast (DIC) imaging [10, 14, 16, 17, 27, 33, 87]. Although these techniques provide excellent visualization at the 0.5 µm scale in a single plane, none are able to provide the fine-scale and ultra-architectural details of the elastic fibre network.

At the smaller scale, scanning electron- (SEM) [28, 81], atomic force- (AFM) [92] and transmission electron-microscopies (TEM) [93] have been mainly used for disc fibre characterization (i.e. measuring diameter and relative orientation). However, limited studies reported the application of these techniques in ultrastructure visualization of the disc, i.e., SEM investigations on the collagen framework of the disc using chymotrypsin-treated samples [94, 95] and architectural relationships between disc and vertebral bones [96]. We have developed a technique to isolate AF elastic fibres at the SEM level using sodium hydroxide (NaOH)-sonication digestion and heat treatment [97]. Using a similar technique, the elastic fibre ultrastructure of artery walls and ligaments has been examined [74, 75, 98, 99]. In these studies the architectural arrangement of artery and ligament elastic fibres was determined by selective digestion using NaOH [100, 101], NaOH-sonication [74, 75, 98, 99], autoclaving [102] or formic acid [74, 102]. These digestion methods, which were used to expose and isolate elastic fibres, revealed the soft tissue structure of elastic networks which form a structural framework that acts to provide tissue structural integrity. The studies also confirmed that isolated elastic fibres remained chemically intact with the fibre structure being very close to pure elastin after NaOH-sonication digestion [74-76]. While different digestive methods do not affect the elastic fibre architecture, major structural changes occur subsequent to the dehydration process after digestion [103]. It was reported that freeze drying [103] and low temperature vacuum oven [104] methods resulted in less damage to these delicate elastic fibre networks.

In summary, a fundamental visualization of the AF elastic network ultrastructure is important for determining its structural contribution to disc mechanical properties, disc structural integrity and behaviour under complex loading conditions. Furthermore, an accurate knowledge of the elastic fibre network structural organization would be helpful

in understanding its basic mechanical role, including how stress is distributed throughout the AF layers and the ILM. Little is known about the ultra-structural organization of the ILM elastic fibres in the disc. Therefore, the aims of this study were twofold. First, to present an ultrastructural analysis of the elastic fibre network in the ILM and intra-lamellar region, including CS and IP lamellae, of the AF using Scanning Electron Microscopy (SEM) and second, to compare the elastic fibre orientation between the ILM and intra-lamellar region. This study was performed using an established rapid matrix digestion technique that preserved elastic fibre structural integrity and organization. The effective method for visualization of elastic fibre ultra-structural organization in the ILM and the adjacent lamella of the AF, was recently described [97].

4.3 Materials and methods

4.3.1 Sample preparation

Four lumbar sheep spines (18-26 months old) were obtained from a local abattoir, separated into bone-disc-bone segments (level L1/2) and stored at -20°C until required for analyses. Segments were then thawed overnight at room temperature while wrapped in saline soaked gauze. Each disc was dissected from the vertebral bodies. A 10 mm length of the anterior AF was separated from each disc (Figure 4.1a) and mounted with optimal cutting temperature compound (O.C.T, Tissue-Tek®) at an angle of approximately 30° to the transverse plane to identify the cutting plane (Figure 4.1b), and stored at -20°C until used. Two samples from adjacent sections (thickness 30 µm) were cut using a cryostat microtome (Leica Biosystems, CM3050) from each of four discs (Figure 4.1c) and were stored at -20°C for further analysis.

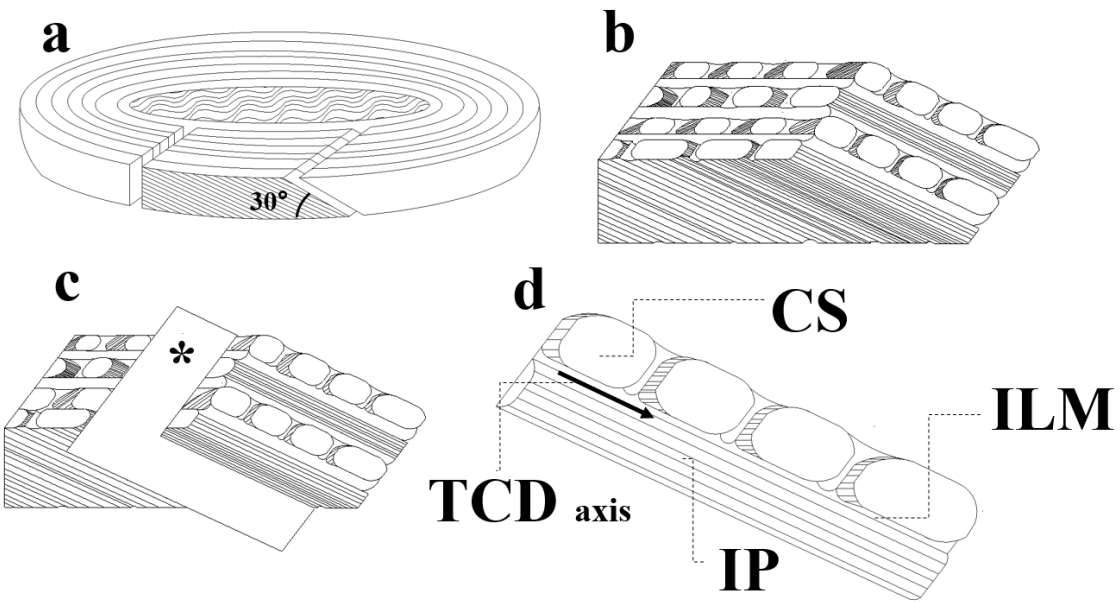

*Figure 4.1 Schematic drawing showing sample preparation. (a) Anterior AF strips (10 mm in length) were separated from the disc, (b) Frozen section preparation at an angle of 30° to the transverse plane and (c) Samples were cut by microtome to a thickness of 30µm along the cutting plane (denoted by *), (d) Schematic of two adjacent lamellae and their reference axis being parallel to the circumferential direction (TCD) for measuring fibre orientation, prepared at an angle of approximately 30° to the transverse axis along cutting plane. The IP (in-plane), CS (cross-section) lamellae of adjacent intra-lamellar and the ILM (inter-lamellar matrix) regions are identified.*

4.3.2 Sample digestion

Partial NaOH digestion was performed to prepare the AF samples for ultrastructure visualization of elastic fibres using SEM [97]. Briefly, samples from adjacent sections were digested in 0.5 M NaOH solution and sonicated (SONIC-950WT, MRC, Germany) for 15 min at 37°C, soaked in distilled water and placed in a water bath at 70 °C for 5 min to remove collagen fibres, leaving the elastic network intact as no cleavage of peptide bonds was seen after alkaline digestion [105]. All digested samples were then dried in a vacuum oven (VO3, LABEC, Australia) at 37°C and -80 kPa overnight.

4.3.3 Scanning electron microscopy

All SEM images were acquired from the exposed surface of each sample. The samples were mounted on aluminium stubs with double adhesive tape, then sputter coated (EmiTech K575X) with platinum at 2 nm thickness. For SEM imaging, the voltage was set at 5 kV and the distance from the sample to the beam source was kept constant for all

performed imaging. As elastic fibres were not visible at low magnifications (>200 µm), the samples were scanned at high magnification first (<50 µm). Once elastic fibres in the digested region were identified, a lower magnification was used as a starting point from which sequential images were acquired at the region of interest at progressively increasing magnifications.

4.3.4 Quantitative analysis

To quantify elastic fibre orientation as well as their distribution, an open source software (ImageJ) was used [79]. Fibre orientation and their distribution in the ILM and intra-lamellar region were measured relative to the tangent to the circumferential direction (TCD) axis (Figure 4.1-d). The OrientationJ plugin was used to measure the orientation of structures in the input binary (8-bit) images, with Cubic Spline Gradient selected as the structural tensor for fitting the data. The results of orientation distribution were presented as orientation (°) versus distribution of orientation (fibre count). Results of the quantitative analysis (orientation magnitude and distribution of orientation) were presented as the average of five regions of interest in each sample for both intra-lamellar region and the ILM at the same magnifications.

4.3.5 Statistical analysis

An independent samples t-test was conducted (IBM SPSS Statistics for Windows, Version 22.0. Armonk, NY: IBM Corp.), having a test variable of orientation between the ILM and intra-lamellar regions using an alpha of 0.05.

4.4 Results

4.4.1 Intra-lamellar region

As previously described, the collagen fibres of the CS in the intra-lamellar region are approximately perpendicular to the cutting plane; hence, elastic fibres are almost

parallel with the collagen fibres. Therefore, it is unlikely that elastic fibres in the CS could be visualized after eliminating collagen fibres via the digestion and heat treatment process (Figure 4.2). As shown in Figure 4.2c, the digestion process is less efficient in the IP regions, where tightly packed parallel collagen fibres are exposed in cutting plane, compared to the CS,. The cross section of a collagen bundle is shown (denoted by arrow head) in Figure 4.2d whose collagen fibres run into the cutting plane (denoted by arrow). It was observed that elastic fibres were removed from different digested regions of the CS (denoted by *) during the digestion process. Therefore, visualization of elastic fibres was not possible in the CS lamellae.

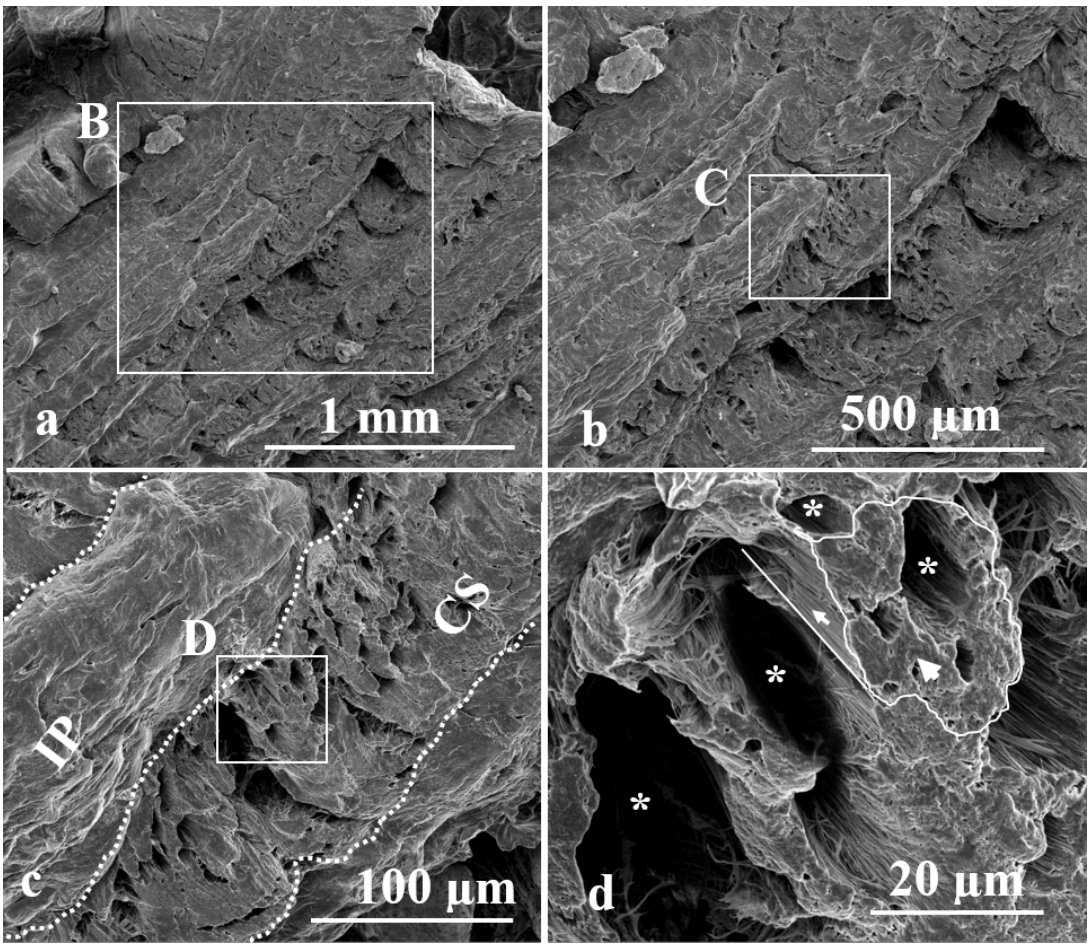

*Figure 4.2 SEM images of cross section lamella (CS) in a digested sample. (a) Lamellae of a digested sample under low magnification. The white boxes denoted by B, C and D correspond to higher magnified images shown in (b), (c) and (d), respectively. (d) Digested regions (denoted by *) revealed that visualization of elastic fibres was not possible in the CS at a cutting angle of approximately 30°. A collagen bundle's cross section (denoted by arrow head) and fibres (denoted by arrow) is presented. White lines in figure (c)*

identify boundaries between lamellae and in figure (d) represent cross section and fibres of a collagen bundle

In digested samples it was possible to observe elastic fibres (Figure 4.3) in IP; however, remnants of non-digested matrix and other components (i.e. collagen) still obscured the underlying elastic fibres. A loose network of elastic fibres could be observed in the IP (Figure 4.3f), which were comprised of almost parallel large fibres (0.3-0.5 µm diameter) and very fine interconnecting fibres of less than 0.3 µm diameter. This loose network of parallel large and fine interconnecting fibres, as a key structural feature, was observed across all digested samples (Figures 4.3f- 3i).

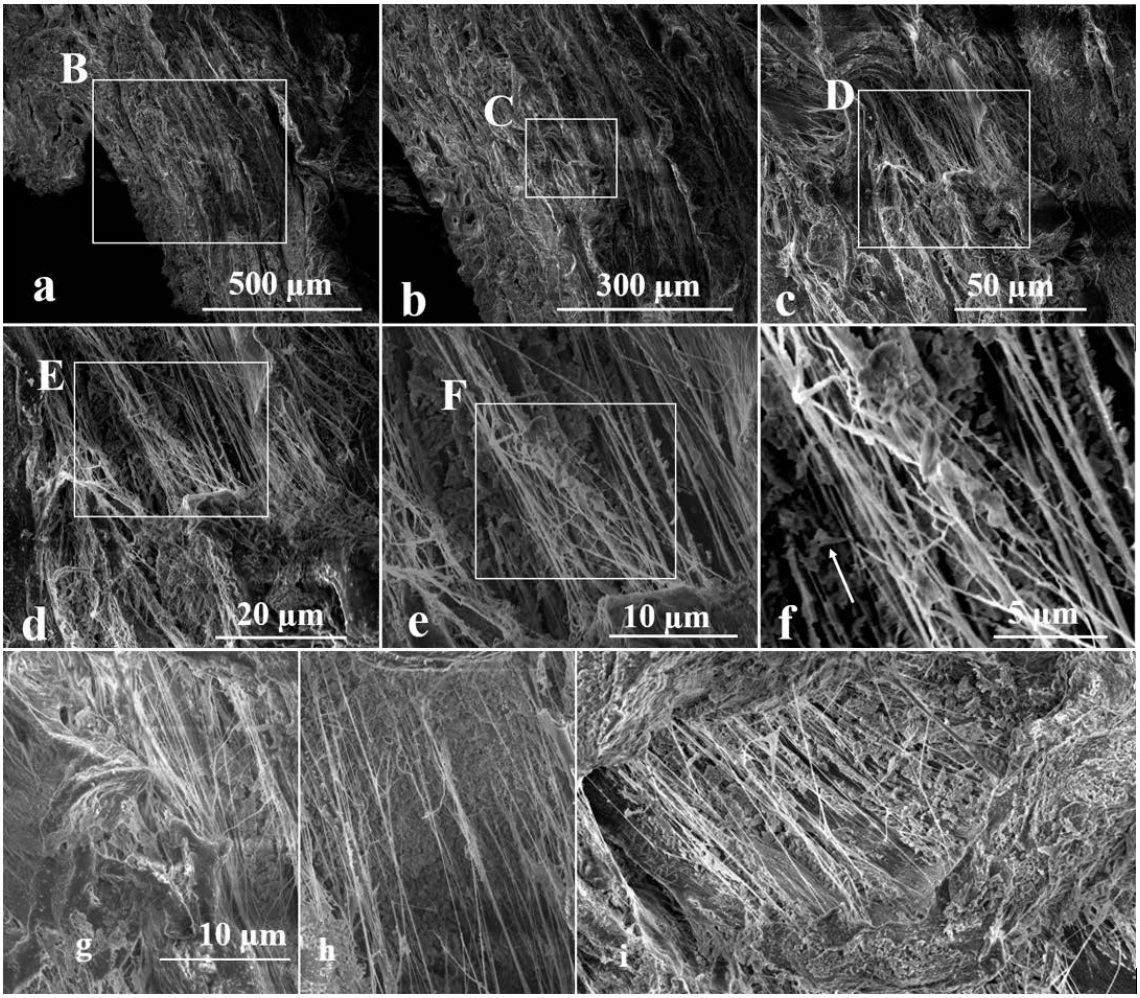

Figure 4.3 SEM images of In-plane lamellae (IP) in a digested sample reveal the elastic fibre ultra-structural organization in one sample at different magnifications (a-f) and in three other samples at the same magnification of 10 µm (g, h, i). The white boxes denoted by B, C, D, E and F correspond to higher magnified b, c, d, e and f images, respectively. TCD axis for panels (f-i) is denoted by arrows.

4.5 Inter- lamellar region

Figure 4.4 shows SEM images of the ILM elastic fibre organization of a digested sample, spanning six magnifications ranging from 300 to 5 µm. As shown in Figure 4.4, elastic fibres within the ILM form a complex network compared to the intra-lamellar region.

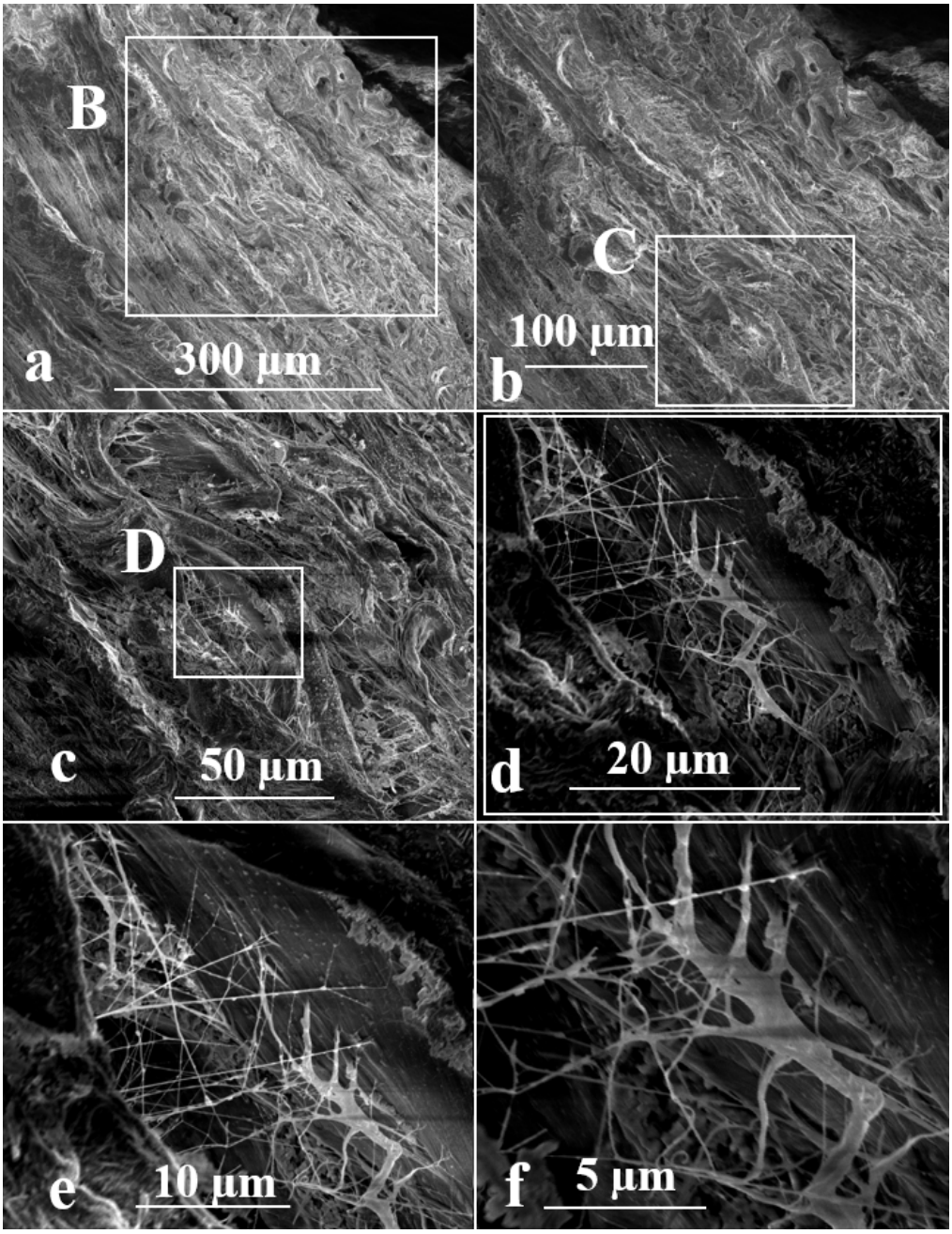

Figure 4.4 SEM images showing the structural organization of elastic fibres in the inter-lamellar matrix (ILM). Low magnification (a, b) revealed the elastic fibre network structure of the ILM located between two adjacent lamellae. Focusing in on the ultrastructure of elastic fibre network within the ILM under increasing magnification (c-f) revealed the complexity of the ultrastructure. The white boxes denoted by B, C and D correspond to higher magnified b, c and d images, respectively.

In the ILM, elastic fibres create a dense network that includes thick and thin fibres (Figure 4.4d- f). The thick elastic fibres have a diameter of approximately 1-2 µm; however, the diameter of thin elastic fibres was approximately 0.1 µm (Figure 4.4f). These thick and thin elastic fibres appear to create a web-like meshwork that connect together (Figure 4.4e). Within the ILM, elastic fibres have different ultrastructure characteristics that distinguish them from other parts of the AF. This network is denser with more complex structures of different size and shape than those located in the intra-lamellar region (Figures 4.4e and 4.3i).

Three different viewing angle of rotations (a, b and c) and a higher magnified (d) ILM including its boundary is shown in Figure 4.5. At the ILM-intra lamellar region boundary, where elastic fibres seem to penetrate into the adjacent lamella, two different kinds of anchoring may occur. Thick fibres of the ILM elastic network merge into the adjacent lamella to be oriented in parallel to the collagenous bundles in the intra-lamellar region (denoted by arrows in Figure 4.5). Thin elastic fibres form a delicate interconnected meshwork that runs from one side to the other of the ILM and branch out at the boundary (denoted by * in Figure 4.5).

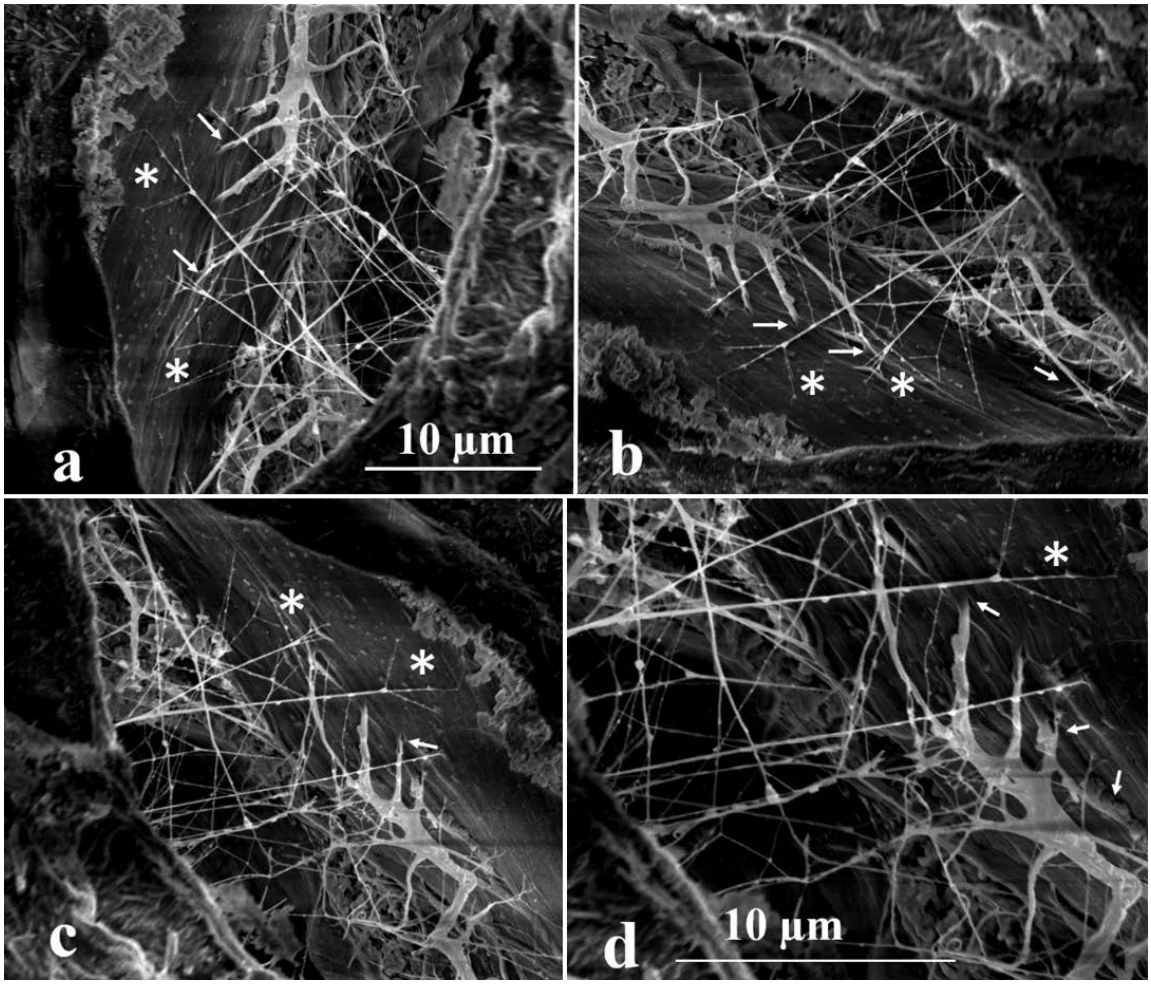

Figure 4.5 The elastic network in the same inter-lamellar matrix (ILM) shown at three different viewing angles of rotation (a, b, c). A higher magnified image of figure (c) is presented in (d). White arrows and stars indicates two different elastic network boundary junctions for thick and thin elastic fibres respectively.

Within the ILM, the frequently occurring features (dense elastic network with complex structure, different size and shape of elastic fibres) are presented in Figure 4.6.

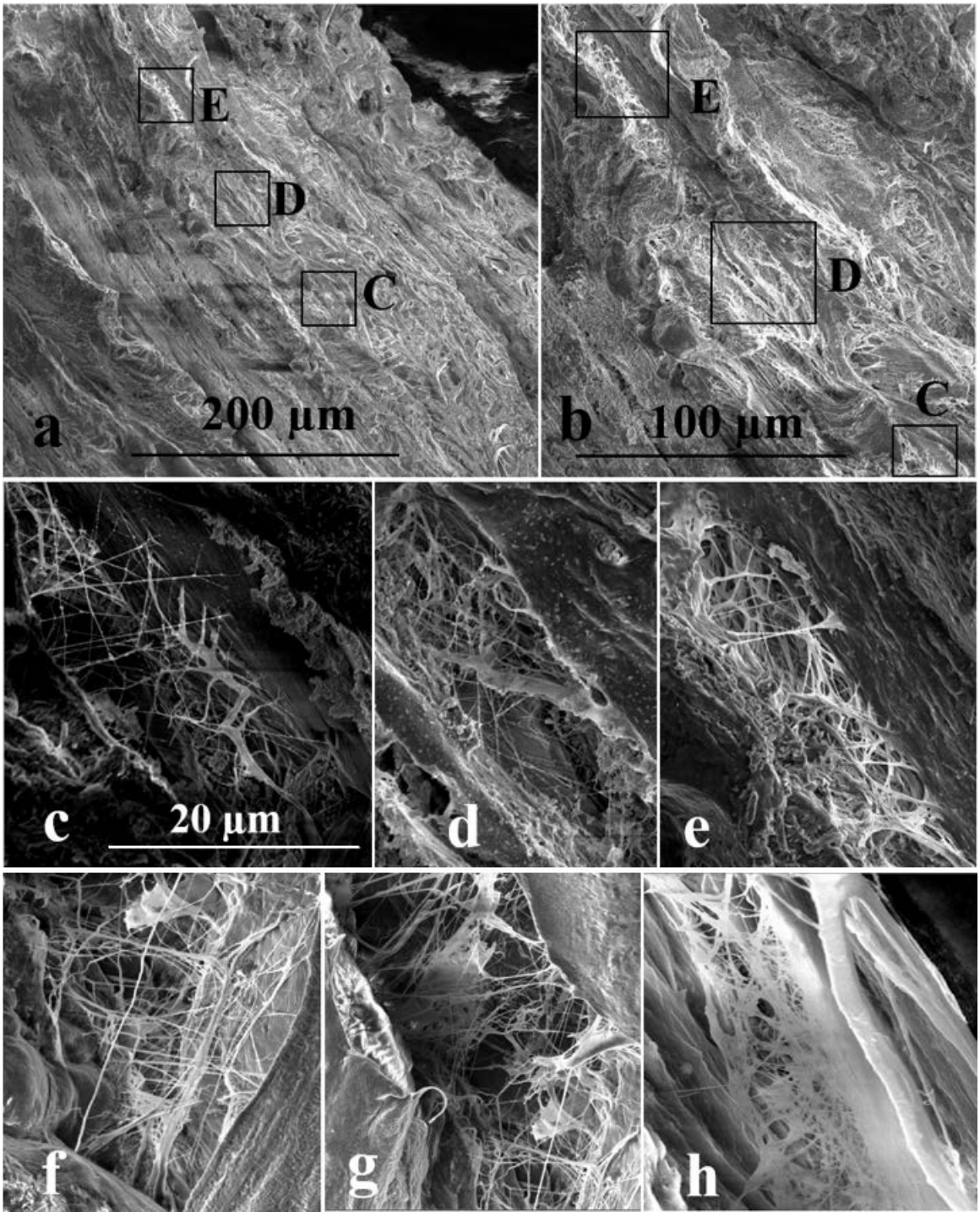

Figure 4.6 SEM images of the elastic network of the inter-lamellar matrix (ILM). (a, b) show lamellae of a digested sample under low magnification. The boxes denoted by C, D and E correspond to higher magnified c (partially), d and e images respectively showing three different regions of the ILM in the same sample (all having 20 µm scale bar). Three ILM regions from three different samples (f, g, h) are shown with the same magnification of 20 µm.

3.3. Quantitative analysis

Figure 4.7 shows the distribution and orientation of fibres in the ILM and intra-lamellar region of the AF relative to the TCD axis.

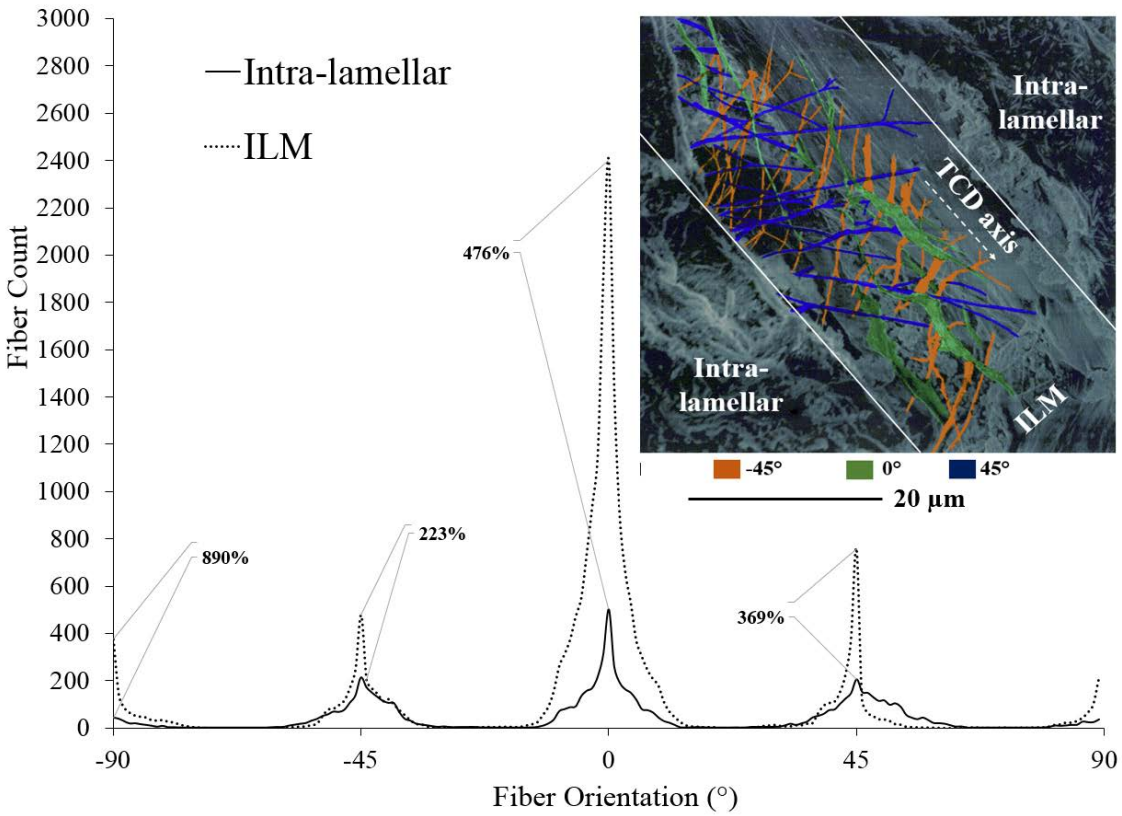

Figure 4.7 Elastic fibre orientation versus number of fibres in the ILM and intra-lamellar region for digested samples, relative to the TCD axis. Percentage values showing % increase of fibres with respect to the ILM.

For the second aim, and after analysing the distribution of fibre orientation, four and three different symmetrically organized angles of orientation were detected in both ILM and intra-lamellar regions respectively (~ ±90°, 45°, 0° and -45° for the ILM and 0 and ± 45° for the intra-lamellar region, Figure 4.7), with the majority of fibres orientated near 0°. The strong peaks for the ILM, compared to the intra-lamellar region, are consistent with the results indicating that the ILM elastic fibre density is higher than those of the intra-lamellar region. Table 4.1 shows the results corresponding to characterization of orientation for all four digested samples.

Table 4-1 Summary of ultrastructural "Fibre Orientation" relative to the TCD axis, between the ILM and intra-lamellar regions for each specimen.

Sample	Fibre Orientation (°) (Mean ± SD)	
	ILM	Intra-lamellar region
Specimen 1	7.69 ± 0.24	6.53 ± 0.28
Specimen 2	10.14 ± 0.36	8.41 ± 0.40
Specimen 3	6.23 ± 0.12	6.39 ± 0.24
Specimen 4	8.24 ± 0.32	7.36 ± 0.36
Mean ±SD	**8.07±1.6**	**6.62±0.5**

There was no statistically significant difference between the orientation of elastic fibres within the ILM and intra-lamellar regions (p=0.171).

4.6 Discussion

The results of this study were consistent with similar studies that were performed under light microscopic analysis [13, 45]. It was previously described that within the AF lamella, elastic fibres were parallel to each other, which was consistent with the findings from the present study. However, the parallel assembly of elastic fibres (Figure 4.3) formed a small part of the whole structural organization of elastic fibres in the AF lamellae regions. By removing the matrix and collagen fibres, it was demonstrated that large parallel fibres were connected to each other by very fine elastic fibres that formed a loose network. It is likely that this new interpretation of elastic fibre ultrastructure hasn't been previously reported due to the limitation of conventional staining techniques, light microscopy methods or the masking effect of the matrix.

A dense network including thick (diameter of approximately 1-2 µm) and thin (0.1 µm diameter) elastic fibres was seen in the ILM and this introduces a structural organization of elastic fibres in the AF that has not been previously described (Figures 4.5, 4.6). Within the ILM, elastic fibres have different ultrastructure characteristics that distinguish them

from other parts of the AF. This complex network, consisting of different size and shape fibres, differs to those located in the intra-lamellar region.

For both ILM and intra-lamellar regions, the dominant elastic fibre orientation was near 0°, with two symmetrical peaks of approximately ±45°. Additionally, in the ILM a peak at ±90° with a fibre count similar to those at ± 45° was found. In both regions, the dominant orientation was not significantly different, confirming that the majority of fibres were parallel to the TCD axis. In the intra-lamellar region, a small fraction of thin fibres are introduced that connect thicker parallel fibres to each other at an angle of 45°. In the ILM, the fraction of the fibres that were oriented at ±45° and ±90°, compared to non-oriented fibres (0°), was increased

This observation was consistent with SEM images that revealed a dense network having a criss-cross structure. It appears that interconnecting elastic fibres in the ILM were not organized randomly as their angle of rotation was symmetrical. The corresponding results of the elastic fibre distribution of orientation measurement in the ILM and intra-lamellar region may be affected by the remnant of undigested matrix in those regions. In spite of careful considerations to minimize the effect of non-elastic component on measurement of elastic fibres orientation, by adjusting image properties (brightness, contrast, threshold …), the existence of undigested components obscured the underlying elastic fibres presents a limitation of the performed quantitative analysis. Based on our previous study describing the method for visualization of disc's annulus elastic fibres [97], it was mentioned that the overall sample preparation method may change the overall structural organization. After matrix digestion and removing collagen fibres, it was revealed that the elastic fibre principle angle of rotation was significantly larger by approximately 2°compared to the adjacent undigested sample. While this

difference was statistically significant, the magnitude was small and it is likely that large elastic fibres align approximately parallel with collagen fibres, particularly when under load. Our previous study showed that in spite of the effectiveness of the method on visualization of AF elastic fibres, identification of collagen and elastic fibres using SEM images and possible shrinkage of samples during sample preparation (digestion and drying) need to be considered for further analysis [97]. The best way to identify elastic fibres in SEM images is their physical appearance and size. As described before, collagen fibres present as wavy tape- or cord-shape with a width (diameter) of 1-20 µm, approximately. Micro-fibrils of diameter 30-100 nm are usually observed as a delicate meshwork. Elastic fibres are about 0.2-1.5 µm in diameter, and are generally straight or twisted strands that sometimes branch to form a course network [69, 97].

The findings presented reveal a well-organized elastic fibre network with a complex ultrastructure that spreads across the ILM. The organization of the elastic network in the ILM may play a significant role in distributing shear and tensile stresses uniformly through the AF, and also provide a mechanism for energy absorption during loading [94]. Structurally, it seems that a continous network of elastic fibres could provide disc structural integrity via connecting the AF lamellae together. The density, fibre orientation and complexity of this complex network in the ILM is different from those within the intra-lamella space.

Previous studies on the disc elastic fibre organization used different light microscopy imaging techniques, and weren't able to present their structural organization details. Therefore gaining further insights into the structural analysis was a challenge in fine scale light microscopic studies. A detailed understanding of the ILM ultrastructure is crucial to elucidate the role of the ILM's structure on the structural integrity of the adjacent lamellae. The present study used extracellular matrix partial digestion to

address significant gaps in understanding of disc microstructure and will contribute to multidisciplinary ultrastructure-function studies.

While the present study used only four discs in this study, several samples from these discs were investigated by SEM imaging. In those samples, significant differences in fibre orientation between the ILM and intra-lamellar region were found. Further study will be required using a larger number of specimens in different disc regions (e.g., anterior, lateral and posterolateral) to investigate the ultrastructure of elastic fibres. The application of alkali digestion to visualize disc elastic fibres has not been previously reported. Therefore, further studies investigating the effect of alkali digestion on AF elastic fibres properties are important (Appendix B).

Also as variations in annular structure between species occur with age, degeneration and disease, the methods from this study may be used for further investigations [80]. Imaging of the elastic fibre network using two different cutting planes (transverse and oblique) and serial adjacent cuts would be helpful for visualization of their 3D characteristics as well as to quantify the elastic fibre spatial orientation and their contribution to AF integrity and mechanical properties.

4.7 Conclusion

The structure of the elastic fibre network in the ILM is considerably more complex in comparison with the adjacent intra-lamellar region. A well-organized network of thick and thin elastic fibres form a network across the ILM and appear to connect two adjacent lamellae. The results presented reveal a well-organized elastic fibre network with a complex ultrastructure that spreads across the ILM, which are composed of elastic fibres having different diameters. The density and distribution of fibre orientation, together with the complexity of this network in the ILM is different to those

within the intra-lamella region. Further study is required to determine the mechanical properties of this network within the ILM.

5 Chapter 5 - Study 3: Ultrastructural organization of elastic fibres in the partition boundaries of the annulus fibrosus within the intervertebral disc

In the previous chapters (Chapters 3 and 4, Studies 2 and 3) a novel technique for visualization of elastic fibres across the AF was presented and their ultrastructural organization in intra- and inter-lamellar regions of the AF was compared. Using the same technique in those studies, the ultrastructural organization of elastic fibres in the partition boundaries (PBs), which are located between adjacent collagen bundles, is presented in this chapter. For the first time it was revealed that a continuous network of elastic fibres may provide disc integrity by connecting adjacent collagen bundles together, while branching from the ILM. More-accurate multiscale computational models of the disc can be developed using the data from this study, which will provide new insights on the mechanics of the disc.

The study presented in this chapter has been published in the following journal and conference proceedings:

Tavakoli J, Costi JJ. Ultrastructural organization of elastic fibres in the partition boundaries of the annulus fibrosus within the intervertebral disc, Acta Biomaterialia (I.F. = 6.319), 68, 67-77, 2018.

Tavakoli J, Costi JJ. Ultrastructural organization of the elastic network within the disc annulus fibrosus. Proceedings of the 29th Annual Meeting of the International Society of Biomechanics (ISB), Brisbane, Australia, July 2017.

Tavakoli J, Elliott DM, Costi JJ. Visualization of the Elastic Network of the Annulus Fibrosus , Proceedings of the 63rd Annual Meeting of the Orthopaedic Research Society (ORS), San Diego, USA, March 2017.

5.1 Abstract

The relationship between elastic fibre disorders and disc degeneration, aging and progression of spine deformity have been discussed in a small number of studies. However, the clinical relevance of elastic fibres in the annulus fibrosus (AF) of the disc is poorly understood. Ultrastructural visualization of elastic fibres is an important step towards understanding their structure-function relationship. In our previous studies, a novel technique for visualization of elastic fibres across the AF was presented and their ultrastructural organization in intra- and inter-lamellar regions was compared. Using the same novel technique in the present study, the ultrastructural organization of elastic fibres in the partition boundaries (PBs), which are located between adjacent collagen bundles, is presented for the first time. Visualization of elastic fibres in the PBs in control and partially digested (digested) samples was compared, and their orientation in two different cutting planes (transverse and oblique) were discussed. The ultrastructural analysis revealed that elastic fibres in PBs were a well-organized dense and complex network having different size and shape. Adjacent collagen bundles in a cross section (CS) lamella appear to be connected to each other, where elastic fibres in the PBs were merged in parallel or penetrated into the collagen bundles. There was no significant difference in directional coherency coefficient of elastic fibres between the two different cutting planes ($p = 0.35$). The present study revealed that a continuous network of elastic fibres may provide disc integrity by connecting adjacent bundles of CS lamellae together. Compared to our previous studies, the density of the elastic fibre network in PBs was lower, and fibre orientation was similar to the intra-lamellar space and inter-lamellar matrix.

5.2 Introduction

Elastic fibres are critical components of the extracellular matrix in biological structures, whose defects affect tissue elasticity and contribute to pathologies (e.g. cutis laxa, Williams-Beuren syndrome, scoliotic discs, etc.) degeneration and aging [32, 84, 87, 106]. The role of elastic fibres in the intervertebral disc is not clearly understood, although few studies revealed their contribution to radial integrity of the annulus fibrosus (AF) [15, 24, 85]. On the other hand, the relationship between elastic fibre disorders and disc degeneration suggests that more structure-function studies need to be performed to identify the impact of elastic fibres on disc mechanical properties [107-111]. A clinical observation found that compared to healthy discs, scoliotic discs have a disorganized and sparse elastic network, which could contribute to the progression of spine deformity [107]. It was demonstrated that with increasing age and disc degeneration, elastic fibre morphology appears to become more disorganized [108]. In addition, an increase of metalloproteinase level in scoliotic discs leads to elastin degradation [109, 110] as well as activation of elastase enzymes in degenerated discs [111].

Early efforts to establish the presence of elastic fibres as an organizational constituent of the disc using Scanning Electron Microscopy (SEM) were unsuccessful [112, 113]; however, they were observed by Buckwalter et al. in 1976 [89]. Several other investigators confirmed the presence of elastic fibres in the disc; however, their observations did not reveal elastic fibre ultrastructure [34, 82, 114, 115]. Based on low elastin content [38, 58, 116], and its irregular distribution across the disc, elastic fibres were thought to play no role in disc function [70]. However, a light microscopy study revealed that there was an abundant elastic fibre network distributed across all regions of the disc [45]. Elastic fibres were found to be comprised of a central elastin core

component integrated with the surrounding fibrillin framework [117], after which it was revealed that both elastin and fibrillin were extensively distributed across the AF [13]. This understanding has been developed through other studies to highlight the potential role of elastic fibres on disc structural and mechanical properties [11, 16, 38, 70, 118]. Early microstructural investigation indicated that elastic fibres have different oblique and longitudinal orientations within the AF [90] and are more dense in the outer compared to the inner AF [119]. Dissimilarity of the AF elastic fibre density in circumferential and radial locations was also explained in a microscopic study [16]. At the light microscopy scale (20× magnification), it was discovered that the long elastic fibres of the nucleus pulposus extend radially towards the AF, while some were oriented towards the endplates [45, 70]. Also it was found that elastic fibres of the AF appeared to be aligned parallel to the collagen fibres within the lamellae [11, 13, 45] and were more dense and of complex arrangement in the inter-lamellar matrix (ILM) [9, 11, 13, 45]. A study showed that elastic fibres enhanced the AF lamellae interconnectivity, while surrounding collagen bundles [88]. This study revealed that collagen bundles in a cross section (CS) lamella are subdivided by a dense structure of elastic fibres, a region identified as a partition boundary (PB), which may divide the entire lamella or appears as incomplete dividers [88]. The PBs were more likely to be seen in CS, rather than in-plane lamellae (IP) [88]. Identification of CS and IP lamellae depends on the cutting plane and has been defined elsewhere [27, 48]. Briefly, collagen bundles in oblique sections are parallel in an IP lamellae, and perpendicular to the cutting plane in a CS lamella.

Although these light microscopic studies showed that elastic fibres were found throughout the AF within three different regions including intra-lamellar, ILM and PB, none were able to provide the fine-scale and ultra-architectural details of the elastic

fibre network. On the other hand, since all fibrous elements including collagen and elastic fibres, are intermingled with each other and masked by the matrix, their ultra-structural organization was not possible to be visualised under low (light microscopic level), nor at higher magnifications (SEM).

Visualization of the AF elastic fibre ultrastructural organization in intra-lamellar region and the ILM has recently been achieved using a novel technique incorporating sodium hydroxide-sonication digestion followed by heat treatment [97]. However, less is known about elastic fibres ultrastructural organization within the PBs. It was demonstrated that large parallel elastic fibres were connected to each other by very fine elastic fibres and form a loose network within the intra-lamellar region. An ultrastructural study of elastic fibres revealed that a dense and complex network, including thick (approximately 1-2 µm in diameter) and thin (0.1 µm diameter) elastic fibres, exist in the ILM [120]. It was demonstrated that interconnecting elastic fibres in the ILM were not organized randomly, which supports the hypothesis that they may be involved in distributing stresses through the AF, while enhancing its structural integrity. Based on the literature review, there is evidence that elastic fibres, having a complex pattern of interconnectivity, exist in three main regions of the AF (Table 5.1).

Investigation of the ultrastructural organization of elastic fibres within the PBs will help to improve the knowledge of the AF elastic fibre interconnectivity within the ILM, PB and intra-lamellar regions. Understanding the ultrastructural organization of elastic fibres in PBs will support further studies on the AF structure-function properties, the role of elastic fibres on herniation, and their impact on mechanical behaviour of the disc. In addition, elastic fibre ultrastructural analysis can be utilized to develop a 3D map of

disc elastic fibre distribution to design tissue engineered scaffolds for AF repair and replacement.

Table 5-1 Three main regions where elastic fibre structural characteristics were described under low (light microscopy) and high (SEM) magnifications.

Region	Location	Structural characteristics
Intra-lamellar	Within the lamella	*Low magnification:* Long elastic fibres are in parallel to the collagen fibres [15, 38, 45, 107]. *High magnification:* A loose network (not randomly distributed) of elastic fibres was observed in the intra-lamellar region, which are comprised of thick fibres aligned parallel to the collagen fibres (0.3-0.5 µm diameter), and very fine interconnecting fibres of less than 0.3 µm diameter [120].
Inter-lamellar (ILM)	Between adjacent lamellae	*Low magnification:* A complex and dense structure was present in the ILM [9, 13, 16, 45, 107]. *High magnification:* A dense network including thick (diameter of 1-2 µm) and thin (0.1 µm diameter) elastic fibres was seen in the ILM. This complex network was not randomly distributed, consisting of different size and shape fibres, differs to those located in the intra-lamellar region [120].
Partition Boundaries (PB)	Between collagen bundles	*Low magnification:* Elastic fibres are the main component of the PB [88]. *High magnification:* No study was performed.

Therefore, the aims of this study were: first to present an ultra-structural analysis of the elastic fibre network in the PBs of the AF using Scanning Electron Microscopy (SEM); and second, to investigate whether the elastic fibre orientation and distribution within the PBs change when viewed from two different cutting planes.

5.3 Materials and methods

5.3.1 Sample preparation

Samples for this study were prepared (Figures 5.1a, 5.a-1 and 5.a-2) similar to the method that was described in previous chapter (Chapter 4, Study 3). However, nine sample were used and the cutting planes were identified at two angles of approximately

0° and 30° to the transverse plane (Figures 5.1b and 5.1c). From each of the eighteen tissue sections, samples from adjacent sections (30 µm thickness) were cut using a cryostat microtome (Leica Biosystems, CM3050) in oblique (Figure 5.1d) and transverse (Figure 5.1e) cutting angles. Control (undigested) and digested samples were prepared for elastic fibre visualization through scanning electron microscopy [97, 120]. The digestion of samples and scanning electron microscopy (SEM) performed similar to the previously described method.

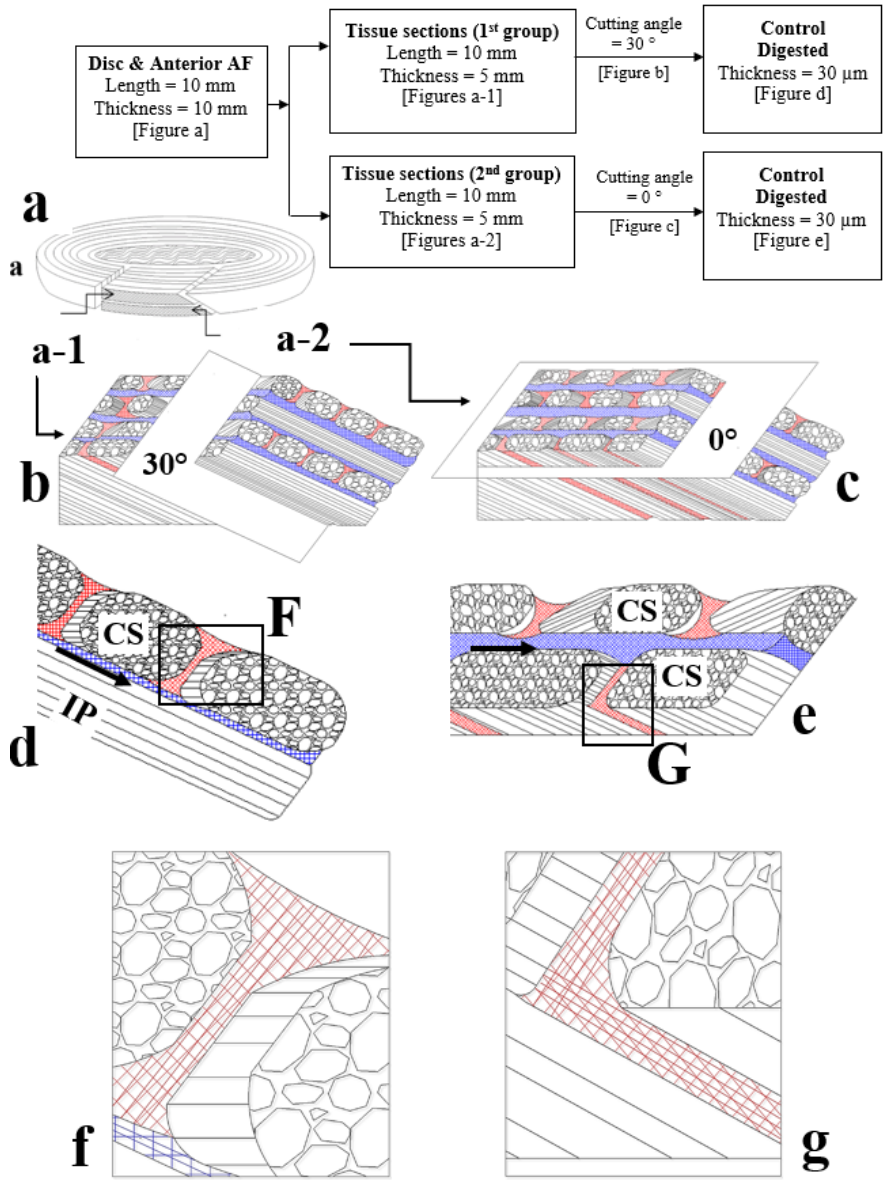

Figure 5.1 Sample preparation methodology and schematic drawing. Anterior AF strips (10 mm in length) were separated from the disc and were cut into half, transversally (a). Frozen sections prepared at two angles of approximately 30° (oblique cut, b) and 0° (transverse cut, c) relative to the transverse axis.

Zoomed-in schematic drawings of two adjacent lamellae of samples that were cut by microtome to a thickness of 30 µm along the cutting planes are shown (d, e) and can be utilized to identify different anatomic locations of PBs (red shaded lines) relative to the ILM (blue). F and G boxes represent magnified regions as shown in f and g images, respectively, to identify the orientation of elastic fibres in the PBs. PBs connect collagen bundles together, while the ILM provides cohesion strength between adjacent lamellae (d, e). The TCD axis is shown at both transverse and oblique cutting planes by black arrows (d, e).

5.3.2 Quantitative analysis

SEMs of elastic network in the PBs were used to assess the degree of elastic fibre alignment relative to the tangent to the circumferential direction (TCD plane), which passes vertically through the ILM (Figures 5.1d, 5.1e and 5.7-b), using an open source software (ImageJ) [79]. All SEM images were manually edited to remove non-elastin components, using a graphics editor software (paint.NET for Microsoft Windows, v3.5.10, Rick Brewster, dotPDN LLC) utilizing Magic wand editing option and selecting a 15% tolerance. The manual editing technique and its effect on coherency coefficient values was evaluated by conducting an intra-rater repeatability analysis. SEM images were randomly selected from five out of the nine specimens from each of the oblique and transverse samples. The manual editing technique was repeated 3 times each, giving a total of 30 sample images. The OrientationJ plugin was used to measure the directional coherency coefficient of elastic fibres in the input 8 bit images, utilizing a pre-filter option with the Laplacian of Gaussian (Sigma) equal to zero. Fibre count-orientation analysis was conducted in the binary images with Cubic Spline Gradient selected as the structural tensor for fitting the data [121].

5.3.3 Statistical analysis

An independent samples t-test was conducted (IBM SPSS Statistics for Windows, Version 22.0. Armonk, NY: IBM Corp.), having a test variable of directional coherency coefficient of elastic fibres within the PBs between two different cutting plane angles (transverse and oblique) using an alpha of 0.05. To assess intra-rater repeatability of the manual image editing technique for measuring directional coherency coefficients, an Intra-class

Correlation Coefficient (ICC) for reliability was conducted, as described by Koo and Li [122].

5.4 Results

5.4.1 Comparing control and digested samples

To clarify the effect of digestion, a comparison between control and digested samples was performed. Figure 5.2 presents the SEM images of the PB at different magnifications for both control (Figures 5.2a-b) and digested samples in oblique (Figures 5.2c-d) and transverse (Figures 5.2e-f) cutting planes. The PBs, located between collagen bundles, divide the AF collagenous compartment (collagen bundles) irregularly and alternately, while running through the lamella. As shown in Figures 5.2a and 5.2b, these PB structures (some denoted by stars) can be distinguished more readily in the CS lamellae containing collagen bundle cross sections rather than those having parallel collagen fibres (IP lamellae). However, identification of their ultrastructural organization wasn't possible at high and low magnifications for control samples using SEM imaging (Figures 5.2a-b) since all intermingled fibres were obscured by the matrix. At 100 µm scale bar (1702×) in a control sample (Figure 5.2b), almost parallel traversing PBs in the CS lamellae seemed to separate collagen bundle compartments.

As shown in Figures 5.2c-f, removing proteoglycans together with a significant decrease in matrix masking effect led to a better visualization of the PBs at both cutting angles, oblique (Figures 5.2c-d) and parallel (Figures 5.2e-f) to the transverse plane. Gradual removal of matrix that occurred as a result of digestion, revealed a progressive improvement in visualization of fibres within the CS compared to the IP lamellae in all samples. It appeared that a CS lamella experienced faster digestion compared to the IP, where tightly packed parallel collagen fibres were presented. Following the digestion of the AF matrix, organization of collagen bundles in a CS lamellae was observed in an

oblique cutting plane (30°). In a CS lamella, collagen bundles that were covered by remnants of undigested matrix were perpendicular to the sample surface (a typical bundle cross section denoted by dashed lines in figure 5.2d) whose collage fibres ran inward (denoted by arrow).

Digestion of adjacent lamellae in a transverse cutting plane (0°) facilitated the organization of PBs to be visualized (denoted by stars in Figures 5.2f). Compared to the control (undigested) samples digestion clarified how PBs might run between adjacent lamellae, while connecting them together (Figure 5.2f). Referring to control samples, it was hard to see whether collagen bundles were divided completely by PBs. However, in digested samples (Figures 5.2e and 5.f), it was apparent that the size, orientation and pattern of PBs were irregular and they frequently divided the entire CS lamella or connected to other PBs, while linking adjacent lamellae. The compartmentalization of the entire lamella seems to result in creating a fenestration across all adjacent CS lamellae. Large fenestrae, shown by arrow heads in Figure 5.2f, were introduced after orthogonal collagen bundles were removed following digestion.

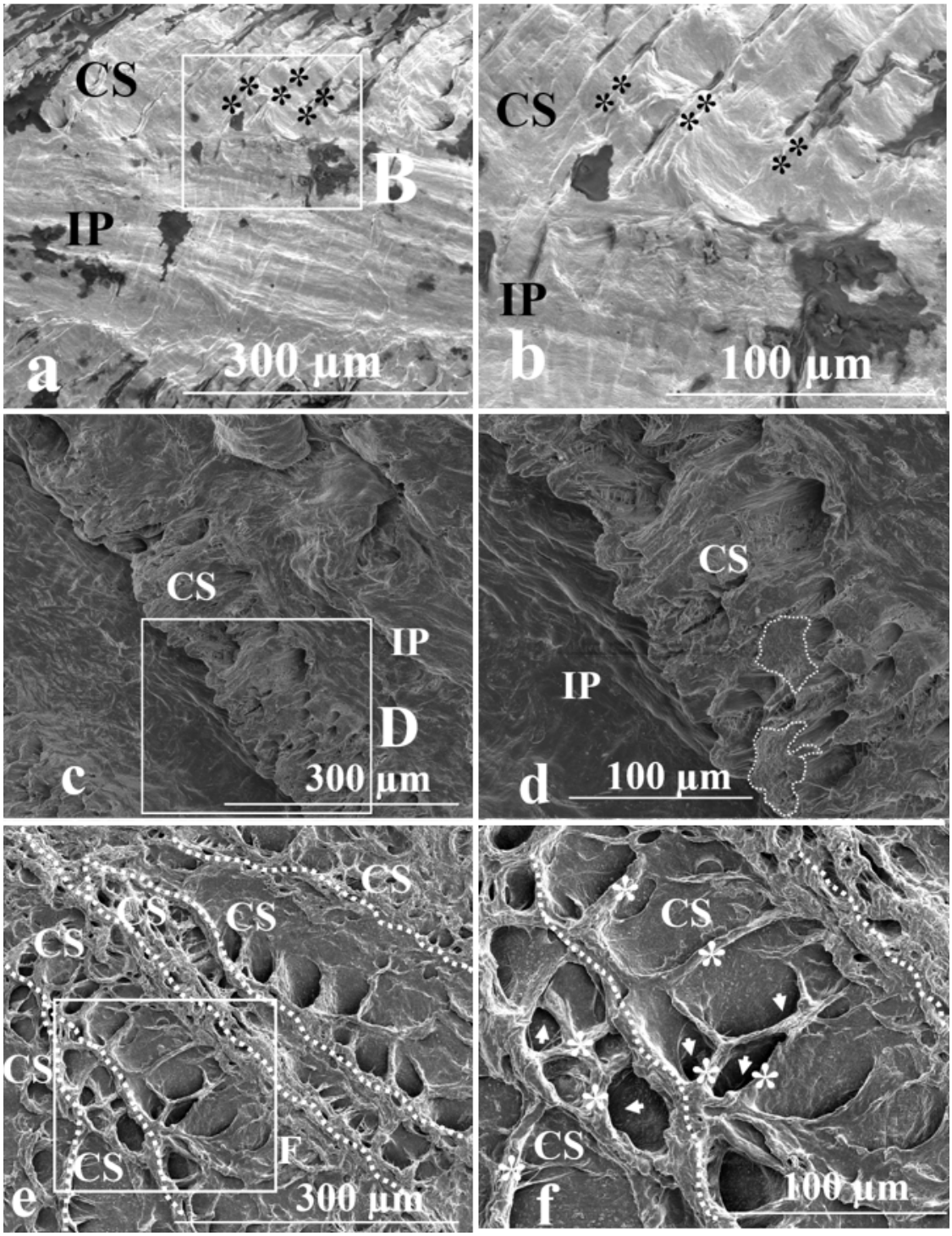

Figure 5.2 Comparison between control and digested samples. SEM images of the PBs (some of which are denoted by stars) organization under different magnifications for both control in oblique plane (a 600×, b 1702×), digested (c 492×,d 1126×) and additional digestion (e 606×,f 1336×) samples in two different oblique (c, d) and transverse (e, f) cutting planes. Images a, c and e were obtained from different samples. SEM images demonstrate the different organization of PBs in CS and IP lamellae. White dashed lines show collagen bundle cross sections in a CS lamella (d) and boundaries between adjacent CS lamellae (e, f), respectively. B (a), D (c) and F (e) boxes represent magnified regions as shown in b, d and f images, respectively. Arrow heads (f) indicate fenestrae that were created after digestion and removal of matrix.

5.4.2 Partition boundaries ultrastructure in the transverse plane (0°)

Figure 5.3 shows SEM images of elastic fibres ultrastructural organization of a PB in a digested sample, spanning six magnification ranges from 160× to 7559×. Elastic fibres within the PB formed a complex and dense network comprised of thick (approximate diameter 1-2 µm) and thin (approximately 0.1 µm in diameter) fibres (Figure 5.3d-f). Thick elastic fibres within the network were parallel to each other and made an angle relative to the transverse plane, while connecting adjacent lamellae (Figure 5.3f). It appeared that collagen bundles were enclosed by this network of elastic fibres (Figure 5.3d, e).

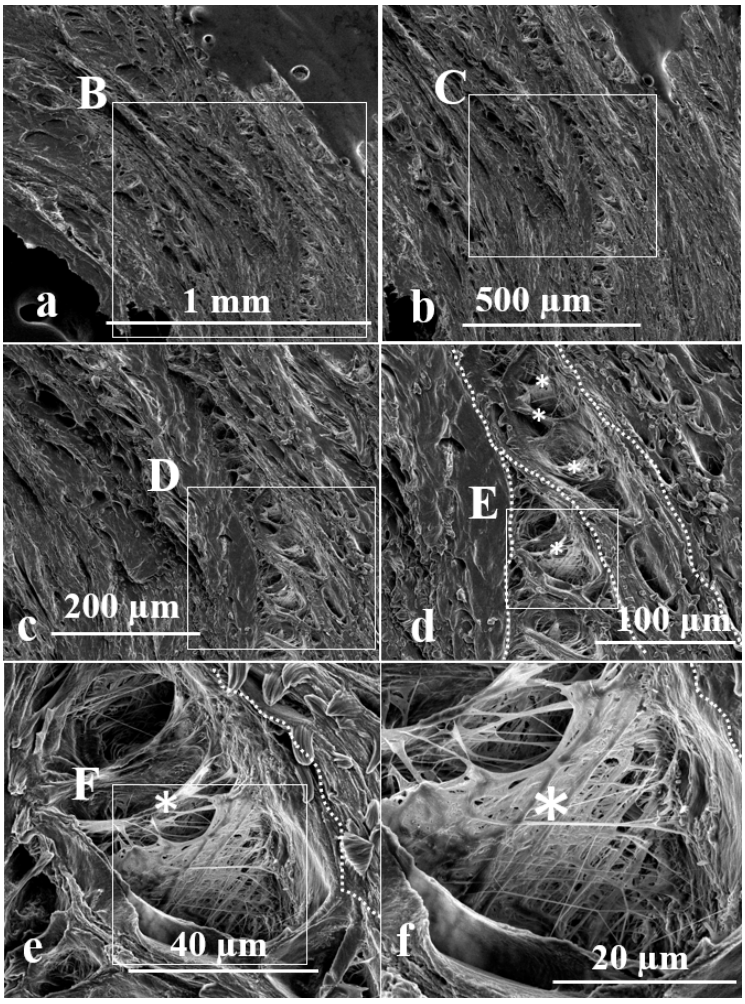

Figure 5.3 Ultra-structural organization of PB elastic fibres under different magnifications in the transverse (0°) cutting plane. Thick and thin fibres create a network structure. The white boxes denoted by B, C, D, E and F correspond to higher magnified b, c, d, e and f images, respectively. Magnification factors of SEM

images in Figures "a" to "f" were 160×, 275×, 600×, 1166×, 3876× and 7559×, respectively. White dashed lines and stars show boundaries between adjacent CS lamellae and PBs, respectively.

Within the PBs in the transverse plane, the frequently occurring features (dense elastic network with complex structure, different size and shape of elastic fibres) are presented in Figure 5.4. The dense elastic network was visible after digestion in all samples. The empty spaces, located between the PBs, were collagen bundle cross sections that were removed after digestion.

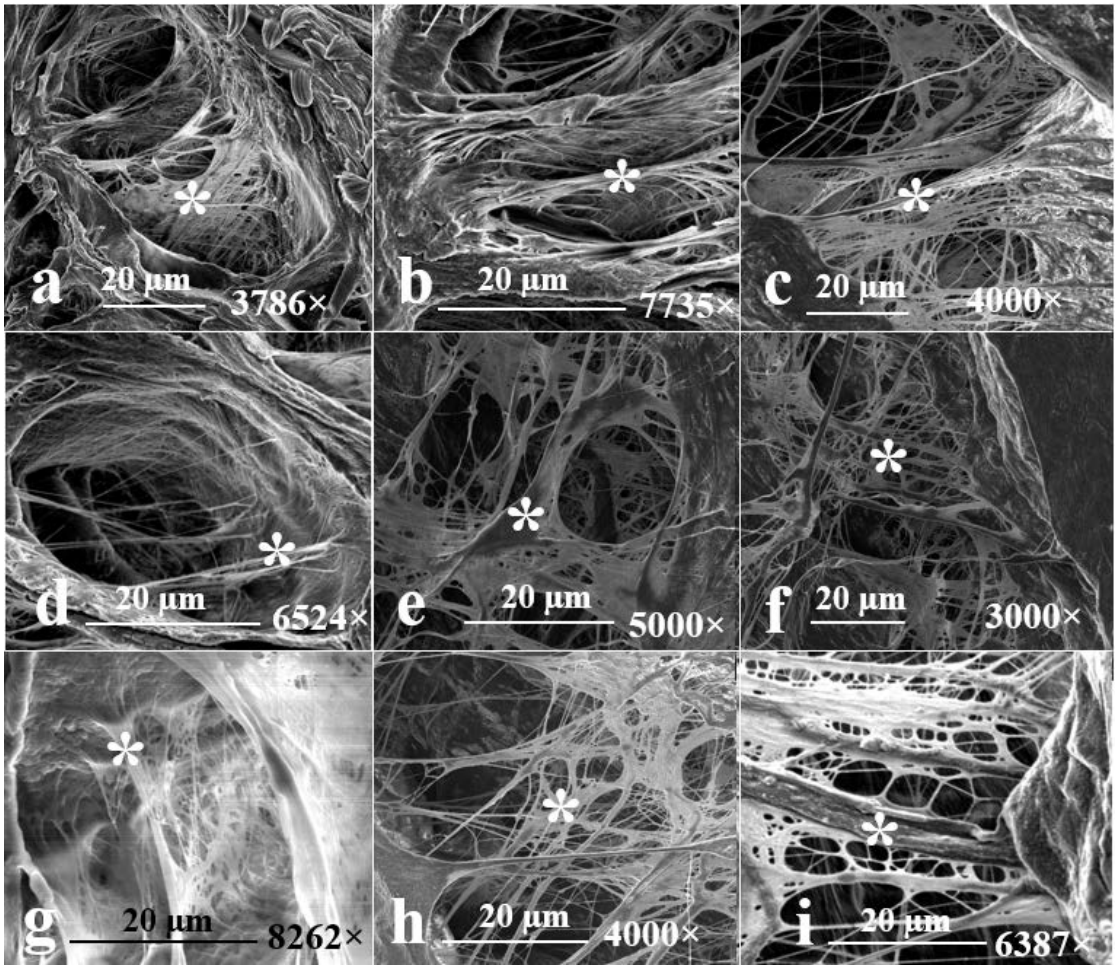

Figure 5.4 Frequently occurring features of a network comprised of thin and thick elastic fibres across all nine digested samples (transverse plane (0°)) at 20 µm scale bar. Partition boundaries are denoted by stars in all figures.

5.4.3 Partition boundaries ultrastructure in the oblique plane (30°)

Figure 5.5 shows SEM images of elastic fibre organization in a selected PB from an oblique cutting plane spanning six magnifications ranging 471× to 14848× (Figures 5.5a-f) and at four different viewing angles of rotation under 14848× magnification (Figures

5.5g-j). Elastic fibres within the PB formed a complex network and seemed to connect collagen bundles in a CS lamellae. Under higher magnification (Figures 5.5e-f), the ultrastructural organization of elastic fibres (denoted by white arrow heads, Figure 5.5f) in a PB (that was located between two adjacent collagen bundles) was apparent. For better clarification the cross section of two adjacent collagen bundles was identified by white dashed lines and denoted by stars. In Figures 5.5e-f, the orientation of collagen fibres from adjacent bundles was identified by white arrows, while being interconnected by elastic fibres in the PB.

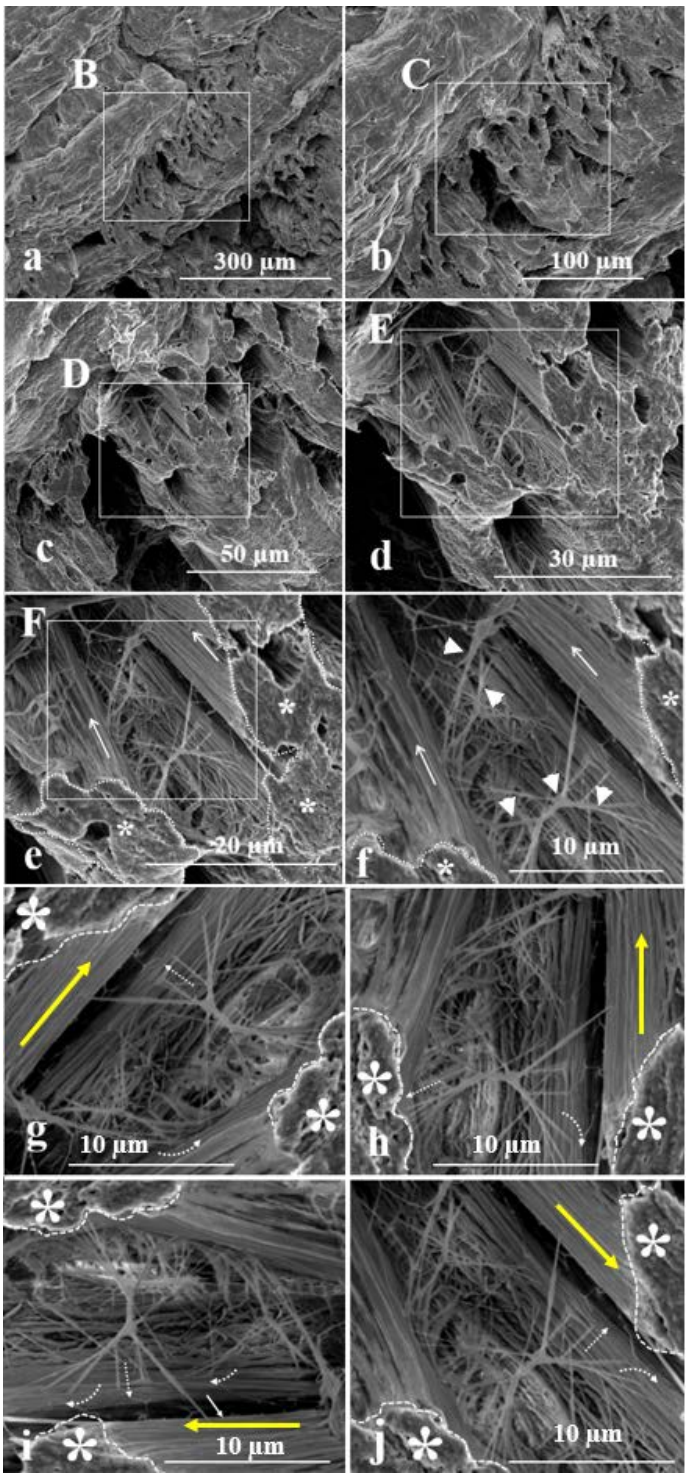

Figure 5.5 SEM images of a cross section (CS) lamella at an oblique cutting plane reveal the elastic fibre ultra-structural organization in one sample under different magnifications (a-f, having magnification factor of 471×, 1126×, 2356×, 5352×, 8534×, 14848×, respectively). The white boxes denoted by B, C, D, E and F correspond to higher magnified b, c, d, e and f images, respectively. Elastic fibres (denoted by white arrow heads) between two adjacent collagen bundles, whose cross sections were surrounded by white dashed lines and denoted by stars (e-f), are shown. Collagen fibres bundles are denoted by white arrows. The elastic network in the same PB (at an oblique cutting plane) shown (yellow arrows) at four different viewing angles of rotation (g-j) under same magnification (14848×). With dashed curved and straight arrows indicate two different possibilities that exist at collagen bundles- PB boundaries. Some elastic fibres merge into the adjacent collagen bundles to be oriented in parallel to the collagen fibres (denoted by curved arrows). While other elastic fibres seem to penetrate directly into the adjacent bundles (denoted by straight arrows).

Four different viewing angles of rotation of a high magnified PB are shown in Figures 5.5g-j. At the PB-adjacent collagen bundle boundaries, where elastic fibres seem to penetrate into the adjacent bundles, two different kinds of anchoring were observed. Some elastic fibres merged into the adjacent collagen bundles to be oriented in parallel to the collagen fibres (denoted by curved arrows). While other elastic fibres seemed to penetrate directly into the adjacent bundles (denoted by straight arrows).

Similar to the transverse cutting plane, a dense network of thick and thin interconnecting elastic fibres (1.5 to 0.2 µm diameter, respectively) was observed as a key structural feature of PB in the oblique cutting plane across all digested samples at 30° (Figures 5.6a-i).

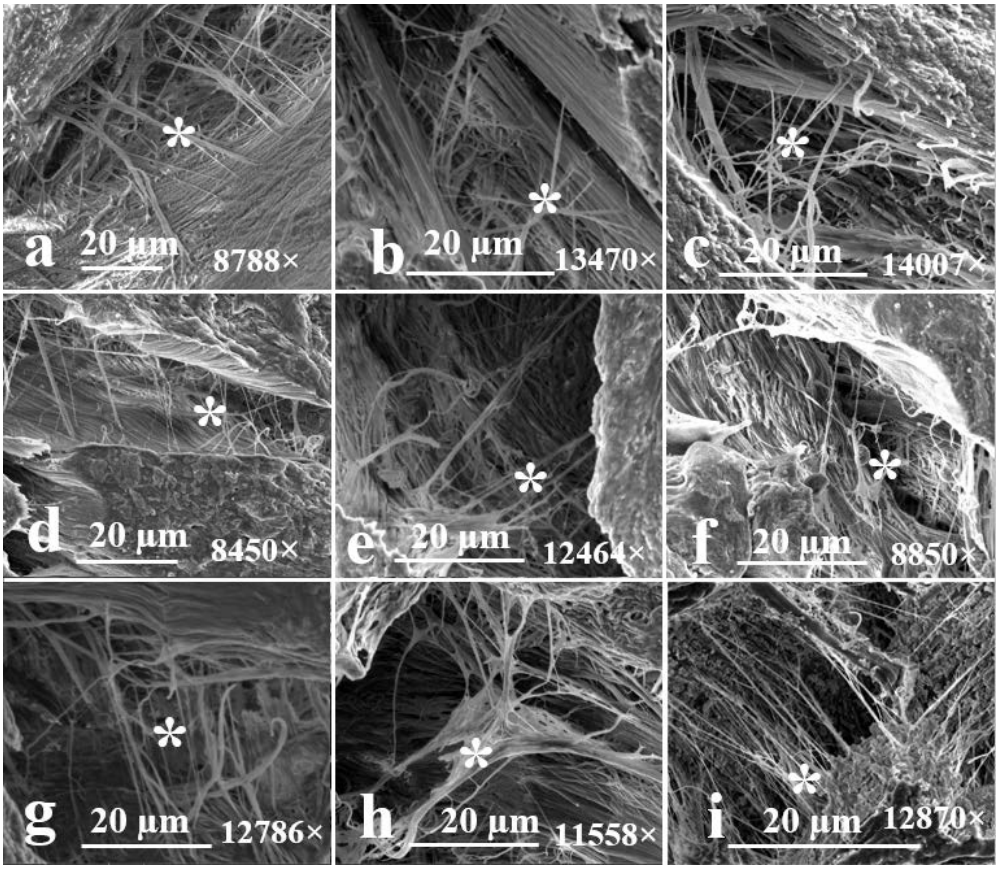

Figure 5.6 Frequently occurring features of the elastic fibre network (denoted by stars), including thick and thin fibres across all nine digested samples (oblique cutting plane).

5.4.4 Quantitative analysis

The quantitative analyses (Figures 5.7a and 5.7c) show the directional coherency coefficient and the organization of elastic fibres in the PB of digested samples at two different cutting plane angles (transverse and oblique). The directional coherency coefficient and the orientation of elastic fibres was measured relative to the TCD plane (Figure 5.7b).

Mean (95%CI) values for directional coherency coefficients of elastic fibres were equal to 0.306 (0.04) and 0.20 (0.03) in the transverse and oblique cutting planes, respectively (Figure 5.7a). A coherency coefficient close to 1 indicates a strongly coherent orientation of the local fibres, and a value of zero denotes no preferential orientation. There was no significant difference in directional coherency coefficient of elastic fibres between the two different cutting planes ($p = 0.35$). Fibre count-orientation analysis detected principal symmetrically organized angles of rotation (±45°, 0° and ±90°) in both cutting planes (figure 5.7c).

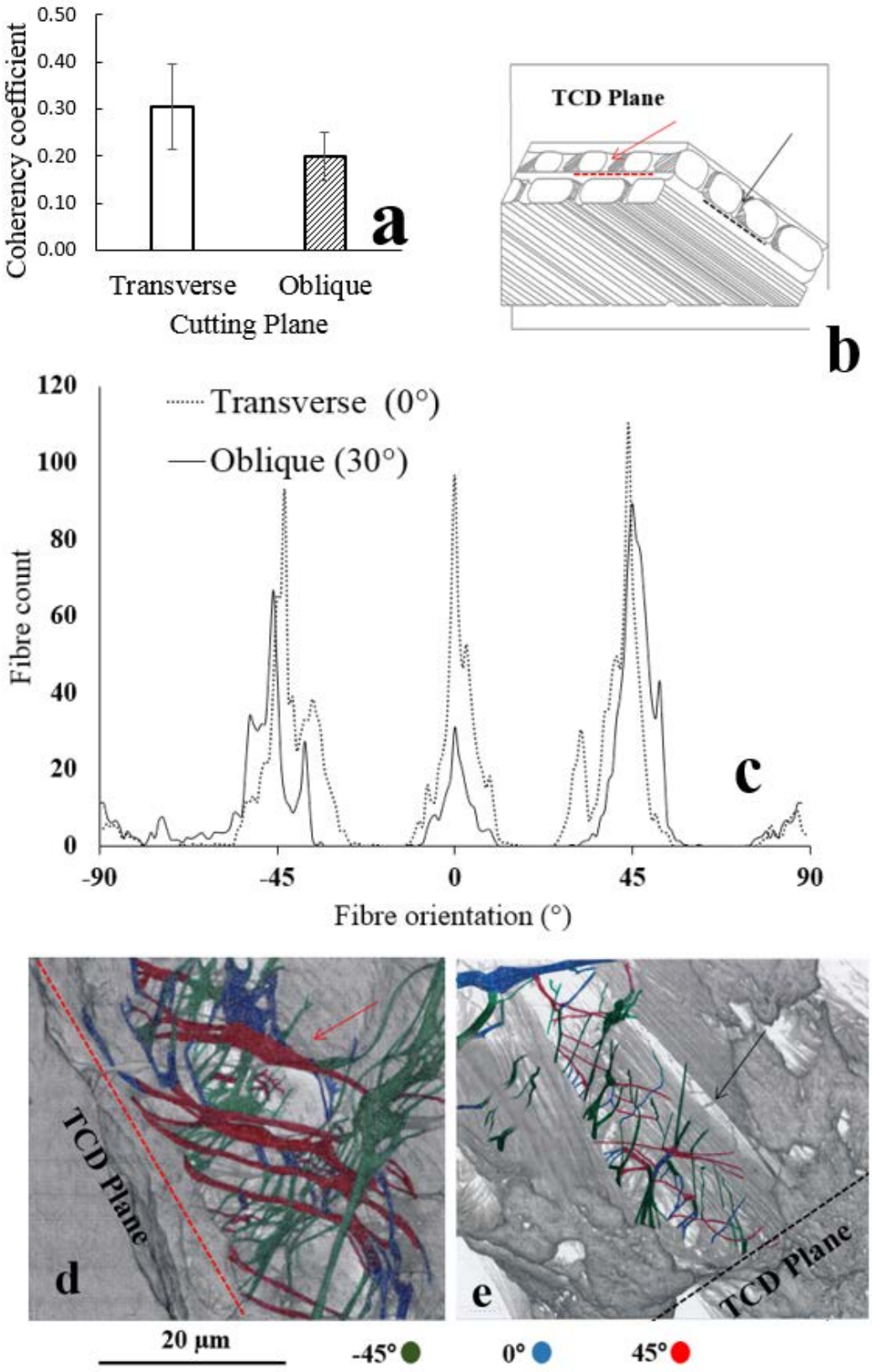

Figure 5.7 Directional coherency coefficient of elastic fibres in PBs reported as Mean (95% CI) for all digested samples in two different cutting planes (a). Fibre directional coherency coefficient and their orientation were measured relative to the TCD plane (b). Three principal angles of rotation ±45° and 0° (c) were coloured in green, red and blue in inverted images of two PBs at two different cutting angles of 0° (d) and 30° (e), respectively. Red and black arrows show corresponding locations of the PBs indicated in the schematic drawing (b) and SEM images (d-e).

A geometric 3D presentation of PBs was obtainable based on SEM images in both transverse and oblique cutting planes (Figure 5.8).

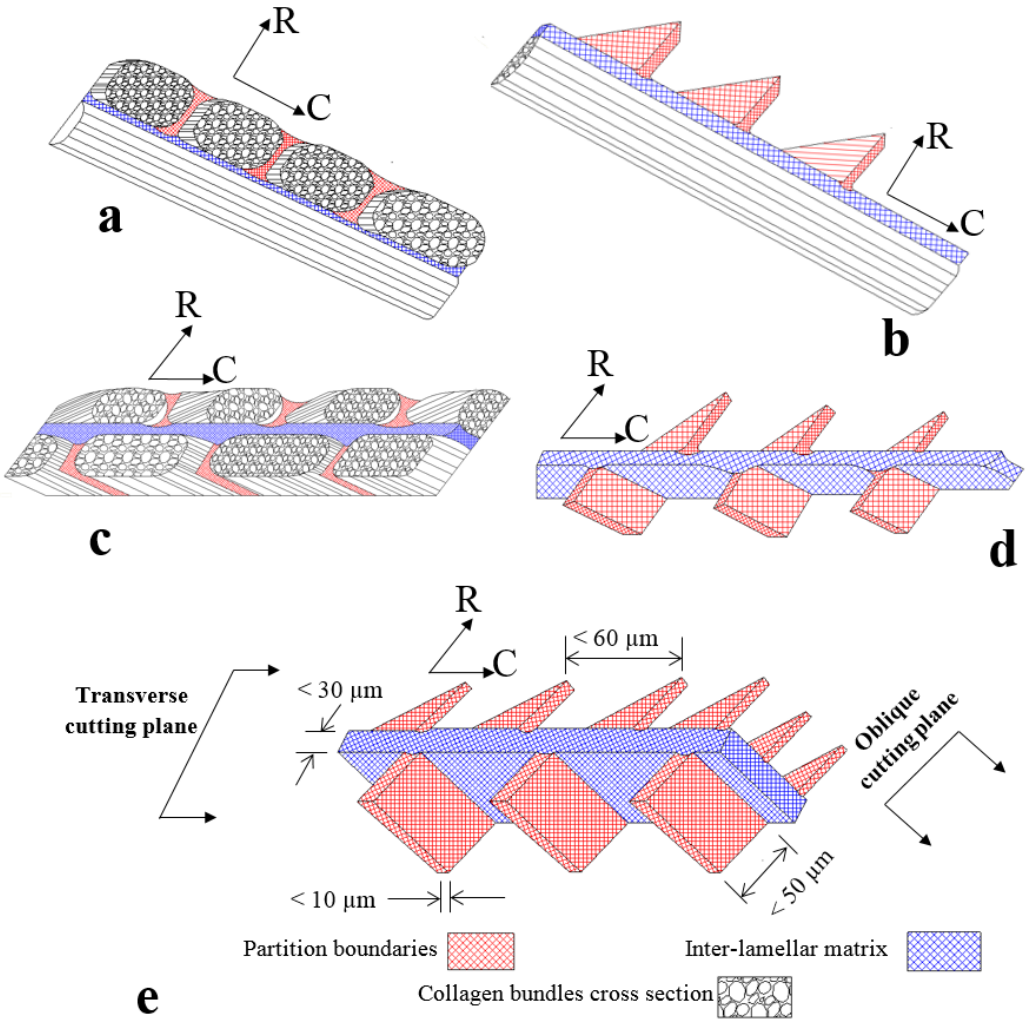

Figure 5.8 Schematic 3D presentation of PBs in an oblique (a, b) and a transverse cutting plane (c, d) is shown. PBs are in red and the ILM identified in blue. Figures b and c show schematic drawing of PBs after collagen bundles removal from the adjacent lamellae. Geometrical analysis of PBs is presented in panel e. Radial and circumferential directions were denoted by R and c, respectively.

PBs were less than 10 µm thick and their length in the radial direction was less than 50 µm for those PBs that don't completely divide CS lamellae. The length of a complete PB, which connects two adjacent ILM in radial direction, is approximately 120-150 µm. The distance between two adjacent PBs in a CS lamellae was measured as less than 60 µm, and the ILM thickness was less than 30 µm (Figure 5.8e).

5.5 Discussion

The current study was designed to identify the ultrastructural organization of elastic fibres in the PBs, which is an initial and important step toward identification of the mechanical role of elastic fibres in the disc. Referring to our previous studies, where the ultrastructural organization of elastic fibres within the ILM and intra-lamellar region were visualized, it was found that the distribution of elastic fibre orientation was similar in both intra- and inter-lamellar regions. The present study showed that the distribution of elastic fibre orientation was similar to the ILM and intra-lamellar regions. It seems that the organization of elastic fibres in all three regions are similar; however, their function may be different. The presence and arrangement of elastic fibres in PBs were described previously under light microscopy in both cross section (CS) and in-plane (IP) lamellae [88]; however, their ultra-structural organization has not been previously described. Using a technique to remove collagen, proteoglycans and matrix from the AF, while leaving elastic fibres intact [97], the ultrastructural organization of the elastic fibres in the inter- and intra-lamellar regions were successfully described [120]. Utilizing the same technique, current SEM study has described the ultrastructural architecture of the elastic components in the PBs of the AF lamellae.

In spite of using a novel method for visualizing elastic fibres that enabled us to present SEM images of PBs elastic network, there are a few limitations that need to be addressed. An ovine model was used for the current study based on its structural and biochemical similarities to the human disc; however, using human samples are more clinically relevant. The findings of this study may be affected by remnants of undigested matrix or undigested components; however, only regions where undigested tissue did not obscure elastic fibres were analysed for quantitative analysis. On the other hand, the sample preparation method including digestion, indirect heat treatment and drying,

was found to alter the fibre orientation by approximately 2° compared to the control samples [97]. Therefore, it is unlikely that this orientation affects the overall quantitative analysis as it is small in magnitude [76]. Like other SEM studies, identification of elastic fibres by their physical appearance and size is another limitation. Elastic fibres were distinguished from other fibrous components as they are generally twisted or straight strands (0.2-1.5 µm in diameter) that sometimes branch to introduce a course network [69, 74, 75]. Further studies will be required to investigate the elastic fibre characteristics in different disc regions (e.g., anterior, lateral and posterolateral) or showing the effect of age, degeneration or disease on elastic fibre ultrastructural organization.

Based on SEM images obtained from transverse cutting planes, the frequent presence of PBs dividing the CS lamellae across the AF (Figures 5.2a, b, e, f and 5.3d, e) indicated a well-organized interconnecting structure comprised of elastic fibres. Consistent with other studies, collagen bundles in the CS lamellae of the AF provide a segmental structure that is surrounded by a network of elastic fibres in the PBs and inter-lamellar matrix (Figure 5.3b) [27, 48, 88]. This compartmentalization of the AF by traversing PBs was seen in SEM images in the transverse cutting plane (Figures 5.2e-f). SEM imaging of a control sample did not reveal elastic fibres in the PBs due to the presence of matrix and collagen constituents, while PBs appear to constitute a constant or definite pattern that recurs at uniform intervals (denoted by stars in Figure 5.2a-b). As a consequence of partial digestion, a fenestration structure of various sizes was seen to randomly scatter across the CS lamellae (cutting plane = 0°) indicating that PBs are irregularly distributed across the AF (Figures 5.2e-f). Previously it was believed that PBs divide collagen bundles. However, we have shown that PBs both divide and enclose collagen bundles. This PB arrangement is in agreement with findings that indicated the role of elastic fibres

on AF radial integrity [15, 24]. Also their contribution to enhance disc mechanical properties is unknown.

By removing the matrix and collagen fibres, it is now possible to visualize elastic fibre organization within the PBs, and to our knowledge this new interpretation of elastic fibre ultrastructure has not been previously reported. In both cutting planes (transverse and oblique), a dense network including thick (1-2 µm diameter) and thin (less than 0.2 µm diameter) elastic fibres were seen in the PBs (Figures 5.3f and 5.5f).

Analysing the ultrastructural organization of elastic fibres in the PBs in the oblique plane revealed that elastic fibres connect adjacent collagen bundles in a CS lamella by two mechanisms: merging with and becoming orientated in parallel to the collagen fibres; or by a sharp penetration into adjacent collagen bundles (Figures 5.5g and j). A similar anchoring mechanism was reported within the boundaries between the inter-lamellar matrix and adjacent lamella [120]. Based on the proposed 3D geometrical model of the PB (Figure 5.8), a possible function of elastic fibres in the PBs is to structurally reinforce adjacent collagen bundles during loading. Could PBs not only enclose collagen fibre bundles, but rather form a branching elastic fibre network between these bundles to provide some form of reinforcement.

Quantitative analysis revealed that there was no significant difference in structural organization of elastic fibres between the transverse and cutting planes. While at least three principle orientations of elastic fibres in the PB were identified, the relatively low magnitudes of coherency coefficients would suggest that the organization of elastic fibres in the PBs represented a more isotropic than anisotropic structure. However, investigations comparing a random network of fibres representing a more isotropic structure, to a preferential fibre orientation that more closely indicates an orthotropic structure with well-organized fibres at 0° and ±45° (Figure 5.7c), the coherency

coefficients were the same. The frequently occurring features including a dense elastic network, having a complex structure with different size and shape of elastic fibres, were seen across all nine specimens in both cutting planes (Figures 5.4 and 5.6).

Based on the presented results the likely mechanical role of PBs in the AF can be speculated, however, a study of the mechanical properties of the PBs is required to provide new mechanical insights, and the current study represents the first steps towards this. The same method that was carefully developed for visualization of the elastic fibre organization in the ILM and lamellae, was utilized to present an ultrastructural understanding of the elastic fibre network in the PBs, which is new knowledge that has not been presented before. Furthermore, with the new proposed 3D geometry of the PBs resulting from the present study (Figure 5.8), more-accurate multiscale computational models of the disc can be developed, which will provide new insights on the mechanics of the disc.

5.6 Conclusion

A detailed understanding of the PB ultrastructure is crucial to elucidate its role on the structural integrity of the adjacent collagen bundles, as well as adjacent lamellae. The present study used extracellular matrix digestion to address significant gaps in understanding of disc ultrastructure, and will contribute to multidisciplinary ultrastructure-function studies. The findings presented reveal a well-organized elastic fibre network with a complex ultrastructure that spreads across the PB in both transverse and oblique cutting planes. The present study revealed that a continous network of elastic fibres may provide disc integrity by connecting adjacent bundles of CS lamellae together.

6 Chapter 6 – Study 4: New findings confirm the viscoelastic behaviour of the inter-lamellar matrix of the disc annulus fibrosus in radial and circumferential directions of loading.

The previous chapters (Chapters 3-5, Studies 1-3) revealed new insights into ILM elastic fibre ultrastructure identifying a dense and complex network of thick (diameter of 1-2 μm) and thin (0.1 μm diameter) fibres that were not randomly distributed. Based on those ultrastructural studies it is likely that the ILM plays a role in the mechanical properties of the AF. Utilizing a novel approach for sample preparation (isolating ILM samples) for minimizing the contribution of lamellae into the mechanical properties of the ILM, this chapter explored the viscoelastic and failure properties of the ILM. For the first time, the viscoelastic and failure properties of the ILM were quantified.

The study presented in this chapter has been published in the following journal and conference proceeding:

Tavakoli J, Costi JJ. New findings confirm the viscoelastic behaviour of the inter-lamellar matrix of the disc annulus fibrosus in radial and circumferential directions of loading, Acta Biomaterialia (I.F. = 6.319), 71, 411-419, 2018.

Tavakoli J, Costi JJ. New insights reveal the mechanical role of the Inter-lamellar matrix and the elastic fibre network in the annulus fibrosus of the intervertebral disc (Poster), The 64th Annual Meeting of the Orthopaedic Research Society (ORS), New Orleans, USA, March 2018.

6.1 Abstract

While few studies have improved our understanding of composition and organization of elastic fibres in the inter-lamellar matrix (ILM), its clinical relevance is not fully understood. Moreover, no studies have measured the direct tensile and shear failure mechanical failure and viscoelastic properties of the ILM. Therefore, the aim of this study was, for the first time, to measure the viscoelastic and failure properties of the ILM in both the tension and shear directions of loading. Using an ovine model, isolated ILM samples were stretched to 40% of their initial length at three strain rates of 0.1%s^{-1} (slow), 1%s^{-1} (medium) and 10%s^{-1} (fast) and a ramp test to failure was performed at a strain rate of 10%s^{-1}. The findings from this study identified that the stiffness of the ILM was significantly larger at faster strain rates, and energy absorption significantly smaller, compared to slower strain rates, and the viscoelastic and failure properties were not significantly different under tension and shear loading. We found a strain-rate dependent response of the ILM during dynamic loading, particularly at the fastest rate. The ILM demonstrated a significantly higher capability for energy absorption at slow strain rates compared to medium and fast strain rates. A significant increase in modulus was found in both loading directions and all strain rates, having a trend of larger modulus in tension and at faster strain rates. The finding of no significant difference in failure properties in both loading directions, was consistent with our previous ultra-structural studies that revealed a well-organized (±45°) elastic fibre orientation in the ILM. The results from this study can be used to develop and validate finite element models of the AF at the tissue scale, as well as providing new strategies for fabricating tissue engineered scaffolds.

6.2 Introduction

With a unique hierarchical structure, the annulus fibrosus (AF) of the intervertebral disc is comprised of annular lamellae with alternating orientation of collagen fibres embedded in a proteoglycan-rich ground matrix [43]. The inter-lamellar matrix (ILM), with a thickness of approximately 20 µm, lies between lamellae and consists of collagen type IV, cells, several glycoproteins and matrix; however, elastic fibres were recognized as its main component [9, 10, 12, 89, 90]. Microstructural studies of the ILM revealed higher elastic fibre density relative to the intra-lamellar region [11, 13, 16, 45], while further insight into ILM elastic fibre ultrastructure identified a dense and complex network of thick (diameter of 1-2 µm) and thin (0.1 µm diameter) fibres that were not randomly distributed [120].

The clinical relevance of the ILM is not fully understood. However, loss of structural boundaries between lamellae in scoliotic discs, which are more vulnerable to degeneration, along with evidence interpreting an increase of irregularity and interdigitating of lamellae structure with age, may show a correlation between the ILM disorganization and disc degeneration [107, 108]. Investigation of AF radial cohesion identified a complex hierarchy of interconnecting fibres in the ILM-lamella boundary that demonstrates the role of the ILM in lamellae connectivity [27]. Furthermore, based on studies of AF delamination, tears, patterns of herniation of the whole disc and lamellae peel strength, it is likely that the ILM plays a role in providing AF structural integrity [18, 19, 57, 123]. Therefore, failure of the ILM may contribute to the initial stages of herniation and disc degeneration [8, 17, 23]. Knowledge of the structure-function relationship in the ILM is crucial in identifying the loading conditions that contribute to AF delamination or increased risk of disc herniation. Development of

clinical strategies including tissue engineering scaffold fabrication and herniation treatment requires a greater understanding of the ILM mechanical and structural properties.

In spite of recent progress identifying the ultrastructure of the ILM, there is limited knowledge on its mechanical role. The ILM shear strength has been found to increase with lamella thickness [28], and deform by up to 10 mm, having a mean (SD) peak shear strength of 0.03 (0.05) MPa during delamination [124]. Significantly different shear stress and strain distributions, with a trend of being greater in the lamella than across the ILM, were found in disc mechanical modelling when inter-lamellar connectivity was considered [65, 125]. Also higher strain was reported in the ILM compared to the intra-lamellar region in bovine discs [85].

In the radial direction, the ILM structural connectivity was discussed, yet the mechanical properties of the ILM in tension were not quantified [14, 17, 27]. Compared to the lamella, the stiffness of the outer lamellae interface (i.e. ILM) was higher than the inner AF, (ranging between 43% to 75%).[24]. This result was consistent with a study indicating that AF peel strength was approximately 30% higher in outer lamellae compared to the inner layers [18].

While microstructural-based studies revealed that the density of elastic fibres were higher in the ILM compared to the lamellae [11, 16, 45, 70, 88, 107], ultrastructural studies provided new insights to the organization of elastic fibres in different regions of the disc [97, 120, 126]. A dense network including thick (diameter of 1-2 µm) and thin (0.1 µm diameter) elastic fibres was seen in the ILM. This highly organised complex network was comprised of the majority of fibres oriented at ±45° to the circumferential lamellae, and having different size and shape fibres, compared to those in the intra-lamellar region [120].

Studies on the ILM were categorized into qualitative structural-based research where no mechanical measurement were undertaken [9, 17, 23, 27, 88, 97, 120], or quantitative research where a number of lamellae were used with limited mechanical properties reported [18, 24, 57, 124, 127]. While these studies have improved our knowledge of the possible mechanical role of the ILM, no studies have measured the viscoelastic and mechanical behaviour of the ILM under direct tensile and direct shear loading has not been studied, however peel tests, which would represent a more-tensile loading regime, have been performed.

Studies of multiple and single lamellae have demonstrated that these tissues exhibit increased modulus and failure stress with increasing strain rate, and a higher modulus in shear compared to tension, however no such studies have been conducted on the ILM. Therefore, the aim of this study was to measure the viscoelastic and failure properties of the ILM in both the tension and shear directions of loading. The following hypotheses were proposed:

1. The stiffness of the ILM will be significantly larger at faster strain rates, and energy absorption significantly smaller, compared to slower strain rates.
2. The viscoelastic and failure properties under tension and shear loading will not be significantly different.

The first hypothesis was proposed due to the combination of elastic fibres and extracellular matrix in the ILM, which most likely impart viscoelastic behaviour to the ILM. The second hypothesis is based on the dominant orientation of elastic fibres at ±45°, which suggests a similar mechanical role in both tension and circumferential directions of loading.

6.3 Materials and methods

6.3.1 Sample preparation

Sixteen Ovine spines (18-24 months old) were obtained from a local abattoir, and discs from lumbar FSUs (L4/L5) were dissected from vertebral bodies, sprayed with saline and stored at -20°C in cling wrap until used for sample preparation. While frozen, a 10 mm length of the anterior AF, with the depth to the nucleus pulposus region (~7mm disc height) was separated from each disc. Each AF tissue was moulded with optimal cutting temperature (OCT, Tissue-Tek®, Sakura, Japan) compound to identify the transverse cutting plane. Samples from adjacent sections (thickness 1 mm and length 10 mm) were sliced using a hand microtome (Figure 6.1a-c). Damaged samples or those having less than ten lamellae were excluded from the study. All adjacent samples were labelled and then divided into two groups of 10 for mechanical testing in the radial (tension) and circumferential (shear) directions.

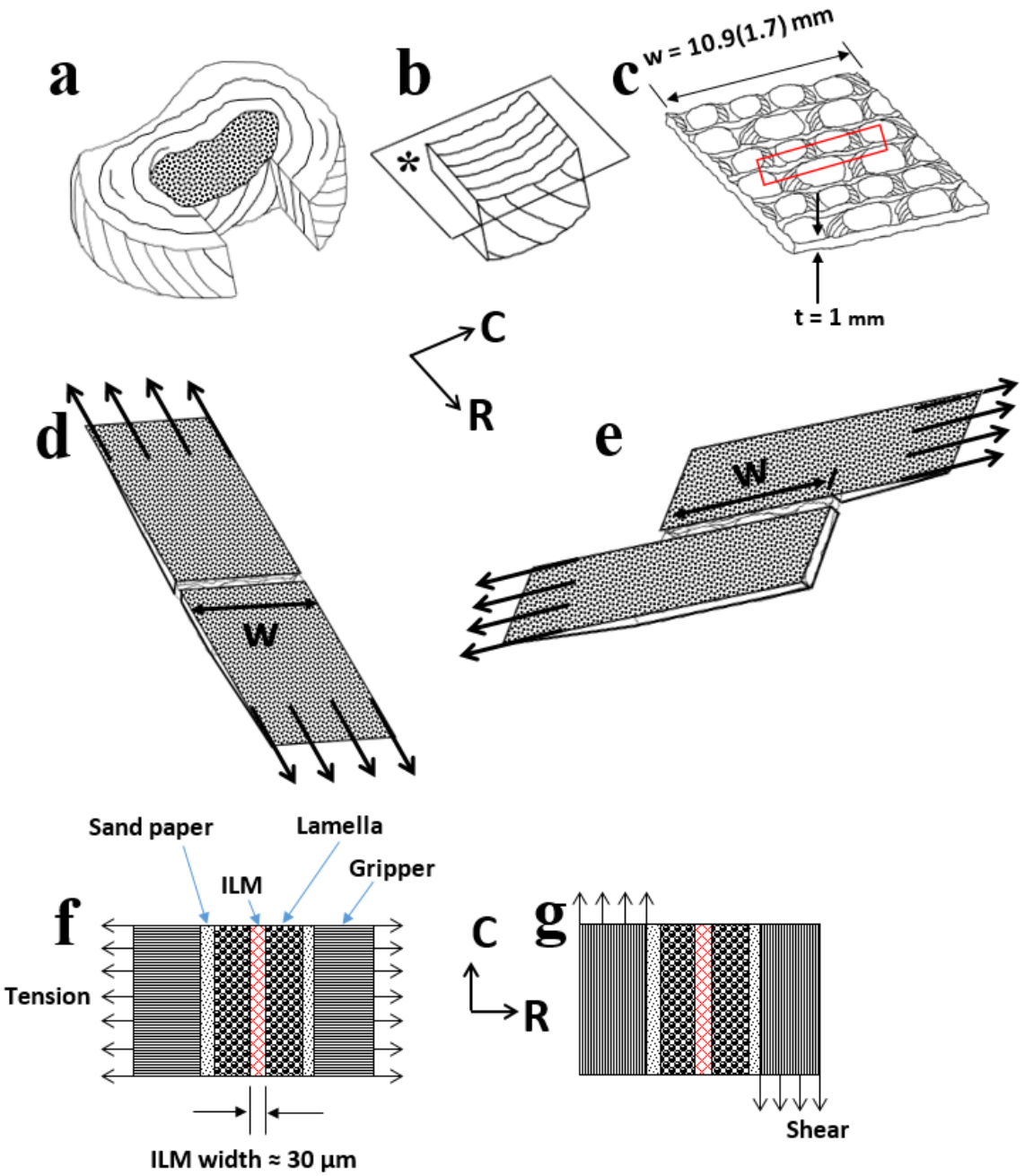

*Figure 6.1 Sample preparation. (a) Anterior AF segments of approximately 10 mm width, were separated from the outer AF to the nucleus pulposus, (b) frozen sections were then cut along the transverse plane (denoted by *), (c) transverse samples were sliced to approximately 1 mm thickness. The region identified by the red rectangle represents the approximate location from which samples were prepared and tested. (d, e) samples of inter-lamellar matrix (ILM) and portions of two adjacent lamellae prepared for shear and tension tests, respectively. Sand paper was attached to the samples using superglue under microscope visualization (directions of applied load are identified by arrows). (f, g) schematic drawings of the samples from axial view to identify the size of the recruited adjacent lamellae compared to the ILM, where the width of the lamellae are greater than the ILM. The mean (95%CI) cross-sectional area of all samples was 10.9 (1.7) mm2 as shown in (panel c). Axes R and C represent radial and circumferential directions, respectively, and dimension t and W indicate the specimen thickness and width, respectively.*

6.3.2 Mechanical testing

To accomplish the ILM mechanical tests, a functional lamellae unit, which consisted of two adjacent lamellae and the ILM between them, was identified from prepared adjacent sections using a stereomicroscope (Motic, SMZ-168, China) (Figure 6.1d-e). The functional lamellae units were isolated from the middle of the AF (approximately 5-6 lamellae inwards) and was consistent for all samples. Previous ultrastructural studies identified an approximate 30 µm width for the ILM. During specimen preparation the total width of the lamella-ILM-lamella complex was approximately 200 µm and careful attention was used to ensure that the ILM was located in the middle of the complex. (Figure 1f -g). This strategy for sample preparation was consistent among all samples. Sand paper (250 grit) was bonded above and below the sample, and on each edge using cyanoacrylate adhesive. The mechanical properties of samples were measured in tension (radial) and shear (circumferential) loading directions.

Pilot failure mechanical tests for the ILM were performed at different strain magnitudes to identify the maximum strain (40%) used in this study, which was low enough (compared to the yield stress) to be non-destructive, yet high enough to include the linear region. The strain rate was estimated based on disc deformation data during compression from Costi et al., 2007 for the outer anterior radial AF displacement [67]. For every 1 mm of applied compressive displacement, the radial strain was 11%, as calculated between the two outermost anterior radial displacement vectors. In order to estimate the compressive displacement of the disc during physiological loading, an in-vivo nucleus pulposus pressure of 1.1 MPa that was measured during standing was used [128]. The equivalent axial compressive force [129] required to create the 1.1 MPa nucleus pressure was then calculated based on an average lumbar (L4-5) disc area of 2011 mm2 [130], which yielded a compressive force of 1475 N. The resulting

physiological compressive displacement was calculated to be 0.29 mm based on a compressive stiffness of normal discs of 5,141 N/mm taken from a loading frequency of 1 Hz [131]. Therefore, the radial strain for a compressive displacement of 0.29 mm was 3.2%. Using a sinusoidal physiological compressive loading frequency of 1 Hz, the peak outer anterior AF radial strain would be achieved in 0.5 s, which yields a strain rate of 6.4%/s. Based on this we chose a strain rate of 10 %/s, and then chose two other strain rates that were each an order of magnitude lower (1 %/s and 0.1 %/s).

All samples were initially equilibrated in 0.15M phosphate buffered saline (PBS) at room temperature for 30 min and immersed in 0.15M PBS at 37°C during tests. Each sample was subjected to dynamic and failure tests using a micromechanical testing machine (BioTester, CellScale, Waterloo, ON ,Canada) having a load cell capacity of 23 N. Three cycles of dynamic loading using a triangle waveform were applied to stretch the samples to 40% of their initial length at three strain rates of 0.1%s^{-1} (slow), 1%s^{-1} (medium) and 10%s^{-1} (fast) under displacement control, followed by a 5 min unloaded recovery period between each rate. Preload and recovery were used to minimise creep between tests. A 100 mN preload was applied before the first cycle. Data frequency acquisition was set to 1, 10 and 100 Hz for slow, medium and fast strain rates, respectively. Finally, a ramp test to failure was performed at a strain rate of 10%s^{-1} at 100 Hz data acquisition.

6.3.3 Data and statistical analysis

Engineering stress and strain were calculated from the final cycle of the dynamic tests (Figure 2), and the failure test using custom-written MATLAB scripts (R2014b, The Mathworks Inc.). Outcome measures of phase angle, extensibility and modulus (toe, linear, average during entire load-unload cycle (average) and average during loading only (average loading)), were calculated from the dynamic tests, followed by the failure test parameters of failure stress and strain, and toughness. Failure stress was defined as

the peak stress recorded during the test, and the corresponding strain was defined as the failure strain. All modulus measures were calculated as the slope of the best-fit line using linear regression. Toe modulus represented the initial region of the loading curve where the elastic fibre network in the ILM was uncoiling, and linear modulus represented the region where the majority of fibres in the ILM were fully recruited. Extensibility was calculated as the strain at the intersection of the toe and linear stiffness lines [132]. The average loading modulus represented the entire loading curve, and average modulus represented the entire load-unload curve. The phase angle, which is a measure of energy absorption, was calculated using a cross spectral density estimate function (MATLAB: csd.m) [15].

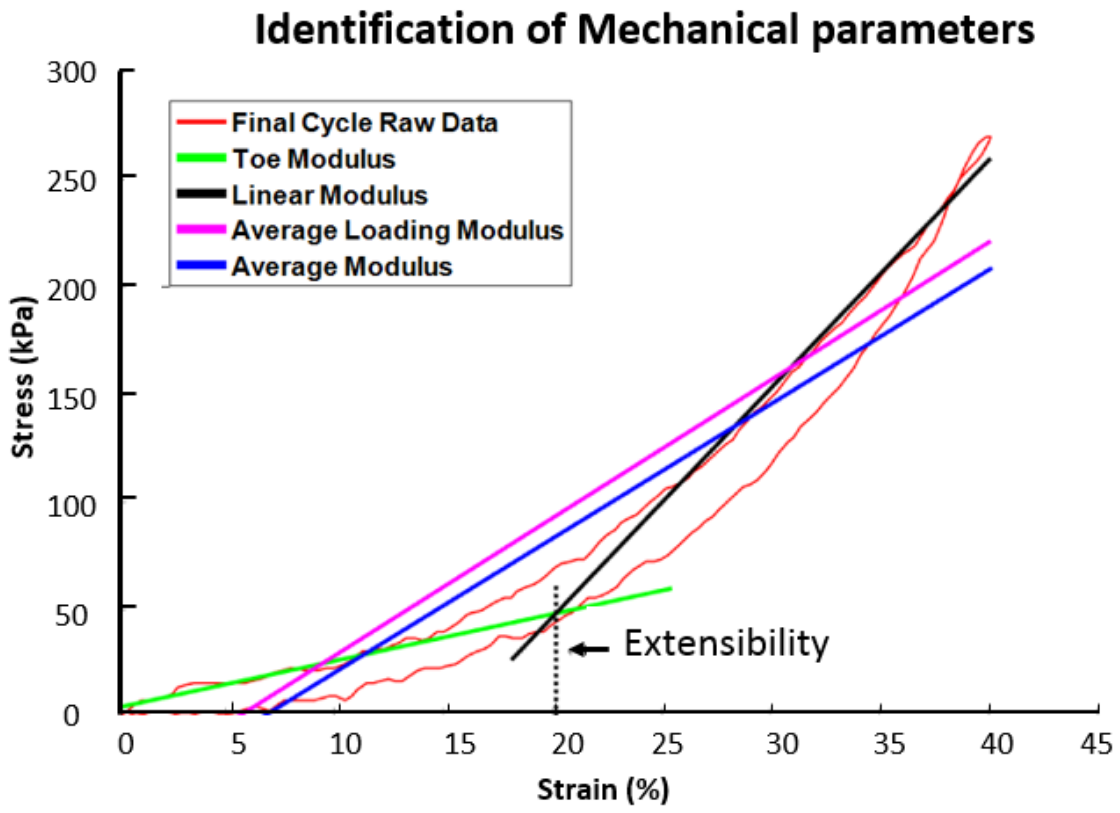

Figure 6.2 Identification of mechanical parameters including final cycle of data, extensibility, toe, linear, average loading and average moduli

For statistical analysis all data were assessed for normality using the Shapiro-Wilk test. For the dynamic test outcome parameters, separate repeated measures ANOVA were conducted (IBM SPSS Statistics for Windows, Version 22.0. Armonk, NY: IBM Corp.) for each variable of phase angle, extensibility, toe modulus, linear modulus and average modulus having fixed factors of direction of load application, (shear and tension), and strain rate (0.1%s^{-1} (slow), 1%s^{-1} (medium) and 10%s^{-1} (fast)) using an alpha of 0.05, with post-hoc multiple comparisons conducted using a Bonferroni adjustment on alpha. Statistical differences for ILM failure properties of failure stress, strain and toughness between tension and shear loadings were assessed using an unpaired t-test, using an alpha = 0.05.

6.4 Results

There was no indication of sample slippage during mechanical testing as identified from observation of the recorded video of each tests, and from the testing curves (Appendix B and Figure 6.3). The mean (95% CI) gripper to gripper distance was 1.172 (0.074) mm. The dimensions of the samples were approximately a thickness of 1 mm, a width of 10.9 (1.7) mm. When tested to failure, all samples failed at the ILM site. According to the Shapiro-Wilk test, it was found that the data for all specimens were normally distributed ($p > 0.05$).

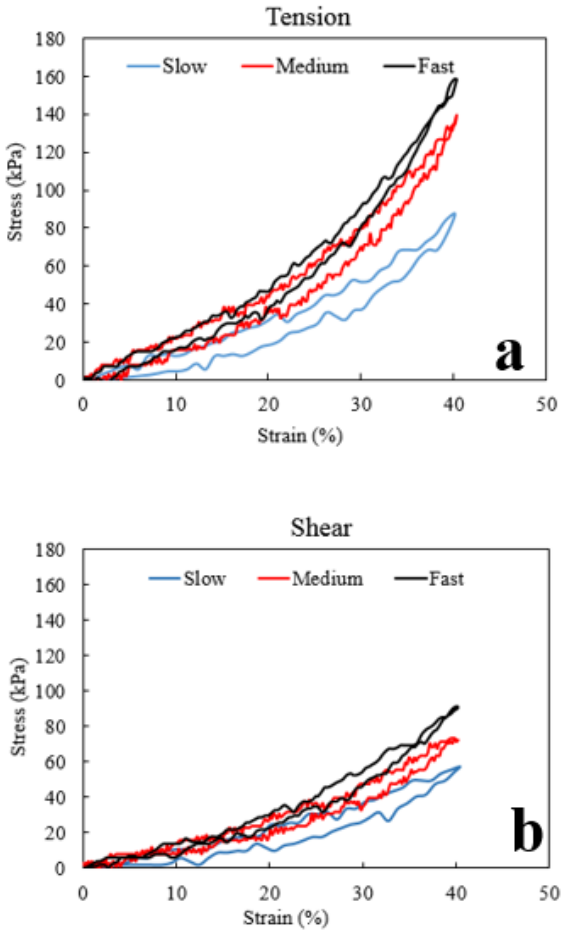

Figure 6.3 The viscoelastic properties (final loading cycle) of the ILM for the same sample tested of the ILM at three different strain rates of 0.1%s^{-1} (slow), 1%s^{-1} (medium) and 10%s^{-1} (fast), in both (a) radial (tension) and for a second sample tested in (b) circumferential (shear) directions obtained from the final loading cycle.

Statistical analysis for phase angle, extensibility, average modulus, toe modulus, linear modulus, and average loading modulus are reported as follows:

6.4.1 Phase angle

The overall effect of strain rate was significant ($p < 0.001$, Table 6.1), with post-hoc comparisons revealing a significantly larger phase angle at slow compared to the medium and fast strain rates ($p < 0.001$, Figure 6.4a). The overall effect of loading direction (tension vs. shear) and the interaction between strain rate and loading direction was not significant ($p = 0.226$ and $p = 0.545$ respectively).

6.4.2 Extensibility

No significant overall effects were found for strain rate ($p = 0.631$), or loading direction ($p = 0.574$) for extensibility, nor their interactions ($p = 0.442$), (Table 6.1, Figure 6.4b).

6.4.3 Average modulus

The overall effects of strain rate ($p = 0.173$) and loading direction ($p = 0.110$) for average modulus, was not significant, nor their interactions ($p = 0.417$), (Table 6.1, Figure 6.4c).

6.4.4 Average loading modulus

The overall effect of strain rate was significant for average loading modulus ($p = 0.017$, Table 6.1), with post-hoc comparisons revealing that the slow strain rate was significantly smaller compared to fast ($p = 0.05$, Figure 6.4d). No significant difference was found between slow and medium ($p = 0.191$) as well as between fast and medium ($p = 0.069$) strain rates. A trend of larger modulus at higher stain rates was seen for the effect of loading direction on average loading modulus ($p = 0.051$). No significant interactions between strain rate and loading direction were found ($p = 0.797$).

6.4.5 Toe modulus

The overall effect of strain rate was significant for toe modulus ($p = 0.005$, Table 6.1), with post-hoc comparisons revealing a significantly larger toe modulus for the fast strain rate compared to medium ($p = 0.019$, Figure 6.4e) and slow ($p = 0.035$). No significant difference for toe modulus was found between slow and medium strain rates ($p = 0.098$). Also the overall effect of loading direction was significant for toe modulus ($p = 0.046$), with post-hoc comparisons revealing that toe modulus was significantly smaller in shear compared to tension ($p =0.046$). No significant interaction was found between strain rate and loading direction ($p = 0.779$).

6.4.6 Linear modulus

The overall effect of strain rate was not significant for linear modulus ($p = 0.061$, Table 6.1). The overall effect of loading direction was significant ($p = 0.009$) for linear modulus, with post-hoc comparisons revealing that the tension group was significantly larger than the shear group ($p = 0.004$). No significant interactions were found between strain rate and loading direction ($p = 0.681$) (Figure 6.4f).

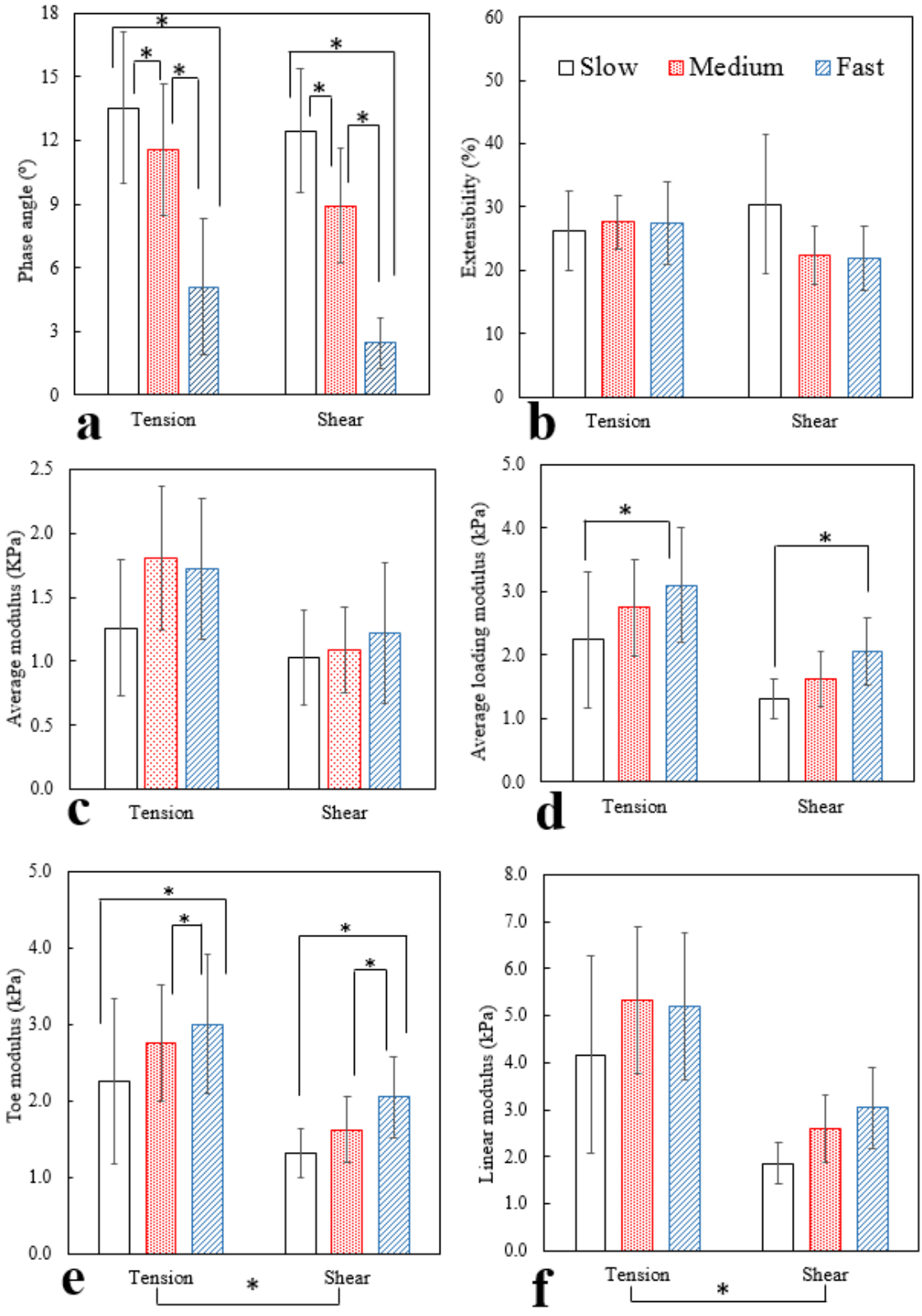

*Figure 6.4 Comparison of selected mechanical properties of the ILM at three strain rates of 0.1%s-1 (slow), 1%s-1 (medium) and 10%s-1 (fast), during tension and shear loading (a) Phase angle, (b) Extensibility, (c) Average modulus, (d) Average loading modulus, (e) Toe modulus and (f) Linear modulus. * denotes significant differences between groups.*

6.4.7 Failure tests

Loading direction (tension and shear) was not significant for failure stress (p = 0.674), failure strain (p = 0.341) and toughness (p = 0.366) (Figure 6.5). The mean (95%CI) ILM toughness was 0.54 (0.22) and 0.79 (0.48) $J.m^{-3}$, in tension and shear directions, respectively, which was not significant (p = 0.366).

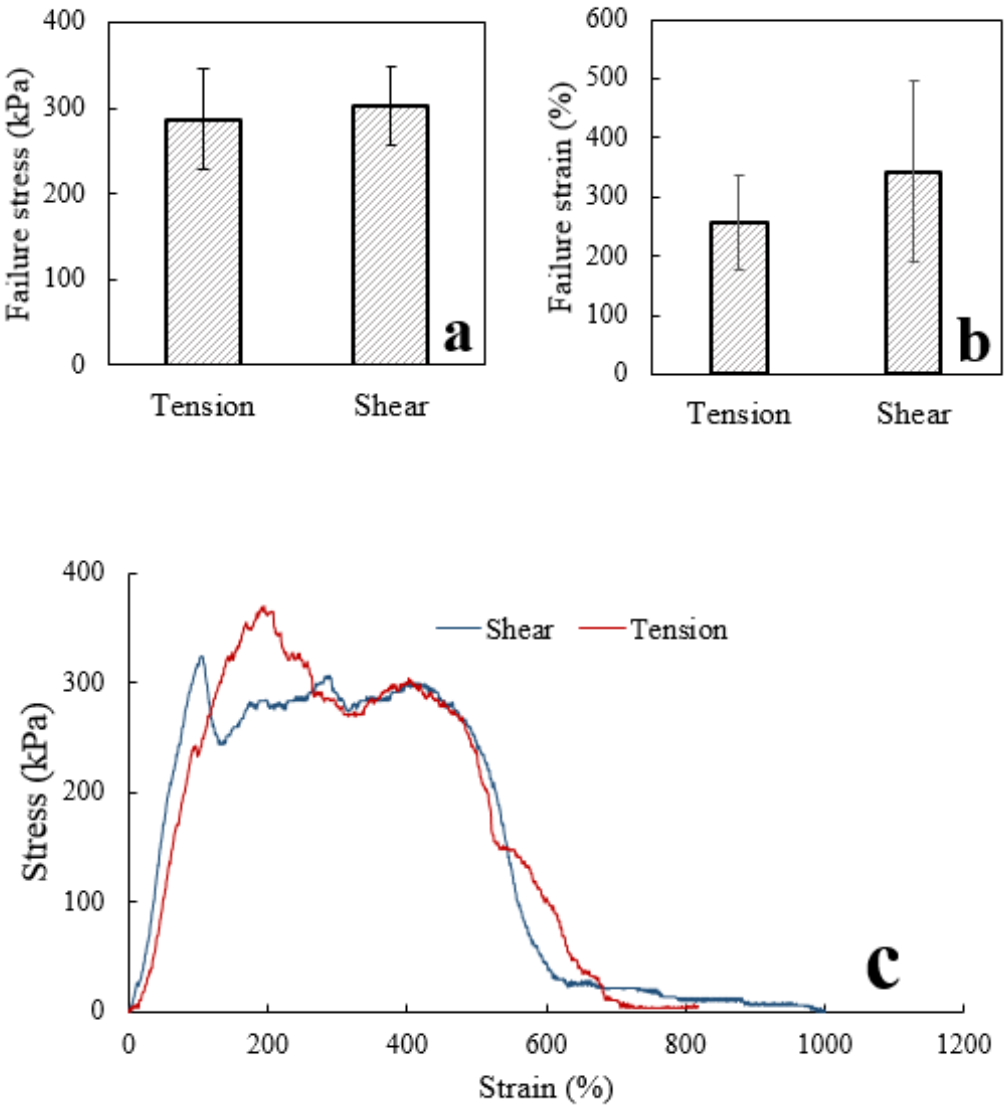

Figure 6.5 Comparison of mean (95%CI) (a) Failure stress and (b) Failure strain of the ILM in tension and shear loading directions. (c) Example stress-strain failure curves during shear and tension loading of the ILM in adjacent samples from the same disc.

*Table 6-1 Summary of ANOVA results for the overall effects of strain rate (slow vs. medium vs. fast) and loading direction (tension vs. shear) and their interactions for each of the micro-mechanical test parameters. The * symbol and NSD were used to indicate significant and no significant difference, respectively.*

Parameter	Strain rate	Loading direction	Interactions
Phase Angle (°)	*(p < 0.001)	NSD (p = 0.226)	NSD (p = 0.545)
Extensibility (%)	NSD (p = 0.631)	NSD (p = 0.574)	NSD (p = 0.442)
Average Modulus (kPa)	NSD (p = 0.173)	NSD (p = 0.110)	NSD (p = 0.417)
Average Loading Modulus (kPa)	*(p = 0.017)	NSD(p = 0.051)	NSD (p = 0.797)
Toe Modulus (kPa)	*(p = 0.005)	*(p = 0.046)	NSD (p = 0.779)
Linear Modulus (kPa)	NSD (p = 0.061)	*(p = 0.009)	NSD (p = 0.681)

6.5 Discussion

Understanding the mechanical function of the ILM is an important step towards developing more accurate multi-scale computational models for disc function, which can lead to improved strategies for tissue engineering and repair. The aim of this study was to measure, for the first time, the viscoelastic and failure material properties of the ILM under tension and shear loading. The findings from this study confirmed both of our hypotheses that the stiffness of the ILM was significantly larger at faster strain rates, and energy absorption significantly smaller, compared to slower strain rates, and the viscoelastic and failure properties were not significantly different under tension and shear loading. We found a strain-rate dependent response of the ILM during dynamic loading, particularly at the fastest rate. The ILM demonstrated a significantly higher capability for energy absorption at slow strain rates compared to medium and fast strain rates. A significant increase in modulus was found in both loading directions and all strain rates, having a trend of larger modulus in tension and at faster strain rates. It was revealed that average loading modulus in tension was marginally non-significant compared to shear (p = 0.051), while it seems with increasing the number of specimens

it become significant. The overall interaction between loading direction and strain rate was not significant for all viscoelastic parameters. When tested to failure, there were no significant differences in failure stress, strain and toughness between ILM tensile and shear loading directions.

The images at different time points during tension (Figure 6.6) and shear (Figure 6.7) tests provide more information for the role of the ILM in the AF during loading in different directions. Time was presented on the abscissa instead of strain, to allow for a direct comparison to the videos in the supplementary files. While it was not possible, at this magnification, to observe the likely sub-failure of the samples that occurred in both directions of loading after 2 s (Figures 6.6b and 6.7b) to the peak stress (denoted by c), the failure was more likely to commence at peak stress (Figures 6.6c and 6.7c). The observed fluctuation for stress after the linear region to the peak stress (point b to c), which were seen to be less that those after initiation of failure and its propagation (point c to e), may represent the changes in ultrastructural organization of the elastic fibres in the ILM, which may arise from the expansion of the elastic fibre network, rotation of fibres, separation between ECM and elastic fibre network and the failure of the thin elastic fibres. The observed fluctuations after initiation of failure (Figure 6.6c, 6.7c) to the point of separation of the lamellae (Figure 6.6e, 6.7e) may represent the failure of the thick elastic fibres in the ILM.

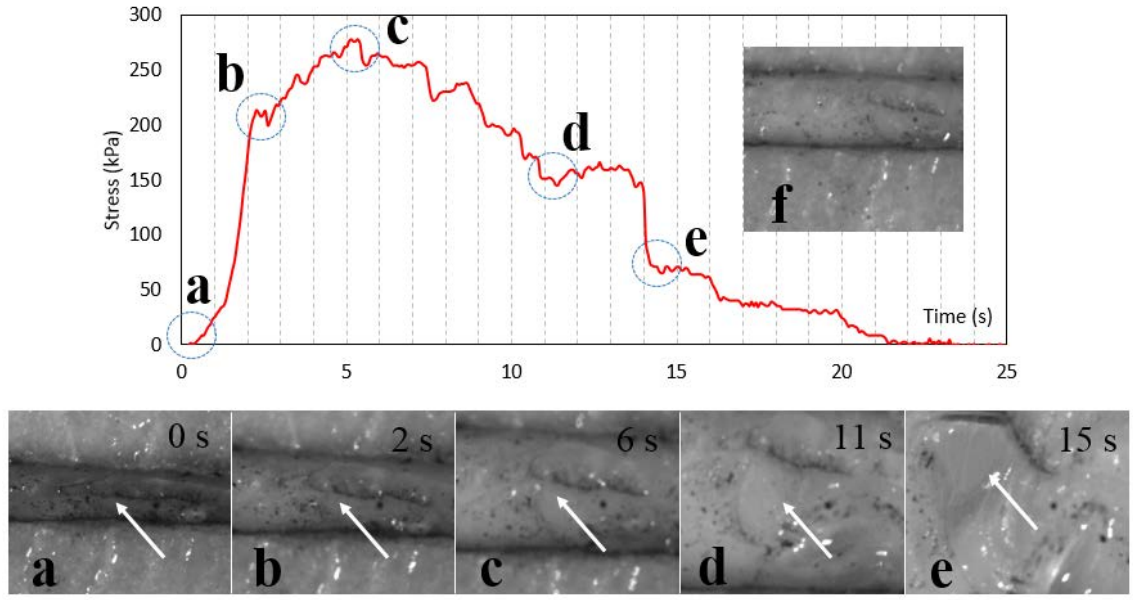

Figure 6.6 Change in stress during the performance of mechanical failure for the ILM in tension (a, b and c) represent rest point, yield stress and maximum stress, respectively and (d, e) indicate the ILM disruption and separation, respectively. The correspondence images show the change in the appearance of the samples during mechanical failure test at different time points (seconds) as indicated in the graph. (f) Represents the sample after stretched to 40% of its initial length. Arrows indicate the approximate location of the ILM in the middle of lamella-ILM-lamella complex (a, b) and initiation (c), propagation (d) of the failure as well as (e) the lamella separation.

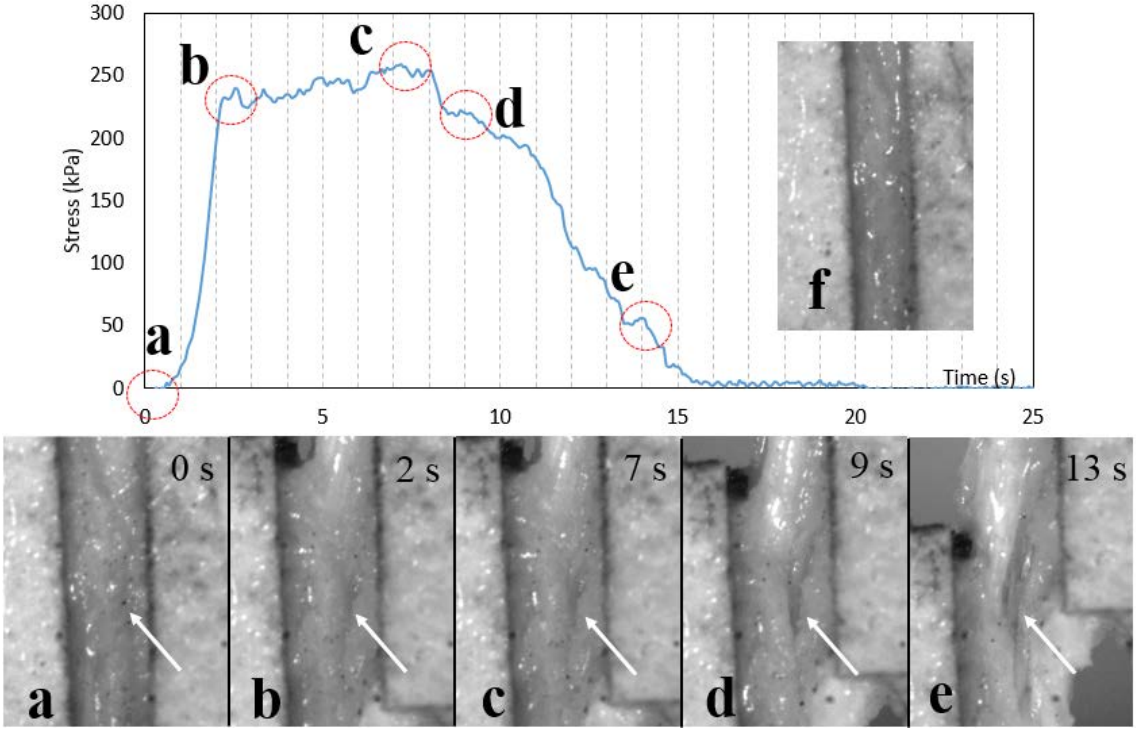

Figure 6.7 The stress-time curve during the performance of mechanical failure for the ILM in shear. (a, b and c) represent rest point, yield stress and maximum stress, respectively and (d, e) indicate the ILM disruption and separation, respectively. The correspondence images show the change in the appearance of the samples during mechanical failure test at different time points (seconds) as indicated in the graph. (f) Represents the sample after stretched to 40% of its initial length. Arrows indicate the approximate

location of the ILM in the middle of lamella-ILM-lamella complex (a, b) and initiation (c), propagation (d) of the failure as well as (e) the lamella separation.

Failure of the lamella-ILM-lamella complex more likely occurred at the ILM site, where the looser network of elastic fibres was present compared to the lamella having dense and highly packed collagen bundles. The lower stiffness of the ILM, together with the orthotropic ultrastructure, suggests a role that is adapted to support 6 degree of freedom deformation of the AF, and absorb more energy than the lamellae.

Our ultrastructural studies of the elastic fibre network in the ILM revealed that the dominant elastic fibre orientation, relative to the circumferential (lamellae) direction, was near 0°, with two symmetrical peaks of approximately ±45°, indicating the presence of an orthotropic structure [120]. This structure likely explains why a lower modulus (toe, linear and average) was found in shear compared to tension, where only those fibres oriented in the direction of applied shear would be recruited. We identified the presence of both thick and thin elastic fibres, with the thicker fibres aligned parallel to the lamellae [120, 133]. It may be that in shear, the thicker fibres experienced the highest stresses and failed first, as observed by the abrupt decrease in stress (Figures 6.5c, 6.6 and 6.7), followed by the thinner fibres taking up the stress and progressively failing. In tension, the network of "crossing" fibres (±45°) were likely all recruited, after which they failed sequentially, resulting in a less abrupt decrease in stress. Based on protein-proteoglycan interactions, supramolecular assemblies (elastic fibres, collagen fibrils) are formed and a structural scaffold is provided by ECM. The mechanical entanglement and binding of this structural scaffold with elastic fibres in the ILM, provides a structurally stable composite, contributing to the mechanical properties of the ILM, which likely to plays an important role in imparting isotropic failure properties [134].

Unfortunately, few studies have been undertaken to identify the role of the ILM on mechanical properties of the AF. The observations implying that the ILM was mainly composed of elastic fibres [9, 13, 45, 88], having an overall low density relative to collagen fibres [34], may address why such studies are lacking. Therefore, comparisons to other studies is limited. The findings of this study strongly support the previous reports that suggested a biomechanical role for the ILM based on the observation of alignment of collagen and elastic fibres after loading [14, 135], and a well-organized ultra-structural arrangement of the elastic fibre network [120]. Only one study has reported human ILM failure strength as a peel strength of 18.4 kPa in the anterior region of degenerated discs (grade 3, [18]), which is an order of magnitude lower than our non-degenerated ovine disc with a mean (95%CI) tension strength of 287 (58) kPa. In addition, the mean (SD) peel strength (normalized to the sample width) of the rabbit ILM was reported to be 0.88 (0.26) N/mm that can compared to the peak tension force (normalized by width) in our study measured as mean (SD) 0.28 (0.093) N/mm. The peak load for delamination of the AF measured by a lap test using porcine cervical discs was reported to be mean (SD) 0.3 (0.02) N/mm, compared to our normalized ovine shear maximum force of 0.396 (0.22) N/mm at the anterior region [57, 124].

From another point of view, based on the results of this study we are able to compare the mechanical properties of the ILM to those of the lamellae. The AF lamella shear failure strength (strain rate: 2 $\%s^{-1}$) was reported as 1.03 ± 0.85 MPa in porcine cervical discs [136], and our measurement showed that the ILM tensile and shear failure strengths were 0.29 (0.58) MPa and 0.30 (0.46) MPa, respectively (Figure 6.4a). These comparisons indicate that ILM material properties are comparable to that of the lamellae, which presents evidence in support of the key role of the ILM on mechanical properties of the AF in the disc.

Calculating strain using gripper-to-gripper distance, instead of utilizing a non-contact method, presents a limitation, however since there was no evidence of sample slippage, the measured strain is representative of global tissue strain. While it is un-likely that the strain is constant across the ILM, the calculation of the ILM strain may be affected by the presence of adjacent lamellae and therefore represents the global strain across the ILM and ILM-lamella boundary. However, our studies have found that ILM has a significantly lower failure stress compared to the adjacent lamellae, indicate that the ILM is weaker (Please see chapter 8). From a structural point of view, the lamella consists of dense and highly packed collagen fibres, while elastic fibres are a looser network within the ILM. Another limitation of this study was the use of an ovine model. There is strong evidence that supports the use of an ovine model based on its structural and biochemical similarities to the human disc [4, 8, 17, 23-25, 47, 48, 137, 138]; however, using human samples would be more clinically relevant. While it is likely that the mechanical properties of the ILM in tension and shear directions of loading are not the same in different regions of the disc, the use of only the anterior region was a limitation of this study. The preparation of adjacent samples from other regions in ovine discs was difficult due to the small disc height; however, different regions could readily be isolated in human discs. Also we would like to acknowledge that using isolated ILM samples, despite its preparation being challenging, was important for minimizing the lamellae contribution to mechanical properties.

6.6 Conclusion

This study identified the mechanical contribution of the ILM to the structural integrity of the AF, in both tension and shear directions of loading. The strain-rate dependent response of the ILM during dynamic loading and its significantly higher capability for

energy absorption at slow strain rates in both directions of loading, confirmed its viscoelastic behaviour. More importantly, the finding of no significant difference in failure properties in both loading directions, was consistent with our previous ultra-structural studies that revealed a well-organized (±45°) elastic fibre orientation in the ILM. The results from this study can be used to develop and validate finite element models of the AF at the tissue scale, as well as providing new strategies for fabricating tissue engineered scaffolds. This research will serve as a foundation for future studies on the relationship between degeneration and ILM mechanical properties, as well as understanding the contribution of the elastic fibre network to the mechanical properties of the ILM.

7 Chapter 7- Study 5: New insights into the viscoelastic and failure mechanical properties of the elastic fibre network of the inter-lamellar matrix in the annulus fibrosus of the disc

While in the previous chapter (Chapter 6, Study 4) a new study was performed for biomechanical characterization of the ILM, the contribution of the elastic fibre network to the structural integrity of the ILM is not yet known. The main fibrous component of the ILM is the elastic fibre network (Chapter 2, Study 1), which have a preferential fibre orientation that suggests an orthotropic structure (Chapters 4 and 5, Studies 2 and 3), therefore it is likely that this network plays a role in imparting mechanical properties to the ILM. This chapter aims to measure the viscoelastic and failure properties of the elastic fibres in the ILM in both tension and shear directions of loading. No studies have been undertaken to identify the role of the elastic fibre network on the mechanical properties of the ILM by removing all components except elastic fibres.

The study presented in this chapter has been published in the following journal and conference proceeding:

Tavakoli J, Costi JJ. New insights into the viscoelastic and failure mechanical properties of the elastic fibre network of the inter-lamellar matrix in the annulus fibrosus of the disc, Acta Biomaterialia, (I.F. = 6.383), 71, 411-419, 2018.

Tavakoli J, Costi JJ. New insights reveal the mechanical role of the Inter-lamellar matrix and the elastic fibre network in the annulus fibrosus of the intervertebral disc (Poster), The 64th Annual Meeting of the Orthopaedic Research Society (ORS), New Orleans, USA, March 2018.

7.1 Abstract

The mechanical role of elastic fibres in the inter-lamellar matrix (ILM) is unknown; however, it has been suggested that they play a role in providing structural integrity to the annulus fibrosus (AF). Therefore, the aim of this study was to measure the viscoelastic and failure properties of the elastic fibre network in the ILM of ovine discs in both tension and shear directions of loading. Utilizing a novel technique, isolated elastic fibres within the ILM from ovine discs were stretched to 40% of their initial length at three strain rates of 0.1%s-1 (slow), 1%s-1 (medium) and 10%s-1 (fast), followed by a ramp test to failure at 10%s-1. A significant strain-rate dependent response was found, particularly at the fastest rate for phase angle and normalized stiffness ($p < 0.001$). The elastic fibres in the ILM demonstrated a significantly higher capability for energy absorption at slow compared to medium and fast strain rates ($p < 0.001$). These finding suggests that the elastic fibre network of the ILM exhibits nonlinear elastic behavior. When tested to failure, a significantly higher normalized failure force was found in tension compared to shear loading ($p = 0.011$), which is consistent with the orthotropic structure of elastic fibres in the ILM. The results of this study confirmed the mechanical contribution of the elastic fibre network to the ILM and the structural integrity of the AF. This research serves as a foundation for future studies to investigate the relationship between degeneration and ILM mechanical properties.

7.2 Introduction

The clinical relevance of elastic fibres in the annulus fibrosus (AF) of the disc is not fully understood. However, in contrast to healthy discs, where well organized and abundant elastic fibres are found in the inter-lamellar matrix (ILM) [120], scoliotic discs that are more vulnerable to degeneration have a sparse and disrupted elastic network and irregular ILM structure [107]. An increase of metalloproteinases level across scoliotic

and degenerated discs may show a correlation between the disorganization of elastic fibres and disc degeneration [109]. Metalloproteinases can degrade elastin and release elastin peptides into the extracellular matrix (ECM) [110]. Elastin peptides are able to trigger a series of biological events, including an increase in cell calcium flux [139], metalloproteinase up-regulation [140], and cell proliferation [141] that lead to change in density and structure of ECM components and affect the mechanical properties of the disc [108].

Early structural studies revealed an irregular distribution and low volume fraction of elastic fibres compared to collagen [38], and suggested that elastic fibres play no substantial role in the mechanical properties of the AF [70]. Later, it was shown that elastic fibres, visualized by histological staining, are organized in the AF, their density is higher in the ILM and they may interact with the ECM [11, 13, 16, 45, 70, 88, 107]. Further insight into the ultrastructural organization of elastic fibres in the ILM identified a dense and complex network of fibres that were not randomly distributed [120]. Despite recent progress identifying the micro- and ultra-structural organization of elastic fibres, their contribution to the mechanical properties of the ILM is less known.

Investigation of the radial cohesion of AF lamellae identified a complex hierarchy of interconnecting fibres in the ILM that demonstrates the role of elastic fibres in lamellae connectivity [27]. It is thought that elastic fibres in the ILM assist lamellae to return to their original position after deformation. While the role of elastic fibres in mechanical properties of the ILM hasn't been studied, it has been suggested that they play a role in providing AF structural integrity [15, 53, 58]. It was shown that enzymatic removal of elastic fibres using elastase resulted in the following observations: tensile toe and linear modulus in the radial direction decreased by 90%, while extensibility increased by 431% in human AF [15]. Using bovine caudal AF an increase of lamellae shear strain in the

radial direction was seen, while shear strain [46] and shear modulus were reported to remain unchanged in the circumferential direction [55].

Enzymatic treatments have been used to remove elastic fibres from the AF, and provide a strategy for measuring the mechanical properties of the AF in the absence of elastic fibres. These treatments are expensive, time consuming and hard to optimize in order to limit the non-specific degradation of other components in the AF [15]. As an alternative, alkali digestion was used in different tissues to selectively remove all components and leave elastic fibres intact [69, 74-76, 98, 99, 102]. While no cleavage of peptide bonds in the elastic fibres has occurred, this method has been selectively used for measurement of the mechanical properties of the elastic fibres [73, 105, 106, 142]. The development of the alkali digestion technique for visualization of elastic fibres of the AF [97] provided new insights to the organization of elastic fibres in different regions of the disc [97, 120, 126], revealing a dense network including thick (diameter of 1-2 µm) and thin (0.1 µm diameter) elastic fibres in the ILM. It was reported that the ILM fibres oriented at ±45° and 0° relative to the collagen fibres in the circumferential lamellae, introduced a highly organised orthotropic network having different size and shape compared to those in the lamellae region. [120]. Based on the orientation of elastic fibres in a well-organized network it is likely that elastic fibres in the ILM play a mechanical role; however, no studies have measured their viscoelastic and failure properties. Therefore, the aim of this study was to measure the elastic, viscoelastic and failure properties of the elastic fibres in the ILM of ovine discs in both tension and shear directions of loading. The following hypotheses were proposed:

1. The elastic fibre network in the ILM exhibits mainly elastic than viscoelastic behavior.

2. The failure properties of the elastic fibres in the ILM will be significantly different under tension and shear loading.

The first hypothesis was proposed as elastic fibres are highly extensible and can deform reversibly with minimum loss of energy. The second hypothesis is based on the observed orthotropic structure of elastic fibres [126], suggesting that their mechanical properties will differ between tension and shear loading. Since there is a lack of mechanical quantification of the elastic fibre network, this mechanical examination could lead to a new understanding of the role of elastic fibres in contributing to AF structural integrity.

7.3 Materials and methods

7.3.1 Sample preparation

Sixteen Ovine spines (18-24 months old) were obtained from a local abattoir and discs from lumbar FSUs (L4/L5) were dissected from vertebral bodies (Figure 7.1a), sprayed with saline and stored at -20 °C in cling wrap until used for sample preparation. While frozen, a 10 mm width of the anterior AF, with the depth to the nucleus pulposus region (~7mm disc height) was separated from each disc (Figure 1b). Each AF tissue was embedded in optimal cutting temperature compound (OCT, Tissue-Tek®, Sakura, Japan) to identify the transverse cutting plane (Figure 1c). Samples from adjacent sections (thickness 1 mm and width 10 mm) were sliced using a hand microtome (Figure 1d) for mechanical testing and histology analysis. Damaged samples or those having less than ten lamellae were excluded from the study. For mechanical testing, all adjacent samples were labelled and then divided into two groups for testing in the radial (tension: N=8) and circumferential (shear: N=8) directions. To prepare the samples for the mechanical tests, a functional lamellae unit, which consisted of two adjacent lamellae and the ILM between them, was identified from prepared adjacent sections using a stereomicroscope (Motic, SMZ-168, China) (Figure 1e-f). Waterproof sand paper (250

grit) was bonded above and below the sample and on each edge, using cyanoacrylate adhesive. Partial digestion (digestion) to remove the majority of components from the ILM region except elastic fibres, was performed before mechanical testing, by placing samples in 0.3M NaOH (Sigma-Aldrich, 1310-73-2) solution at 50°C for 45 min frozen [97]. Before digestion, the sand paper was carefully covered with cling wrap and adhesive tape, to ensure that only the functional lamellae unit was exposed to digestion treatment.

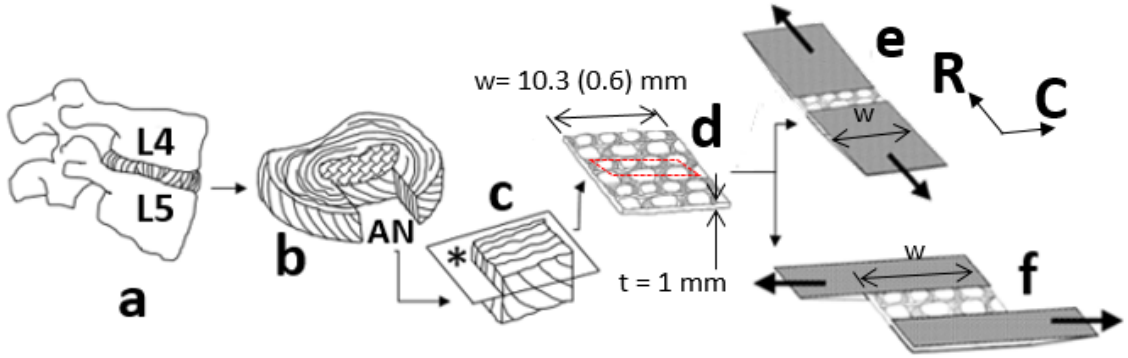

*Figure 7.1 Sample preparation. (a) Fresh functional spine unit (L4/5) were prepared and (b) anterior AF segments (10 mm in width) to the nucleus, were separated from the disc, (c) frozen section cut along the transverse plane (denoted by *), (d) transverse samples having approximately 1 mm thickness. (e, f) samples of inter-lamellar matrix and portions of two adjacent lamellae prepared for shear and tension tests, respectively. Sand paper was attached to the samples using superglue under microscope visualization (directions of applied load were shown by bold arrows). The region identified by the red rectangle represents the approximate location from which samples were prepared. Axes R and C represent radial and circumferential directions, respectively and dimensions t and w indicate the specimen thickness and width, mean (95% CI), respectively.*

Toluidine blue [143] and orcein [97] staining were used to confirm that the majority of ECM components in the ILM (except elastic fibres) were removed after digestion compared to undigested samples. Briefly, serial thin samples (20 µm thickness) were cut transversally from both digested and undigested samples using a cryostat microtome (Leica Biosystems, CM3050). The samples were mounted on poly-L-lysine coated microscope slides and soaked in orcein and toluidine blue solutions for 40 and 10 min, respectively. Then they were rinsed in tap water for 2 min and mounted with DPX

(resinous mounting media). The presence of elastic fibres and ECM was visualized in the histologically prepared samples using light microscopy analysis (Brightfield BX50, Olympus, Japan). The SEM images before and after digestion were captured to visualize the elimination of ECM after performing digestion at high magnification. The samples were dried before SEM imaging (Inspect F50, FEI Company, USA) in a vacuum oven (VO3, LABEC, Australia) overnight at 37 °C and −80 kPa. Dried specimens were mounted on aluminium stubs with double adhesive tape, then sputter coated with platinum at 2 nm thickness. High voltage was set at 5 kV and the distance from the sample to the beam source was kept constant for all performed tests.

7.3.2 Mechanical testing

The mechanical properties of samples were measured in tension (radial) and shear (circumferential) loading directions. All samples were initially equilibrated in 0.15M phosphate buffered saline (PBS) at room temperature for 30 min and immersed in 0.15M PBS at 37°C during tests. Each sample was subjected to dynamic and failure tests using a micromechanical testing machine (BioTester, CellScale, Waterloo, ON ,Canada) having a load cell capacity of 23 N. Three cycles of dynamic loading using a triangle waveform were applied to stretch the samples to 40% of their initial length at three strain rates of $0.1\%s^{-1}$ (slow), $1\%s^{-1}$ (medium) and $10\%s^{-1}$ (fast) under displacement control. A 100 mN preload was applied before the first cycle. Data frequency acquisition was set to 1, 5 and 100 Hz for slow, medium and fast strain rates, respectively. Finally, a ramp test to failure was performed at a strain rate of $10\%s^{-1}$ at 100 Hz data acquisition.

7.3.3 Data and statistical analysis

Since it was not possible to measure the thickness of the samples after digestion, force (normalized to the sample width; normalized force) was reported instead of engineering stress [142]. Normalized force and engineering strain were calculated from the final

cycle of the dynamic tests, and the failure test using custom-written MATLAB scripts (R2014b, The Mathworks Inc.). Outcome measures of phase angle and normalized stiffness (linear, average loading, and average) [131] were calculated from the dynamic tests, followed by the failure test parameters of normalized failure force, normalized failure strain, and normalized toughness at failure [144]. Failure was defined as the peak force recorded during the test. Normalized toughness was calculated as the area under "normalized force - strain" curve at failure, the corresponding strain was defined as the failure strain and strain was measured using gripper to gripper distance. All stiffness measures were calculated as the slope of the best-fit line using linear regression. The average loading stiffness represented the entire loading curve, and average stiffness represented the entire load-unload curve. The phase angle, which is a measure of energy absorption, was calculated using a cross spectral density estimate function (MATLAB: csd.m) [15].

For statistical analysis all data were assessed for normality using the Shapiro-Wilk test. For the dynamic test outcome parameters, separate repeated measures ANOVA were conducted (IBM SPSS Statistics for Windows, Version 22.0. Armonk, NY: IBM Corp.) for each variable of phase angle, extensibility, toe stiffness, linear stiffness and average stiffness having fixed factors of direction of load application, (shear and tension), and strain rate (0.1%s^{-1} (slow), 1%s^{-1} (medium) and 10%s^{-1} (fast)) using an alpha of 0.05, with post-hoc multiple comparisons conducted using a Bonferroni adjustment on alpha. Statistical differences for ILM failure properties of normalized failure force, strain and normalized toughness between tension and shear loadings were assessed using an unpaired t-test, using an alpha = 0.05.

7.4 Results

Results from one sample was excluded from this study after the load-displacement curve identified damage to the tissue that had been noted as a technical error during specimen setup in the micromechanical testing machine. There was no indication of sample slippage during mechanical testing as identified from observation of the recorded video of each test, and from the testing curves (Figure 7.2). The mean (95% CI) gripper to gripper distance was 1.105 (0.069) mm. According to the Shapiro-Wilk test, it was found that the data for all specimens were normally distributed ($p > 0.05$).

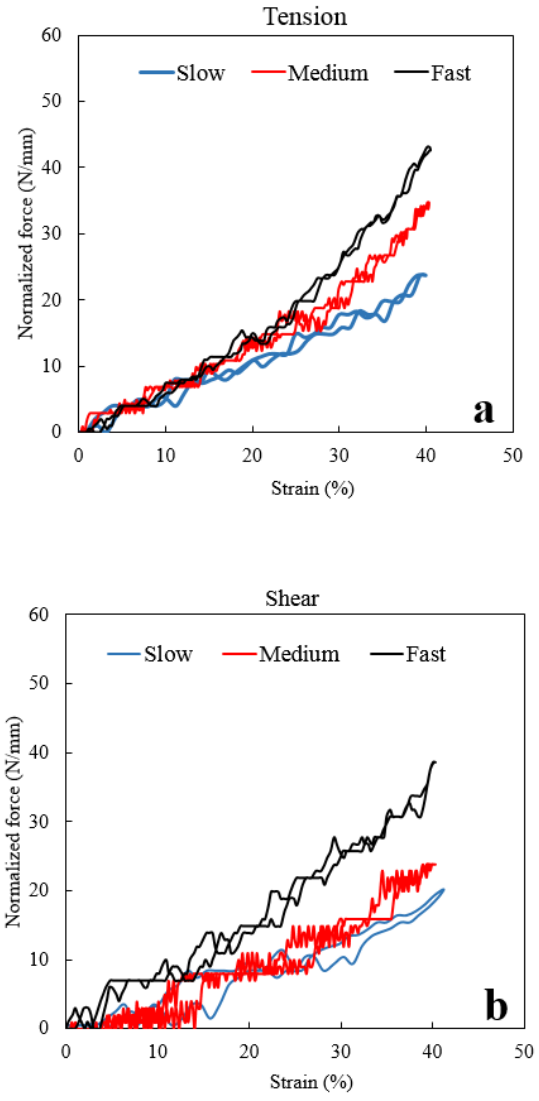

Figure 7.2 Example testing curves of the elastic fibres in the ILM at three different strain rates of 0.1%s^{-1} (slow), 1%s^{-1} (medium) and 10%s^{-1} (fast), in both (a) radial (tension) and (b) circumferential (shear) directions obtained from the final loading cycle.

Statistical analysis for phase angle, extensibility, normalized average stiffness, normalized toe stiffness, normalized linear stiffness, and normalized average loading stiffness were reported as follows:

7.4.1 Phase angle

The overall effect of strain rate (slow, medium and fast) and loading direction (tension vs. shear) was significant ($p < 0.002$, Table 7.1, Figure 3a). The interaction between strain rate and loading direction was significant ($p = 0.007$), with post-hoc comparisons revealing significantly smaller phase angles for slow and medium strain rates between tension and shear directions ($p < 0.008$). There was no significant difference at the fast strain rate between tension and shear ($p = 0.56$).

*Table 7-1 Summary of ANOVA results for the overall effects of strain rate (slow vs. medium vs. fast) and loading direction (tension vs. shear) and their interactions for each of the micro-mechanical test parameters, and statistical differences for digested ILM failure properties of normalized failure force, strain and normalized toughness between tension and shear loadings. The * symbol and NSD were used to indicate significant and no significant difference, respectively. The unit of stiffness is $N.mm^{-2}$ as normalized force (N.mm-1) was used, instead of force.*

	Viscoelastic		
Parameter	Strain rate	Loading direction	Interactions
Phase Angle (°)	*(p < 0.001)	*(p = 0.002)	*(p = 0.007)
Normalized average stiffness ($N.mm^{-2}$)	NSD (p = 0.963)	NSD (p = 0.075)	NSD (p = 0.403)
Normalized average Loading stiffness ($N.mm^{-2}$)	*(p < 0.001)	*(p = 0.046)	NSD (p = 0.211)
Normalized linear stiffness ($N.mm^{-2}$)	*(p = 0.001)	NSD (p = 0.165)	NSD (p = 0.238)
	Failure		
Normalized failure force ($N.mm^{-1}$)	*(p = 0.011)	*(p = 0.011)	-------
Failure strain (%)	NSD (p = 0.172)	-------	-------
Normalized toughness ($J.m^{-4}$)	NSD (p = 0.690)	-------	-------

7.4.2 Normalized average stiffness

No significant overall effects were found for strain rate ($p = 0.963$), or loading direction ($p = 0.075$) for normalized average stiffness, nor their interactions ($p = 0.403$), (Table 7.1, Figure 3c).

7.4.3 Normalized average loading stiffness

The overall effect of strain rate ($p < 0.001$, Table 7.1) and loading direction ($p = 0.046$) was significant for normalized average loading stiffness. Post-hoc comparisons revealed a significantly larger stiffness for the fast strain rate compared to medium and slow ($p < 0.001$, Figure 3d), with medium also being significantly larger then slow ($p < 0.001$). No significant interaction was found between strain rate and loading direction ($p = 0.211$).

7.4.4 Normalized linear stiffness

The overall effect of strain rate was significant for normalized linear stiffness ($p = 0.001$, Table 7.1), with post-hoc comparisons revealing a significantly larger stiffness between medium and slow ($p = 0.022$, Figure 3f), and also between fast and slow ($p = 0.005$) strain rates. No significant difference was found between medium and fast strain rates ($p = 0.095$). No significant overall effects were found for loading direction ($p = 0.165$), nor their interactions ($p = 0.236$).

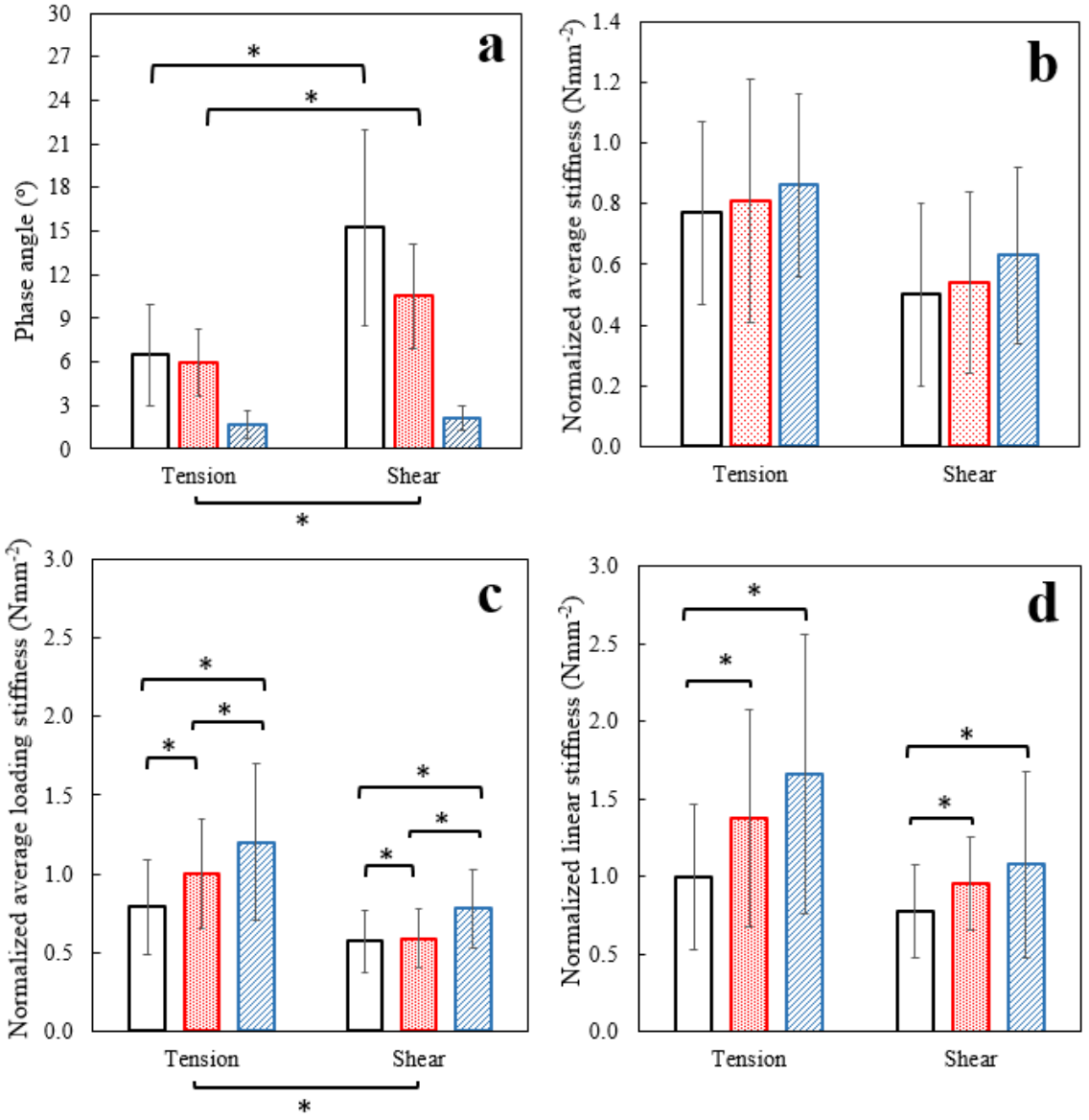

*Figure 7.3 Comparison of selected mechanical properties of the elastic fibres in the ILM (digested samples) at three strain rates of 0.1%s^{-1} (slow), 1%s^{-1} (medium) and 10%s^{-1} (fast), during tension and shear loading (a) Phase angle, (b) Normalized average stiffness, (c) Normalized average loading stiffness and (d) Normalized linear stiffness. * denotes significant differences.*

7.4.5 Failure tests

Loading direction (tension and shear) was significant for normalized failure force (p = 0.011, Table 7.1), with post-hoc comparisons revealing that normalized failure force was significantly smaller in shear compared to tension (p = 0.011). The loading direction was not significant for failure strain (p = 0.172) and normalized toughness (p = 0.690) (Figure 7.4c). The mean (95%CI) normalized toughness for elastic fibres in the ILM was 0.43

(0.19) and 0.50 (0.45) J.m^{-4}, in tension and shear directions, respectively, which was not significantly different (p = 0.690).

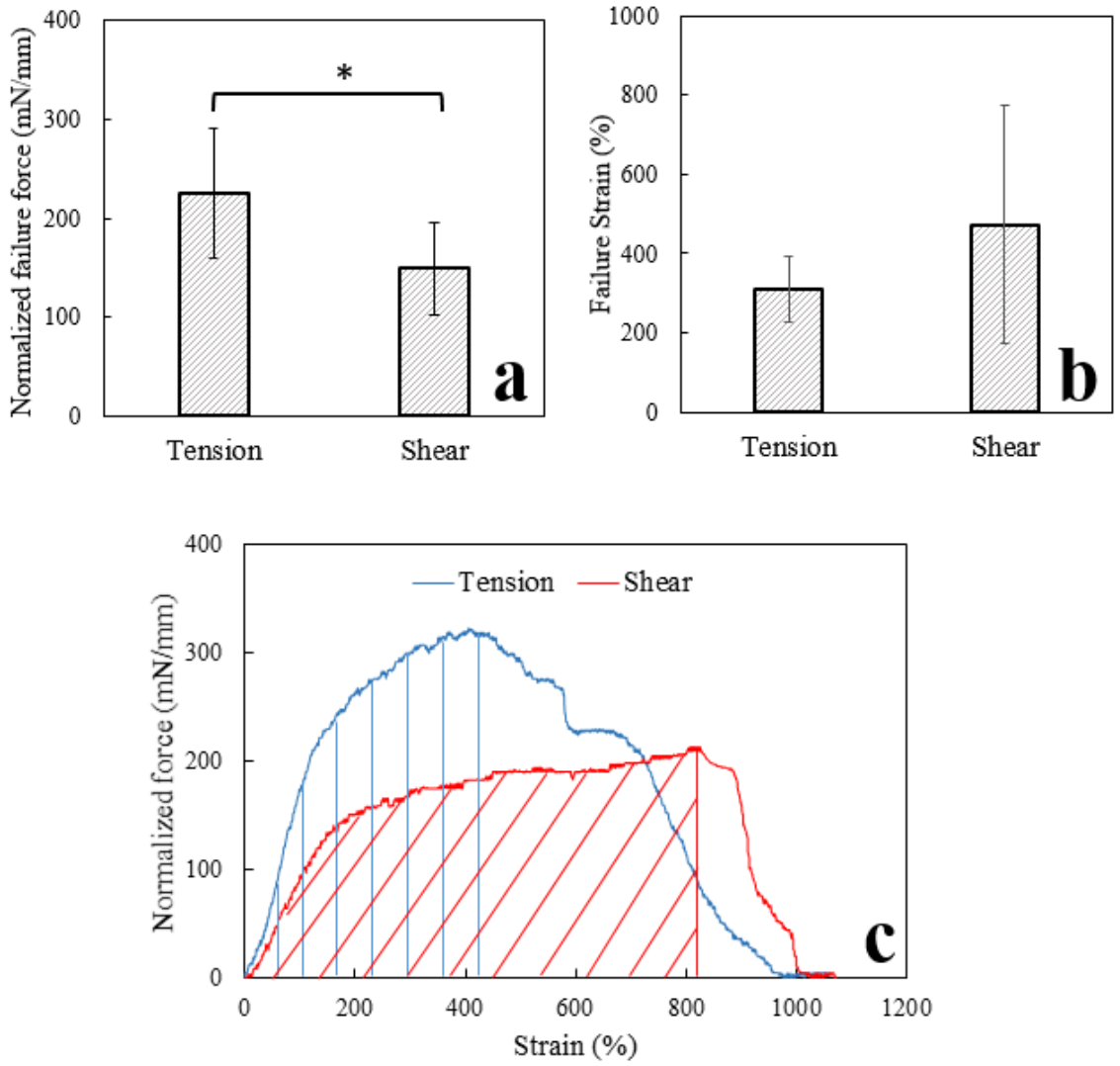

*Figure 7.4 Comparison of mean (95%CI) (a) Normalized failure force and (b) Failure strain of the elastic fibres in the ILM (digested sample) in tension and shear loading directions. (c) Example normalized force vs. strain failure curves during shear and tension loading of the elastic fibres in the digested ILM in adjacent samples from the same disc. The shaded area under the two curves were included for visual comparison of normalized toughness in tension and shear directions and * denotes significant differences between loading directions.*

7.5 Discussion

Understanding the mechanical function of the elastic fibres in the ILM is crucial for identification of their clinical relevance and their impact on the structural integrity of the AF. The results from this study present new findings that can lead to improvement

of regenerative strategies for AF repair, while providing important information for development of more-accurate multi-scale computational models.

The first hypothesis for this study was that the elastic fibre network in the ILM exhibits mainly elastic than viscoelastic behavior. We found a strain-rate dependent response for the elastic fibres in the ILM, particularly at the fastest rate for phase angle, normalized toe, linear and average loading stiffness. The elastic fibres in the ILM demonstrated a significantly higher capability for energy absorption at slow compared to medium and fast strain rates. The findings of significant differences in viscoelastic properties, which were in contrast to our first hypothesis, suggests a viscoelastic behavior for the elastic network in the ILM. In spite of removing bulk of the ECM after digestion that likely reduced extra-fibrillar water content, the presence of intra-fibrillar water in the elastic fibre network might be responsible for the observed viscoelastic behavior [93, 145].

The second hypothesis was that the failure properties of the elastic fibres in the ILM will be significantly different under tension and shear loading. When tested to failure, a significantly higher normalized failure force was found in tension compared to shear loading, which is consistent with the orthotropic structure of elastic fibres in the ILM [120, 133] (Figure 7.5) . There were no significant differences in strain and normalized toughness between elastic fibres in tension and shear loading.

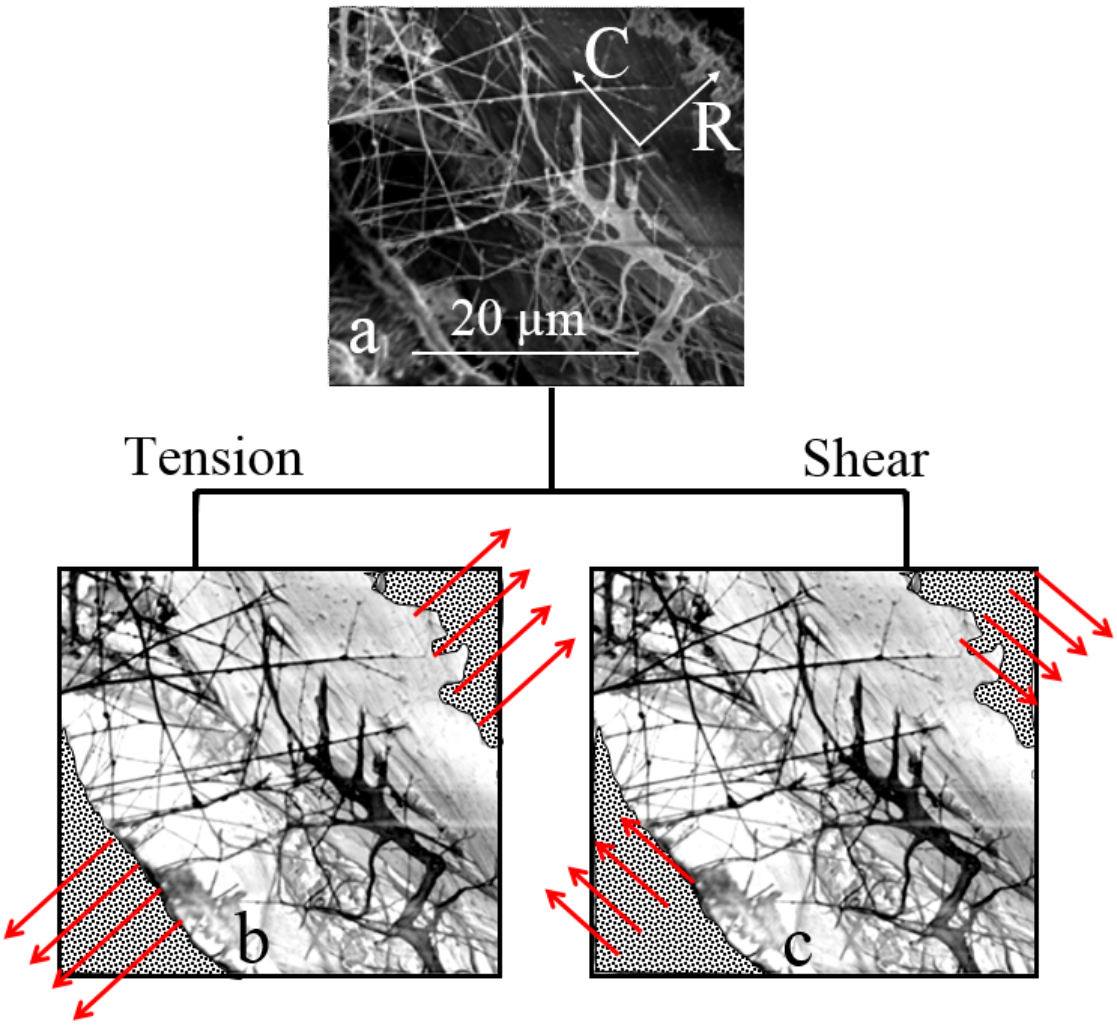

Figure 7.5 Orthotropic structure of the elastic fibre network within the ILM (a), where most fibres were likely recruited under tension (b). However, in shear only those fibres that were oriented in the direction of loading would likely be recruited (c). Axes R and C represent radial and circumferential directions, respectively.

No studies have been undertaken to identify the role of the elastic fibres on the mechanical properties of the ILM, limiting direct comparisons to this study. The findings of this study strongly support a qualitative structural analysis that suggests a biomechanical role for the interconnecting elastic fibres in the ILM [88]. In studies that removed the elastic fibres in human AF, a decrease was found in toe and linear modulus [15] and failure stress in the radial direction [53], as well as an increase in lamellae shear strain [55]. These studies provide evidence in support of the key role of elastic fibres on mechanical properties of the AF in the disc, which are consistent with our results (Figure

7.3). Compared to our previous study on the viscoelastic and failure properties of the intact ILM [146], the phase angles were higher than those for the isolated elastic fibre network (present study) in tension by a factor of approximately two, however the magnitudes were similar in shear. From a multiscale perspective, these findings are consistent with a study that identified the poroelastic behavior of the whole disc [131]. Compared to our results, the phase angle for the intact ILM in tension was larger than the whole disc in both compression and bending at slower strain rates, which may suggest a local role for the ECM, intra- and extra-fibrillar water and their interactions. It is likely that the elimination of ECM components from the ILM after digestion suggests a more nonlinear elastic behavior of the elastic fibre network. Of particulate note, when comparing the dynamic mechanical properties of the intact ILM [146] to the findings of the present study on the isolated elastic fibre network, we observed that both studies revealed strong orthotropic behaviour for toe, linear and average loading moduli/normalized stiffness's, suggesting the dominant role of the elastic fibre network. The extensibility, while not significantly different for all strain rates and loading directions, was approximately the same for both the isolated elastic fibre network and the intact ILM [146], suggesting that only the elastic fibre network is actively recruited during application of tensile and shear strains to the ILM.

To confirm that the majority of tissue components (except elastic fibres) in the ILM were removed after digestion, histology staining with toluidine blue [143] and orcein [97] for ECM (proteoglycan and glycosaminoglycan) and elastic fibres were performed, respectively. Scanning electron microscopy (SEM) images before and after digestion were also compared (Figure 7.6). While orcein staining revealed a high density of elastic fibres in the ILM after digestion (Figures 7.6a, b), the toluidine blue staining indicated the greatest ECM content in the adjacent lamella compared to the ILM (Figures 7.6c, d).

The results from SEM images were consistent with histological evaluation (Figures 7.6e, f).

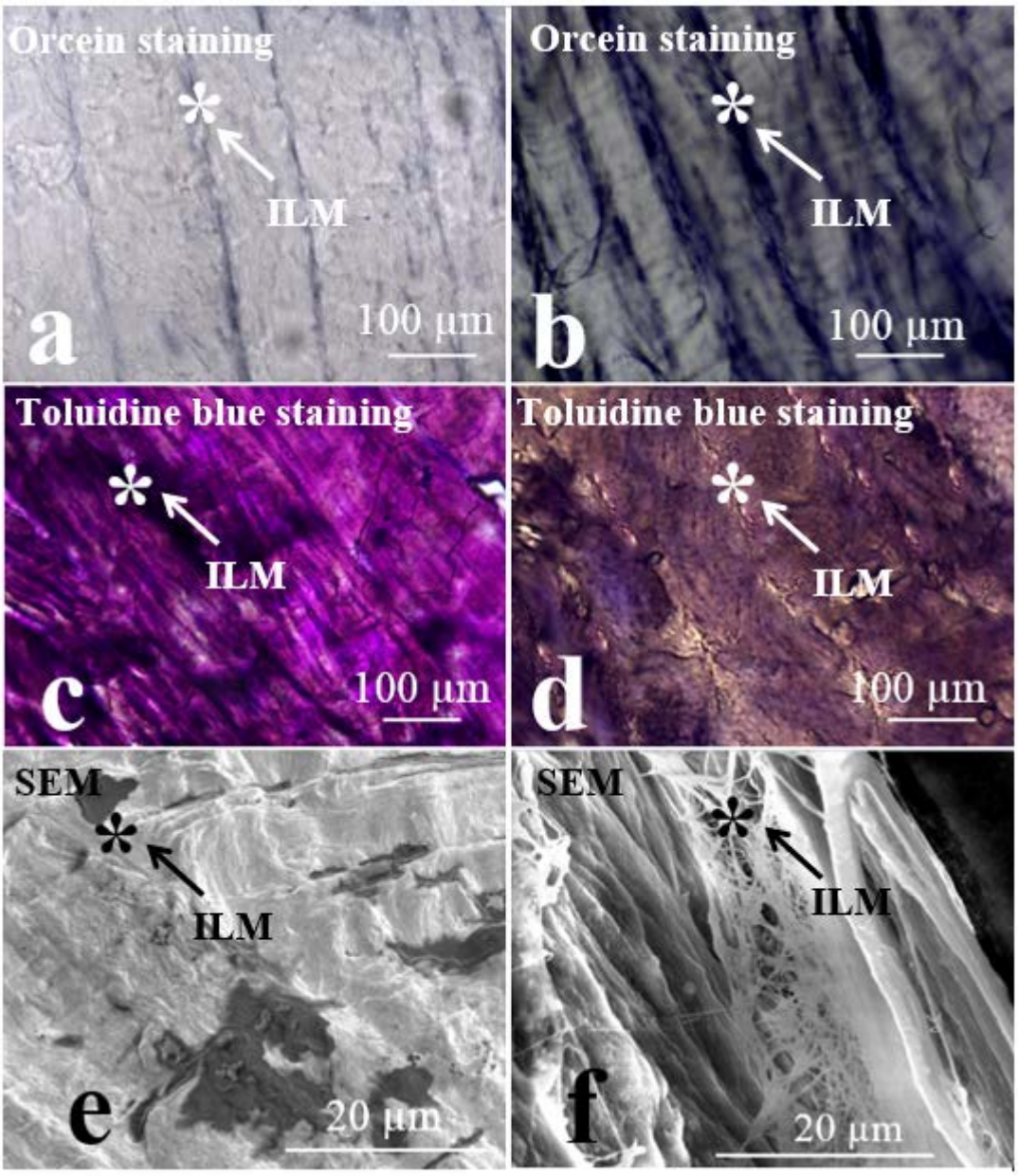

*Figure 7.6 Histology and SEM results. Representative Orcein (a, b) and toluidine blue (c, d) staining and SEM images (e, f) respectively for different undigested (a, c, e) and digested samples (b, d, f). The ILM is denoted by * and arrows in all images.*

Our histology and SEM results clarified the contribution of the elastic fibres to the viscoelastic and failure mechanical properties of the ILM, where the majority of non-elastin components were removed after digestion. The same method has been used to elucidate the role of elastic fibres in different tissues [15, 106, 142, 147]. Among

different digestion methods, alkali digestion has been reported to result in more purified elastin and leaves elastin inter-molecular cross-links intact [105]. In addition, it was shown that the change in elastic fibre orientation was less than 0.5° after digestion [97]. Therefore alkali digestion was considered to be a suitable method for measurement of the mechanical and material properties of the elastic fibres, since minimal inevitable degradation of elastic fibres was found during digestion [105, 142].

Due to the small width of the ILM (20 µm), measurement of strain utilizing a non-contact method was not possible, therefore the reported strain was based on the gripper-to-gripper distance, which presents a limitation of this study. However, since there was no evidence of sample slippage, we believe that the measured strain was representative of tissue strain. An ovine model was used for this study based on its structural and biochemical similarities to the human disc [4, 8, 17, 23-25, 47, 48, 137, 138]; and using human samples would be more clinically relevant. Also we acknowledge that using isolated ILM samples, despite its preparation being challenging, was important for minimizing the lamellae contribution to mechanical properties. Since there is no data on the mechanical and viscoelastic properties of the AF elastic fibre network in the ILM, a variety of normalized stiffnesses were presented to provide modelling studies with a broad range of primary information. The application of different strain rates (slow, medium and fast) wasn't randomized and was ordered from slow to fast to avoid any possible damage to the tissues during the fast rate. Finally, while presenting normalized results was adopted for this study, advanced optical methods could be used to estimate the area of samples in order to calculate stress.

While no differences in failure behavior were found for the intact ILM (i.e. elastic fibres and ECM) [146], a significantly higher normalized failure force was found in tension compared to shear for the isolated elastic fibre network. This difference between failure

directions of loading for the intact ILM and isolated elastic fibre network suggests that the ECM plays an important role in imparting isotropic failure properties, compared to orthotropic behaviour for the elastic fibres only. [33, 71].

7.6 Conclusion

The aim of this study was to measure the viscoelastic and failure properties of the elastic fibre network in the ILM in both tension and shear directions of loading. The results of this study confirmed the mechanical contribution of the elastic fibre network to the ILM, and its likely influence in contributing to the structural integrity of the AF. We found a strain-rate dependent response for the elastic fibres in the ILM during dynamic loading, particularly for phase angle, normalized toe, linear and average loading stiffness. The elastic fibres in the ILM demonstrated a significantly higher capability for energy absorption at slow compared to medium and fast strain rates as well as in shear compared to tension loading. Also, when tested to failure, a significantly higher normalized failure force was found in tension compared to the shear direction of loading. In fact the well-organized elastic fibres that create a highly crosslinked and orthotropic network, significantly contribute to both nonlinear elastic and failure mechanical properties of the ILM. The results of this study, while enhancing our knowledge about the role of the elastic fibres on AF structural integrity, can be utilized in developing and validating advanced multi-scale finite element models of the AF. By understanding the role of the elastic fibre network in influencing delamination and herniation, new strategies for fabricating tissue engineered scaffolds can be proposed. This research will serve as a foundation for future studies to investigate the relationship between degeneration and ILM mechanical properties.

8 Chapter 8 - Study 6: The biomechanics of the inter-lamellar matrix and the lamellae during lumbar disc herniation: Which is the weakest structure?

The previous chapters, for the first time, revealed new insights into the ultrastructural organization and mechanical properties of the ILM. Based on those findings, the relation between structure and function of the ILM became apparent. These studies have improved the understanding of role of the ILM in providing structural integrity to the AF as well as the contribution of the elastic fibre network to the viscoelastic and failure properties of the ILM. However, the clinical relevance of the ILM is not very well known. There are some studies that indirectly address the role of elastic fibres on disc disease and degeneration, but the biomechanical role of the ILM during herniation hasn't been presented before. Based on a multi-scale failure analysis of the ILM and the lamella in an ovine model, this chapter explored the biomechanical properties of the ILM and the lamellae before, during and after lumbar disc herniation.

The study presented in this chapter has been published in the following journal and conference proceeding:

Tavakoli J, Amin DB, Freeman BJC, Costi JJ. The biomechanics of the inter-lamellar matrix and the lamellae lumbar disc herniation. Which is the weakest structure? Annals of Biomedical Engineering (I.F. =3.405), 46(9), 1280-1291, 2018.

J. Tavakoli, DB. Amin, Brian JC. Freeman, JJ. Costi. The biomechanical role of lamellae and the inter-lamellar matrix in lumbar disc herniation. Which is the weakest link? Proceedings of the 44th Annual Meeting of the International Society for Study of the Lumbar Spine (ISSLS), Canada, May 2018.

J. Tavakoli, DB. Amin, Brian JC. Freeman, J. Costi. The biomechanical role of lamellae and the inter-lamellar matrix in lumbar disc herniation. Which is the weakest link? 29th Annual Scientific Meeting of Spine Society of Australia (SSA), Australia, Adelaide, April 2018.

8.1 Abstract

While microstructural observations have improved our understanding of possible pathways of herniation progression, no studies have measured the mechanical failure properties of the inter-lamellar matrix (ILM), nor of the adjacent lamellae during progression to herniation. The aim of this study was to employ multiscale, biomechanical and microstructural techniques to evaluate the effects of progressive induced herniation on the ILM and lamellae in control, pre-herniated and herniated discs (N=7), using two year-old ovine spines. Pre-herniated and herniated (experimental) groups were subjected to macroscopic compression while held in flexion (13°), before micro-mechanical testing. Micro-tensile testing of the ILM and the lamella from anterior and posterolateral regions was performed in radial and circumferential directions to measure failure stress, modulus, and toughness in all three groups. The failure stress of the ILM was significantly lower for both experimental groups compared to control in each of radial and circumferential loading directions in the posterolateral region ($p<0.032$). Within each experimental group in both loading directions, the ILM failure stress was significantly lower by 36% (pre-herniation), and 59% (herniation), compared to the lamella ($p<0.029$). In pre-herniated compared to control discs, microstructural imaging revealed significant tissue stretching and change in orientation ($p<0.003$), resulting in a loss of distinction between respective lamellae and ILM boundaries.

8.2 Introduction

The annual prevalence of lumbar disc herniation is estimated at 3-5%[148]. Herniated lumbar discs and resultant radiculopathy have resulted in almost 15 million office-based physician visits per year, creating a financial burden on society exceeding US$50 billion annually [149]. Approximately 300,000 lumbar discectomies are performed each year in the USA, making it the most common procedure performed by spine and neurosurgeons [150, 151].

Disruption of the annulus fibrosus (AF) is manifested as circumferential and radial tears, and rim lesions [3, 113]. These tears are present after cumulative [4, 136] or sudden overloading [5, 6, 152] events that lead to herniation. Circumferential tears are common and were observed in cadaver discs from the teenage years [7]. It is thought that delamination of adjacent lamellae are the first steps towards the development of circumferential tears, which can lead to early disc degeneration[8]. The failure mechanism of circumferential tears is believed to arise from high inter-lamellar shear stresses, which lead to propagation of these tears [28]. Delamination is a known failure mechanism of composite, laminate structures [153, 154], suggesting that the region at highest risk of failure initiation is at the boundary between lamellae, which is referred to as the inter-lamellar matrix (ILM)[9]. Circumferential disruption of the ILM has been observed as a likely pathway for the nucleus material to follow during herniation [4, 6, 17, 155-158]. Microstructural observations have revealed new insights into AF tissue disruption during herniation [4, 6, 17, 25, 26], as well as the delamination strength of isolated AF samples of the ILM [18, 124]. While these studies have improved our understanding of where herniation may initiate, the possible pathways of its progression, and ILM delamination strength, no studies have measured the mechanical failure properties of the ILM, nor of the adjacent lamellae during progression to

herniation. A new approach is required to understand the mechanical roles of the ILM and lamella during herniation, where the disc should be overloaded without herniation (pre-herniation) to create microstructural damage, and compared to herniated and unloaded controls.

Therefore, the aim of this study was to develop a new multiscale, biomechanical and microstructural understanding of the effects of progressive herniation on the ILM and lamellae in control, pre-herniated and herniated discs. The following hypotheses were proposed:

1. The regional micro-mechanical properties of the ILM, compared to the lamellae, will be significantly reduced during progression to herniation.

2. Pre-herniation of the disc will cause micro tissue damage and structural disorganization.

8.3 Materials and Methods

8.3.1 Sample preparation

An ovine model was used for this study based on its structural, biochemical and biomechanical similarities to the human disc [4, 8, 17, 23-25, 47, 48, 137, 138]. Fresh lumbar spines from two year old animals were obtained from a local abattoir, stored at -20° C and then thawed at room temperature. Soft tissue was removed and spines were cut into L3-4 and L4-5 vertebra-disc-vertebra functional spinal units (FSUs) with intact posterior elements and longitudinal ligaments. Within each spine, L4-5 FSUs were allocated to macro- and micro-mechanical testing (N = 7 pre-herniated, and N = 7 herniated), with the adjacent L3-4 FSUs serving as controls that only underwent micro-mechanical testing (Figure 8.1). Since it has been shown that not all discs will herniate

(herniation rate of 60%) [157] , we tested additional spines to failure until we achieved herniated discs (N=7). In total 19 sheep spines were used.

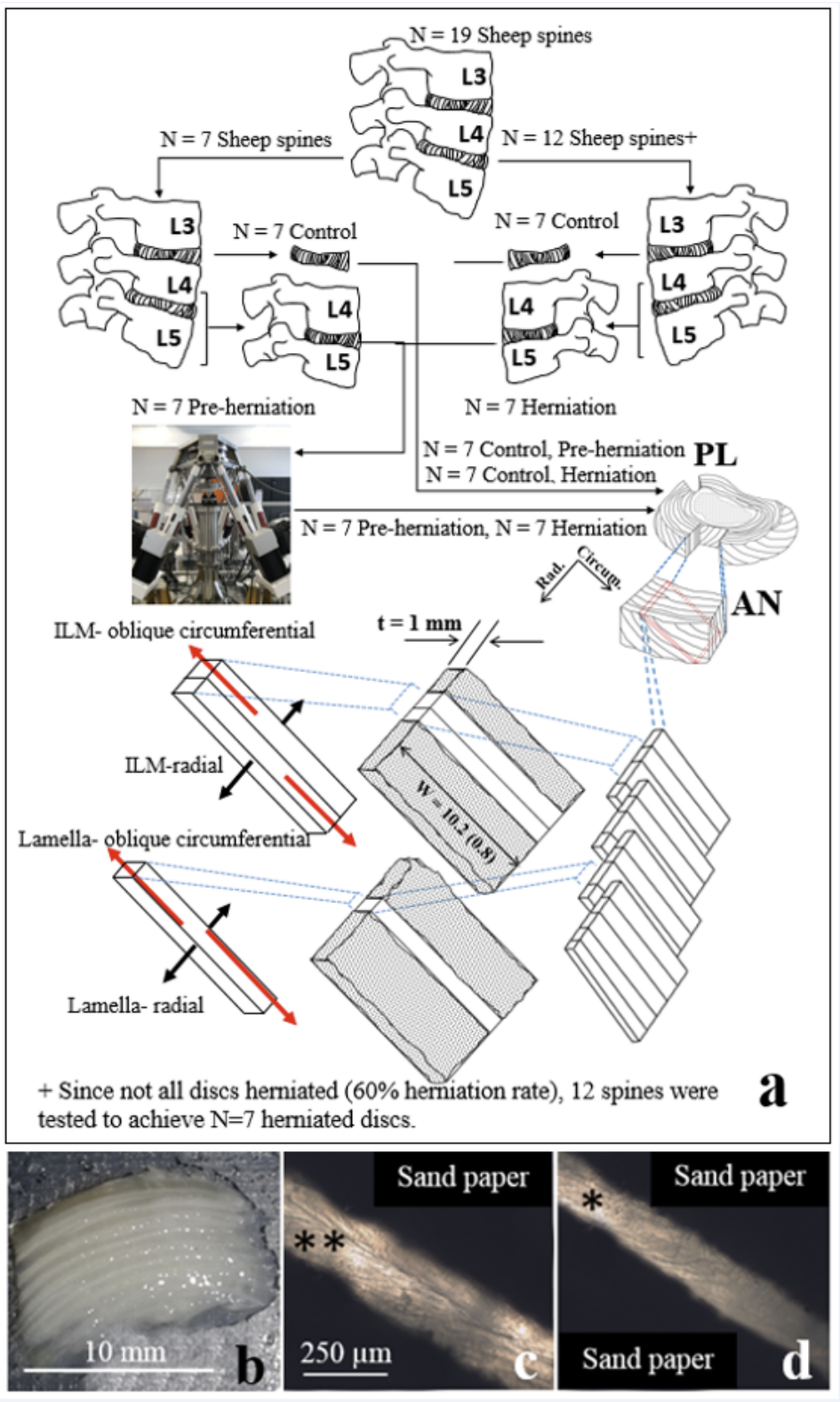

Figure 8.1 Schematic drawing of the study design (a). The pre-herniation (N=7) and herniation (N=7) FSUs were subjected to macroscopic loading. Micro-tensile testing on individual lamella and the ILM from anterior (AN) and posterolateral (PL) regions for control discs (N=14), pre-herniation and herniation FSUs

*was performed in radial and oblique circumferential directions in 224 samples (14 spines× 2 discs per spines × 2 regions per disc (AN, PL) × 2 locations per region (lamellae, ILM) × 2 test loading directions per location (radial, oblique circumferential) =224 samples). The same slicing technique was used for PL region (not shown). Tissue segment (b) and prepared ILM (c) and lamellae (d) samples for micro-mechanical testing was shown and the ILM and lamellae denoted by ** and *, respectively.*

8.3.2 Macro-mechanical Testing

Prior to testing, FSUs were potted in cups, hydrated overnight, and installed in a hexapod robot [128, 130, 159]. Twelve FSUs in the herniation group underwent 13° of flexion about the geometric centre of the disc, followed by a 3 mm compressive displacement at 400 mm/min to create herniation [157]. In the pre-herniation group, the same protocol was used, however 50% of the compressive displacement in the herniation group was applied based on pilot studies finding no evidence of herniation at 1.5 mm of displacement. After loading, the FSU then underwent micro-mechanical testing.

8.3.3 Micro-Mechanical Testing

Discs from the control and pre-herniated/herniation groups were dissected from the vertebral bodies. Tissue segments (10 mm length) from the anterior (AN) and posterolateral (PL) outer AF were separated from each disc, placed in plastic containers (20 mm × 20 mm × 10 mm length× width× thickness) and optimal cutting temperature compound (OCT, Tissue-Tek®, Sakura, Japan) was poured over them. The Moulded samples were stored at -20°C for an hour and adjacent frozen samples (N = 4) were cut from each region (AN, PL) of all discs using a hand microtome at an oblique angle. The mean (95% CI) dimensions of the samples were approximately a thickness of 1 mm, a width of 10.2 (0.8) mm. The oblique cutting angle was chosen to facilitate the identification of both the in-plane single lamellae and the ILM during sample preparation for mechanical testing under light microscopy observation. For the herniated group, samples were taken adjacent to the PL region of nucleus extrusion. All prepared samples

were stored at -20°C for further analysis. Sample preparations for the micro-mechanical tests were conducted using a stereomicroscope (Motic, SMZ-168, China). From each adjacent sample, a single lamella or two adjacent lamellae including the ILM region (ILM-lamellae complex) were identified. Under microscopic observation, a small needle was used to spread cyanoacrylate adhesive, which was mixed with black ink, beyond the identified region (single lamella or the ILM-lamellae complex). Sand paper (250 grit) was placed over the adhesive and bonded to the sample carefully. Sample preparation was performed under microscopic observation to avoid adhesive leakage into the identified region. The micro-mechanical properties of both lamellae and the ILM samples were measured in radial (i.e tension) and oblique circumferential (i.e shear) loading directions. There was no indication of sample slippage during mechanical testing as identified from observation of samples during tests and analysing testing curves. The total number of samples was 224 (Figure 8.1). Samples were hydrated and then attached to a micro-mechanical testing machine (BioTester, CellScale, Canada), preloaded to 100 mN, followed by failure at a strain rate of 10 $\%s^{-1}$ at a sampling rate of 100 Hz. Preload was applied to remove the 'slack' in the sample prior to testing and the magnitude of 100 mN was chosen based on pilot studies. The displacement required to remove this slack region was not included in the strain/displacement measurement.

8.3.4 Microstructural analysis

Four discs from each of control, pre-herniation and herniated groups (N = 12) were used for microstructural analysis after both macro- and micro-mechanical tests. All discs were fixed using 10% formalin in phosphate buffered saline. Tissues from the PL region were dissected from adjacent sections to those harvested for micromechanical testing after being fixed. All dissected tissues were moulded with OCT at approximate angles of 0° and 30° to the transverse plane. Samples (thickness 50 µm) were cut using a cryostat

microtome (Leica Biosystems, CM3050, Germany) from each disc and mounted on microscope slides. Microstructural analysis was performed using light microscopy analysis (SZX 10, Olympus, Japan). Microscopic images of control and pre-herniated samples were analysed to measure lamellae width and orientation using ImageJ [97, 120, 160]. The width was calculated by selecting approximately 30 plot profiles from the control and pre-herniated images of each sample. The plot profile (Fig 6b) displays a two dimensional graph of the intensities of the pixels along a line selection. The X axis represents the horizontal distance along the line and the Y axis shows the vertically averaged pixel intensity. Skeletonized images were used to compare the overall orientation of lamellae and its histogram distribution, relative to X axis (lateral), in control and pre-herniated samples.

8.3.5 Data and Statistical analysis

Failure stress, modulus, and toughness were calculated from engineering stress-strain curves. Failure stress was defined as the peak stress recorded during the test. The modulus measures was calculated as the slope of the best-fit line using linear regression. The toughness, which is a measure of energy absorption, was calculated as the area under stress-strain curve at failure stress. A univariate ANOVA (IBM SPSS Statistics, USA) was conducted for each mechanical parameter having fixed factors of group (control vs. pre-herniated vs. herniation), direction of load application (radial vs. circumferential), type of tissue (lamellae vs. ILM) and region (anterior vs. posterolateral) using an alpha of 0.05, with post-hoc multiple comparisons conducted using a Bonferroni correction on alpha. An unpaired t-test was performed between control and pre-herniated samples for lamellae width and orientation using an alpha of 0.05.

8.4 Results

8.4.1 Macro-mechanical

To obtain the required seven FSUs for the herniation group, 12 FSUs underwent failure testing with five specimens not herniating, and showing signs of endplate failure in the inferior vertebra following dissection. Herniation in the seven FSUs occurred in the posterolateral region of the disc. The mean (95% CI) load to failure for the herniation group was 10.5 (1.5) kN and mean (95% CI) maximum load for the pre-herniation group was 6.4 (1.2) kN (Figure 8.2). Upon visual inspection of the pre-herniated discs, no evidence of herniation was observed.

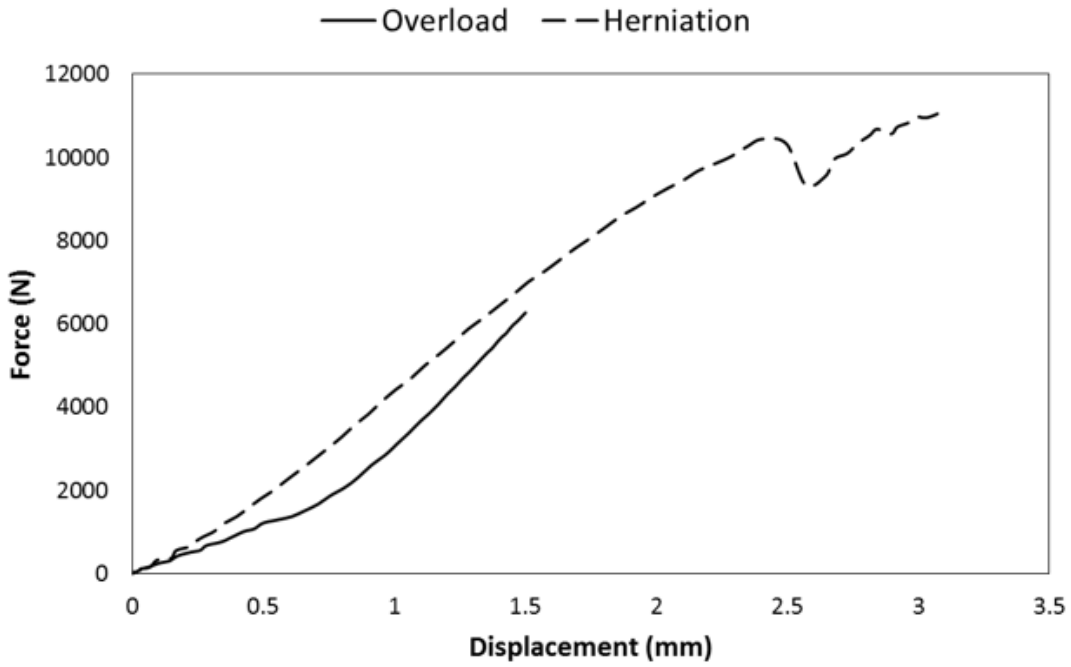

Figure 8.2 Example force-displacement curves from the pre-herniation and herniation groups. No evidence of disc failure was observed during the pre-herniation test, compared to the herniation failure tests.

8.4.2 Micro-mechanical

Within each tissue type (ILM or lamella), there were no significant differences between the two matched control groups for all mechanical parameters and both regions ($p = 1.00$). Therefore, the data for the two control groups were pooled. For failure stress, the overall effects of group, tissue type, and disc region were significant ($p < 0.001$, Table

8.1). Significant interactions were found between group and tissue (p = 0.004, Figure 8.3), as well as region and tissue (p = 0.029). For modulus, no significant overall main effects were found (p > 0.092), with only one overall significant interaction between loading direction and tissue (p = 0.033). For toughness, significant overall effects were found for tissue (p = 0.002) and region (p = 0.020). In addition, the only significant interaction found for toughness was between group and region (p=0.032).

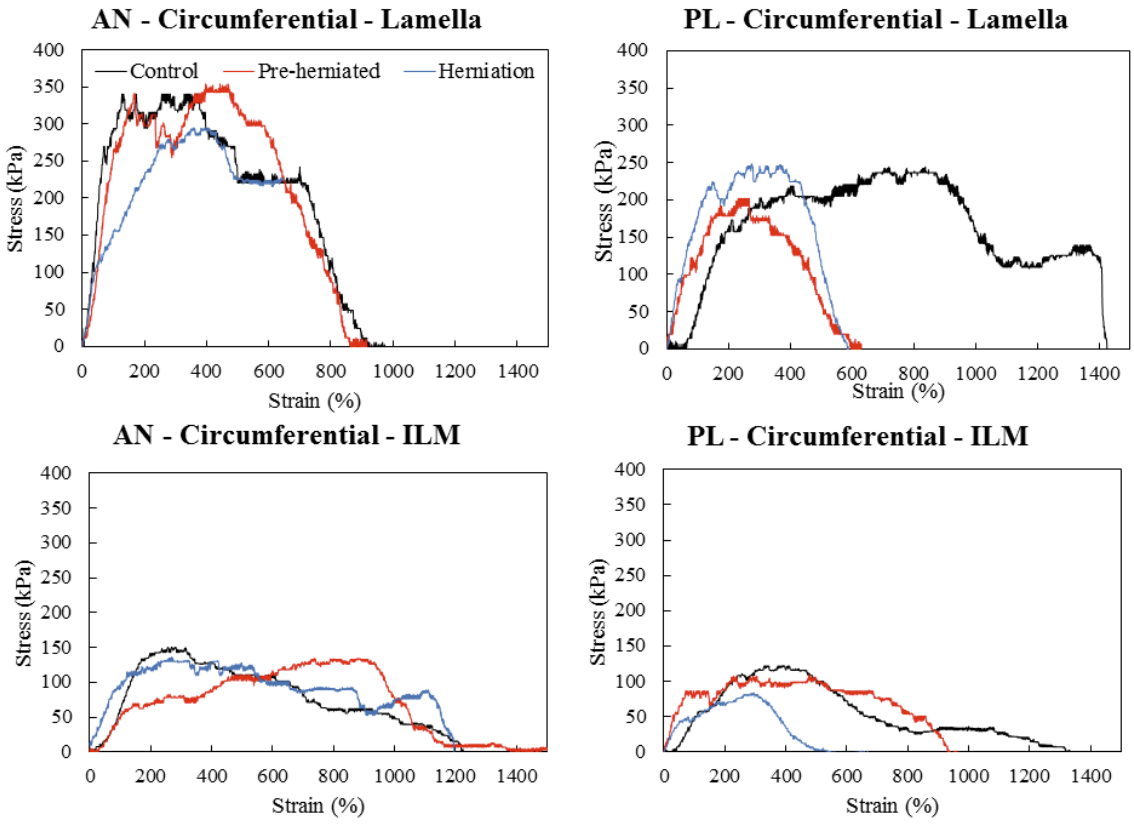

Figure 8.3 Example stress-strain curves from micro-mechanical testing during circumferential loading for all three groups in the posterolateral (PL) and anterior (AN) regions. Samples taken from adjacent samples.

Table 8-1 Summary of ANOVA results for the overall effects of Group (control vs. pre-herniation vs. herniation), Loading Direction (radial vs. circumferential), Tissue Type (lamellae vs. ILM), and Disc Region (anterior vs. posterolateral) and their interactions on each of the dependent micro-mechanical test parameters (Failure Stress, Modulus, and Toughness).

Parameter	Group	Loading Direction	Tissue Type	Disc Region
Failure Stress	Sig. Effect ($p < 0.001$)	No Sig. Effect $p = 0.076$	Sig. Effect ($p < 0.001$)	Sig. Effect ($p < 0.001$)
Sig. Interactions	Group x Tissue Type ($p = 0.004$) Disc Region x Tissue Type ($p = 0.029$)			
Modulus	No Sig. Effect ($p = 0.093$)	No Sig. Effect ($p = 0.253$)	No Sig. Effect ($p = 0.130$)	No Sig. Effect ($p = 0.138$)
Sig. Interactions	Loading Direction x Tissue Type ($p = 0.033$)			
Toughness	No Sig. Effect ($p = 0.678$)	No Sig. Effect ($p = 0.130$)	Sig. Effect ($p = 0.002$)	Sig. Effect ($p = 0.020$)
Sig. Interactions	Group x Disc Region ($p = 0.032$)			

Post-hoc tests revealed that the failure stress for the ILM was significantly lower in the pre-herniation (40%) and herniation (49%) compared to control group during radial loading (Figure 8.4) in the posterolateral region ($p < 0.032$). In circumferential loading (Figure 8.5) the ILM failure stress was significantly decreased by approximately 28% and 48% for pre-herniation and herniation groups compared to the control ($p < 0.032$). However, no significant difference in lamella or ILM failure stress was found between the pre-herniation and herniation groups ($p = 1.00$). Significant post-hoc differences were found in the ILM where control group toughness was greater (76%) than the herniation group during circumferential loading in the posterolateral region ($p = 0.049$).

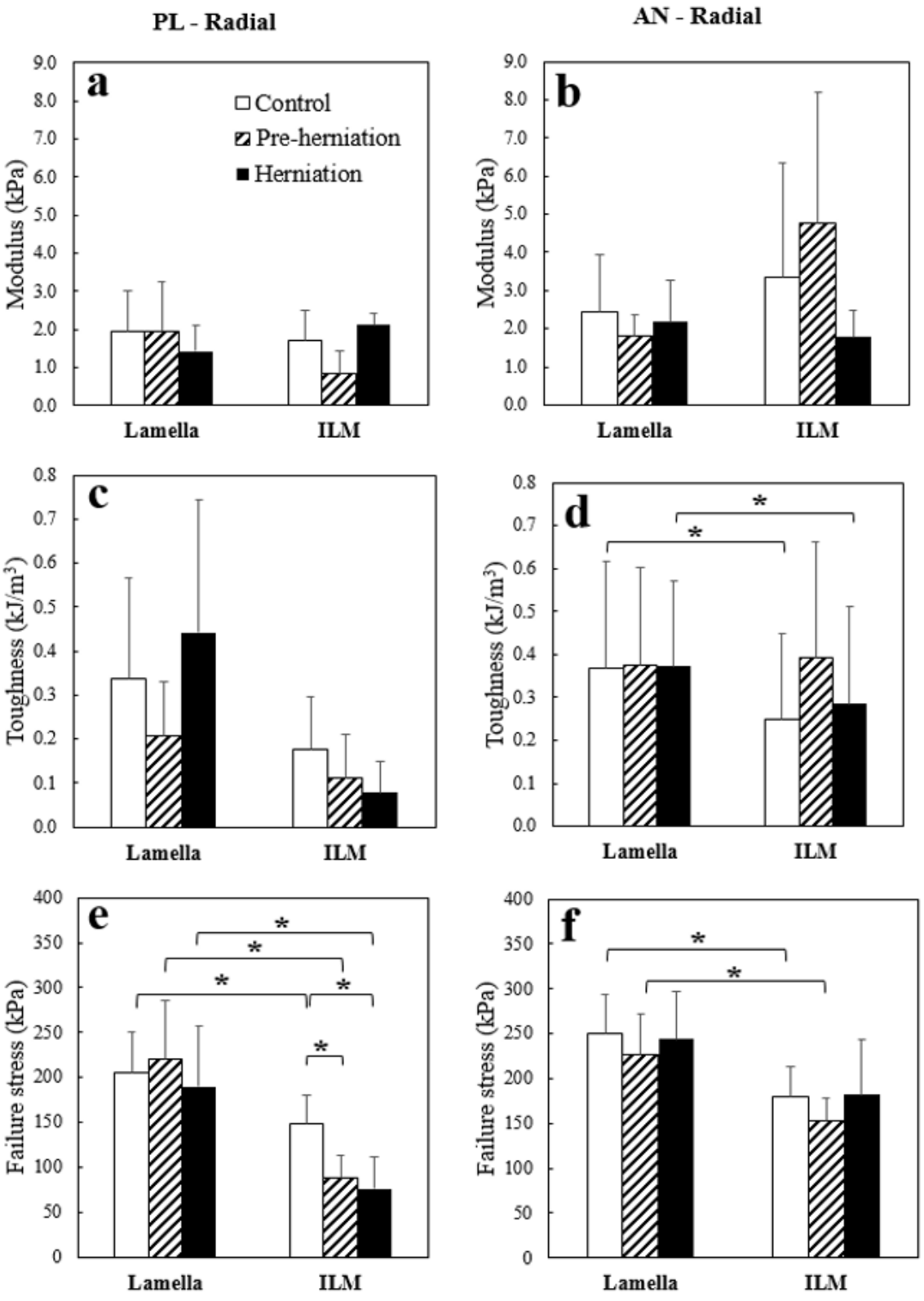

*Figure 8.4 Mean (95% CI) measured micro-mechanical parameters (modulus (a, b), toughness (c, d) and failure stress (e, f)) for ILM and lamella in the posterolateral (PL) and anterior (AN) regions during loading in the radial direction for all groups (control, pre-herniated, and herniation). * denotes significant pairwise differences between- and within-groups and tissue types (Lamella and ILM) ($p < 0.05$)*

Comparing type of tissue, post-hoc tests revealed that the failure stress of the ILM was significantly lower than that of the lamellae under radial loading in the anterior region for the control (28%) ($p < 0.001$) and pre-herniation groups (33%) ($p = 0.003$, Figure 8.3). In the posterolateral region during radial and circumferential loading, ILM failure stress was significantly lower than lamella for all three groups of control (28% and 22%), pre-herniation (60% and 36%) and herniation (60% and 59%) in radial and circumferential directions, respectively ($p < 0.029$, Figures 8.4e, f and 8.5e, f). Under circumferential loading, ILM failure stress was significantly lower than lamella for both pre-herniation (28%) and herniation (36%) groups in the anterior region ($p = 0.016$). Post-hoc tests also revealed ILM toughness to be significantly lower than lamella during radial loading for the control (25%, $p = 0.030$) and herniation (30%, $p = 0.015$) groups in the anterior region (Figure 8.4d).

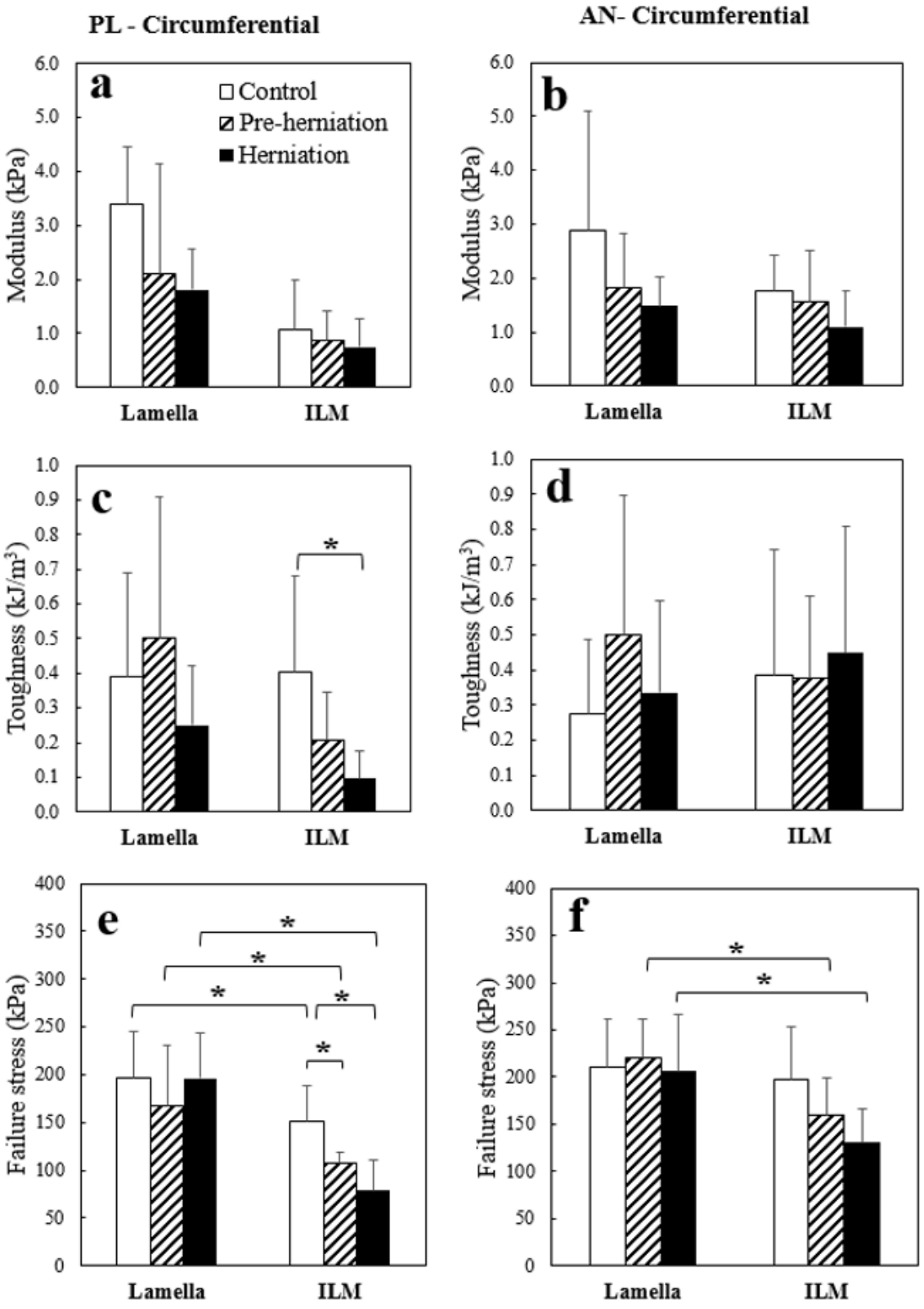

*Figure 8.5 Mean (95% CI) measured micro-mechanical parameters (modulus (a, b), toughness (c, d) and failure stress (e, f)) for ILM and lamella in the posterolateral (PL) and anterior (AN) regions during loading in the circumferential direction for all groups (control, pre-herniation, and herniation). * denotes significant pairwise differences between- and within-groups and tissue types (Lamella and ILM) ($p < 0.05$).*

Comparing disc region, for the lamella, one post-hoc significant regional difference was found where the failure stress in the anterior region was greater (17%) than the posterolateral for the control group during radial loading ($p = 0.015$). For the ILM, the anterior region failure stress was significantly higher than the posterolateral in all three groups: control (18% and 23%, $p < 0.021$), pre-herniation (43% and 32%, $p < 0.008$), and herniation (58% and 40%, $p < 0.015$, Figures 8.4e, f and 8.5e, f) under both radial and circumferential loading, respectively. In addition, toughness in the anterior region was significantly greater (78%) than the posterolateral during circumferential loading in only the herniation group ($p = 0.029$) and during radial loading in both herniation (72%, $p = 0.036$) and pre-herniation groups (65%, $p = 0.030$, Figure 8.4d).

8.4.3 Microstructure

Visual inspection of lamella width from light microscopy images (Figure 8.6) revealed wider lamellae (55%) for pre-herniated compared to control samples. Skeletonized images identified that pre-herniated samples demonstrated a greater level of lamellae disorganization compared to control, where the boundaries of the ILM appeared to merge with lamellae. Results obtained from surface profile plots were consistent with measurements of average lamella width (Table 8.2), which showed an increase in lamellae width after pre-herniation. The lamella width was significantly larger after discs were pre-herniated, compared to control samples ($p = 0.001$). To visualize the degree of lamellae disorganization after pre-herniation, the lamellae orientation and its histogram distribution was measured for control and pre-herniated samples (Figure 8.6, Table 8.2).

A significant difference in the orientation of lamellae between control (43.5 (0.8)°) and pre-herniated (81.6 (6)°) samples (p = 0.002) was found.

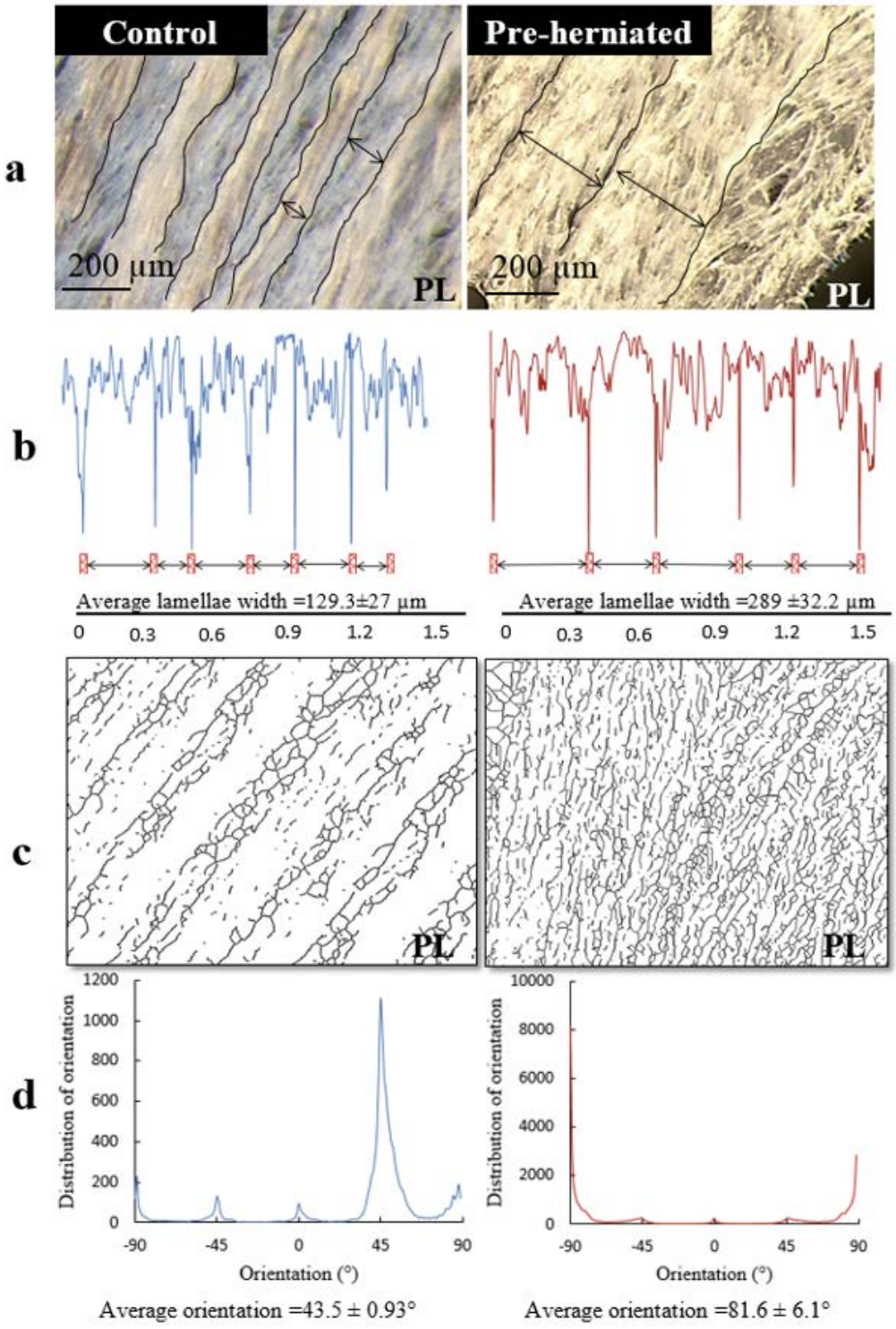

Figure 8.6 Light microscopy images (a) and surface profile plots (b) comparing a control and pre-herniated sample in the outer posterolateral (PL) region revealed a significant effect of pre-herniation on lamellae width (black arrows). The skeletonised images (c) and orientation histogram (d) indicated that pre-herniation altered lamellae orientation. The ILM and lamella were shown by black lines and arrows, respectively.

Table 8-2 Mean (95%CI) measurements of lamellae width and their orientation (relative to the horizontal axis) across four samples for control and pre-herniated FSUs.

Sample	**Lamellae width (µm)**		**Lamellae orientation (°)**	
	Control	Pre-herniated	Control	Pre-herniated
Sample 1	128 (10.4)	332 (26.6)	42 (0.3)	73 (4)
Sample 2	98 (8.28)	292 (20.2)	44 (0.7)	77 (3)
Sample 3	164 (16.6)	276 (23.4)	44 (0.5)	88 (2)
Sample 4	127 (10.8)	256 (21.2)	43 (0.2)	86 (4)
Mean (95%CI)	**129.3 (22.8)**	**289 (27.2)**	**43.5 (0.8)**	**81.6 (6)**

8.4.4 Discussion

The first hypothesis for this study was that the regional micro-mechanical properties of the ILM, compared to the lamellae, will be significantly reduced during progression to herniation. We found that the ILM failure stress, in both radial and circumferential loading, was significantly reduced in pre-herniation and herniation groups, compared to control. However, the failure stress of the ILM after pre-herniation was not significantly different to after herniation (Figures 8.4 and 8.5), suggesting that the ILM was susceptible to mechanical damage at loads below those required to create herniation. In contrast, the lamella exhibited no reduction in failure stress between all three groups. The second hypothesis was that pre-herniation of the disc would cause micro tissue damage and lead to structural disorganization. Light microscopy images revealed significant widening of lamellae, and a significant increase in structural disorganisation from a highly preferential lamellae alignment in control, to a random distribution in pre-herniated discs (Figure 8.6). This micro tissue damage and disorganization resulted in a loss of distinction between respective lamellae and ILM boundaries.

The maximum reported axial compressive failure load that resulted in posterolateral herniation during flexion at a loading rate of 400 mm/min was 11.6 (1.0) kN [157], which

was comparable with our data (10.5 (1.5) kN). In addition, our micro-mechanical results (Tables 8.1 and 8.2) were consistent with other studies. Radial stretching of ox tail lamella indicated that the cohesion stress was 250 kPa, which was similar to lamella failure stress in the anterior and posterolateral regions from this study (250 kPa, and 206 kPa, respectively) [14]. The reported range of failure strength of porcine and human lamella was from 0.18 MPa to 1.88 MPa [136], and 0.14 MPa to 0.46 MPa [60], respectively, in which our results fall. In addition, the peel strength of rabbit ILM, was significantly lower in the posterolateral region than the anterior region, corresponding to the same trends found in this study [57].

We found that the failure stress of the ILM was significantly lower than that of the lamella during both circumferential and radial loading, for pre-herniated and herniated groups compared to control. It is not possible to simultaneously measure the macroscopic properties of the disc while also measuring the micro-mechanical properties at the lamellar interface. Therefore, we used macro-mechanical loading to pre-herniate and herniate the disc, and found significantly reduced mechanical properties of the ILM, which indicated partial failure at this site, compared to the adjacent lamellae. This finding suggests that the ILM may be the weakest structure by providing a pathway for herniation, which has been observed in microstructural studies [17, 155]. In addition, the ILM in the posterolateral region of the disc was significantly weaker than the anterior region, potentially due to a higher number of incomplete lamellae [44]. In support of our findings, the mechanical properties of single and multiple lamella bundles have been found to exhibit both radial and circumferential dependency, with the anterior region being stronger and stiffer than posterolateral [59, 60, 161-163]. Increased mechanical strength of the outer lamellae could be a result of its structure, which is composed of highly packed collagen and elastic fibres compared

to the ILM, which is mainly comprised of elastic fibres [120]. A significant increase in lamella width and orientation was seen after pre-herniation (Figure 8.6), which resulted in lamellae disorganization and disruption. Delamination of the ILM due to high shear stresses [28] potentially severed the elastic fibre network, providing a mechanism for the nucleus to extrude through the ILM via tensile separation of the outer lamellae. Elastic fibres, which provide a well-organized orthotropic network, are the main fibrous element in the ILM. While the presence of collagen fibres in the ILM is less probable, it is unlikely that collagen fibres contribute to the mechanical properties of the ILM, unless they were translamellar bridges [9]. The finding of unaffected modulus that was calculated from the linear region of loading may indicate the contribution of both collagen and elastic fibres, where at 100% strain both lamella and the ILM are loaded, which is consistent with the extensibility of elastic fibres [164]. Further studies using histological staining are required to identify which components (the elastic network of the ILM or collagen fibres at the ILM interface) had failed. Moreover, extracellular matrix within the ILM may interact with elastic fibres and play a role in imparting isotropic failure properties, and likely to contribute to the failure properties of the ILM during progression to herniation.

A microstructural analysis revealed that circumferential progression of the nucleus toward the posterolateral region in the outer AF mainly occurred by ILM delamination (Figure 8.7). Our biomechanical findings support this microstructural observation, indicating that in the outer AF, the ILM is the weakest structure. A study that used a flexion-compression model revealed tears in the mid region of the AF that presented a direct path of extrusion in herniated discs [158]. Another study that tracked the movement of pressurized gel injected directly into the nucleus [17] found that there was a lack of ILM connectivity, which is supported by the biomechanical results of this study,

showing a lower ILM failure stress. While this pressurization study disrupted AF lamellae via a different loading mechanism that may not be physiological, a comparison of nucleus pressures can be performed. Based on the average applied compressive load for pre-herniated discs, and an average ovine disc area of 550 mm^2, the nucleus pressure was estimated to be 17.5 (3.3) MPa [128, 129]. This pressure was higher than from the injected gel study (12.2 (0.4) MPa, posterolateral herniation) [17], and is a factor of seven greater than the in-vivo nucleus pressure of 2.3 MPa measured during lifting a 20 kg weight [128]. Considering these differences to in-vivo pressures, it is not surprising that we measured a significantly reduced failure stress in the ILM after pre-herniation, compared to control, which was no different to that after herniation. Therefore, a threshold of 'safe' compressive loading likely exists, above which a significant reduction in the failure stress of the ILM occurs, which places the disc at greater risk of herniation. The determination of this threshold may be used to support the development of manual handling guidelines to limit lifting motions/repetitions that could cause herniation in both the short- and long-term. Since damage to the disc tissue and cells was found after asymmetric compressive loading [165], the results of the present study may illustrate why delamination contributes to the development of degeneration in the absence of healing.

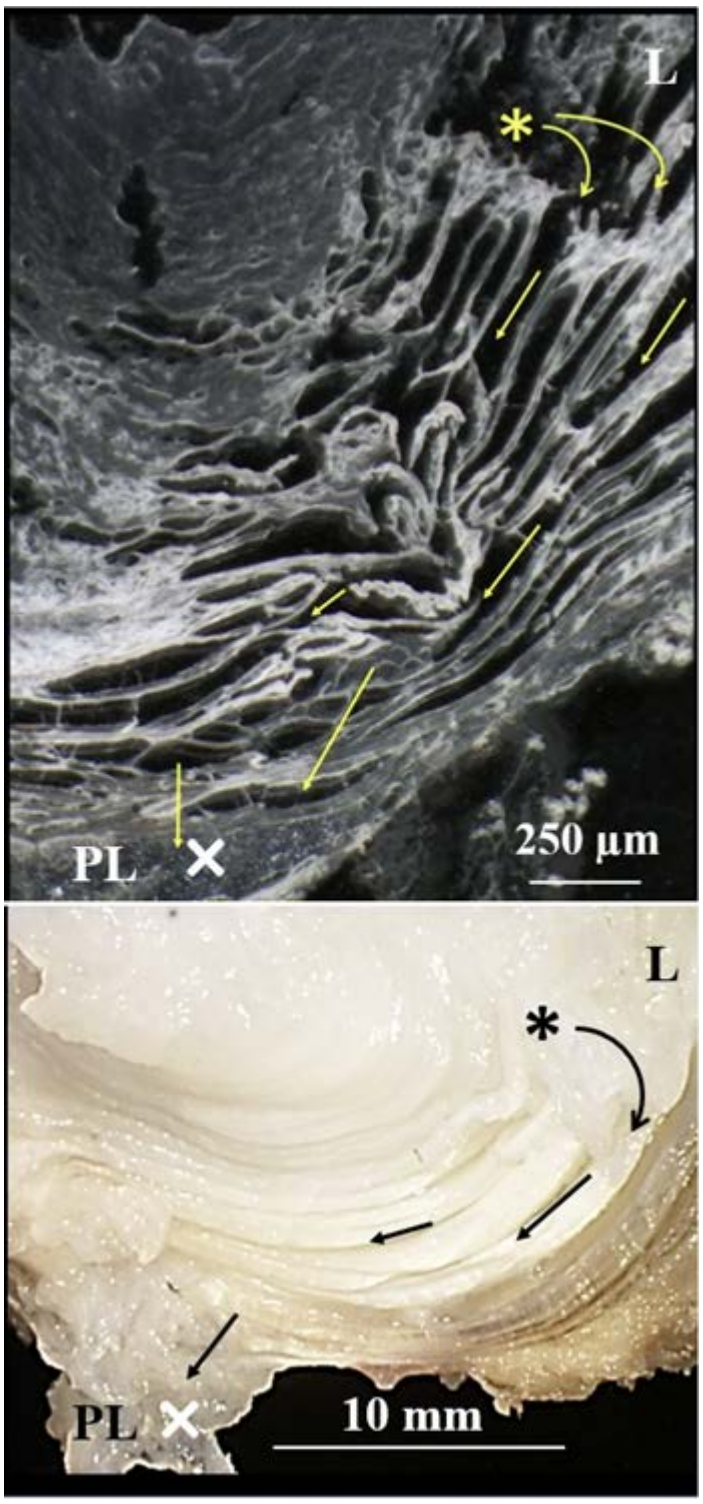

Figure 8.7 Light microscopy (top) and macroscopic (bottom) image of posterolateral (PL) region of two herniated discs revealed an incomplete radial penetration of nucleus into the AF in the lateral (L) region (*), nucleus lateral tracking within the AF (arrows), and herniation site (×).

The limitations of this study included the use of normal ovine discs instead of human, and a small sample size. Ovine discs represent a suitable biochemical, biomechanical, macro- and micro-structural analogy to human discs [4, 8, 17, 23-25, 47, 48, 137, 138].

While there is no consensus whether the disc is degenerated or healthy when herniation occurs [166, 167], we chose two year-old sheep to represent herniation in normal discs without the confounding factor of degeneration. The most notable difference to human discs is geometry and this was accounted for by presenting engineering stress vs. strain. A relatively small sample size of N = 7 per group was used in this study, however we found statistically significant effects for both the mechanical and microstructural parameters.

8.4.5 Conclusion

For the first time, we have demonstrated that compared to the lamella, the ILM is the weaker structure during the progression of herniation in the posterolateral region of the disc. The finding of no differences between ILM failure stress during pre-herniation and herniation suggests that there is a loading threshold above which the ILM loses its structural integrity, which has clinical relevance for recommending safe levels of lifting loads.

9 Chapter 9

9.1 Conclusion and Future Recommendations

The overall aims of this research were to employ a series of multiscale, microstructural and biomechanical studies to evaluate the role of the elastic fibre network on structural integrity of the ILM and its clinical relevance. More specifically, the aims were:

1- To develop a technique for ultrastructural analysis of the elastic fibre network in the disc, while preserving their structural organization.

2- To present an ultrastructural analysis of the elastic fibre network in the AF to compare the architecture of elastic fibres in different regions of the AF and more specifically in the ILM.

3- To measure the viscoelastic and failure properties of the intact ILM and elastic fibre network of the ILM as well as to evaluate the biomechanical properties of the ILM and the lamellae before, during and after lumbar disc herniation.

9.2 Principle Findings

9.2.1 The use of ultrasound and alkali digestion provides a novel technique for visualization of the elastic fibre network in the annulus fibrosus of the disc.

Since elastic fibres are intermingled with other fibrous components of the disc and mostly obscured by the extracellular matrix, it is difficult to demonstrate their ultra-structural organization. Based on the developed novel technique it was identified that sonication of the AF samples in NaOH solution, followed by heat treatment, provide a method for removal of non-elastin components (collagen, micro-fibrils and matrix), and prepared elastic fibres for visualization using SEM. A small difference in fibre orientation was found after digestion compared to the control. The optimum exposure to sonication through the digestion process preserved the organization and ultra-structure arrangement of the elastic network as well as the very delicate elastic fibres can't be

seen usually during light microscopy analysis. Using this technique, ultrastructural analysis of elastic fibres in different regions of the AF could be studied for changes during mechanical loading, injury and disease compared to normal discs. Also, this method can be applied to different discs obtained from other species (bovine, porcine and human) after optimizing time of digestion. The results for this optimization and the detailed process was recently submitted to Materials Science and Engineering C journal as:

Tavakoli J, Costi JJ. A method for visualization and isolation of elastic fibres in annulus fibrosus of the disc, Mater. Sci. Eng. C, 2018, under review.

Also, the relevant images can be found in the following database:

https://researchdata.ands.org.au/ultra-structural-organization-intervertebral-disc/1306246

http://doi.org/10.4226/86/5a680f212c4f1

9.2.2 Elastic fibres within the annulus fibrosus are not randomly organized.

The novel technique that was carefully developed over 18 months, used extracellular matrix partial digestion to address significant gaps in understanding of disc ultrastructure and will contribute to multidisciplinary structure-function studies. Visualization of the ILM under high magnification revealed a dense network of elastic fibres that has not been previously described. Within the ILM, elastic fibres form a complex network, consisting of different size and shape fibres, which differed to those located in the intra-lamellar region. For both regions, the majority of fibres were oriented near 0° with respect to the lamellar circumferential direction, with two minor symmetrical orientations of approximately ±45°. Statistically, the orientation of elastic fibres between the ILM and intra-lamellar region was not different. Also, the ultrastructural analysis revealed that elastic fibres in PBs were a well-organized dense and complex network having different size and shape. Adjacent collagen bundles in a lamella appear to be connected to each other, where elastic fibres in the PBs were merged in parallel or penetrated into the collagen bundles. A continuous network of

elastic fibres that was found across the AF provide disc integrity by connecting adjacent collagen bundles of lamellae together. Compared to the ILM and intra-lamellar region, the density of the elastic fibre network in PBs was lower, and fibre orientation was similar to the intra-lamellar space and inter-lamellar matrix.

9.2.3 The viscoelastic and failure properties of the intact ILM and elastic fibres were characterized for the first time.

The mechanical contribution of the ILM to the structural integrity of the AF as well as the role of elastic fibres in mechanical properties of the ILM were identified in both tension and shear directions of loading. A strain-rate dependent response for both the ILM and elastic fibre network was found during dynamic loading particularly for phase angle and stiffness. The ILM showed higher capability for energy absorption compared to the elastic fibre network with a trend of higher values at smaller strain rates. It was revealed that the ILM and elastic fibre network exhibits more viscoelastic and non-linear elasticity, respectively. The well-organized elastic fibres that create a highly crosslinked and orthotropic network, provide both significant viscoelastic and failure mechanical properties to the ILM. More importantly, for the first time, it was demonstrated that compared to the lamella, the ILM is the weaker structure during the progression of herniation in the posterolateral region of the disc.

9.3 Significance to spinal research

Since previous methods were not able to provide the fine-scale and ultra-architectural details of the elastic fibre network, their ultrastructural organization and role in the intervertebral disc was not clearly understood. The research presented in this thesis is the first to develop a novel technique for extracellular matrix partial digestion to address significant gaps in understanding of disc architecture and relationships between ultrastructural organization of elastic fibres and their function. The biomechanical

characterization of the ILM and the elastic fibre network during measurement of their viscoelastic and failure properties demonstrated their mechanical contribution in the AF. The results of this research can be used to develop and validate advanced multi-scale finite element models of the AF. By understanding the role of the elastic fibre network on delamination and herniation, new strategies for fabricating tissue engineered scaffolds can be proposed.

9.4 Recommendation for future research

Research in this thesis characterised the relationships between structure and function of the elastic fibres of the ILM using an ovine model. Recommendations for future research, based on the findings of this thesis, and from different perspectives are suggested as follows:

While using ovine discs represents a suitable biochemical, biomechanical, macro- and micro-structural analogy to human discs [4, 8, 17, 23-25, 47, 48, 137, 138], further studies will be required using human samples to provide the strongest clinical relevance. On the other hand, since the application of alkali digestion to visualize the elastic fibre network has not been previously reported, further studies investigating the effect of alkali digestion on AF elastic fibre properties are important. Moreover, further studies will be required to investigate the elastic fibre characteristics, and ILM mechanical properties, in different disc regions (e.g., anterior, lateral and posterolateral) for both inner and outer AF, to reveal the effects of age, degeneration or disease on elastic fibre ultrastructural organization.

From a modelling point of view, the findings from this thesis can be utilized to improve existing finite element models of the intervertebral disc [168, 169] by implementing the mechanical role of elastic fibres in the structural integrity of the AF. The measured

viscoelastic properties of the ILM in this thesis needs to be considered in previous finite element models of the AF. While the mechanical results of this thesis are applicable in the radial and circumferential directions, more studies are required to identify the mechanical properties of elastic fibres in the axial direction, especially at the AF-end plate (vertebral body) junction. Some studies have been performed to explain this important subject microstructurally [25, 45]; however, to the best of my knowledge no study has been conducted to measure the biomechanical properties of the elastic fibres at the AF-endplate site. Also there is a lack of knowledge about how elastic fibres are extended from NP towards the AF in the radial direction. Based on the developed method in this thesis, the ultrastructure of the elastic fibres in the transition zone (the region between the AF and NP) can be studied. Hence, the structural interconnectivity between the AF and NP would be identified and the mechanical properties of this region would be characterized. This important approach may serve to clarify from where and how herniation may initiate and propagate, and to establish a 3D structural-based model for herniation.

From a multi-scale perspective, the role of elastic fibres on the biomechanical properties of the whole disc is still a mystery. Based on the results of this thesis and several previous studies, the role of elastic fibres on mechanical properties of the AF at the nano and micro levels were identified [15, 24]. However, more studies are required to measure the mechanical properties of the whole disc under six degree of freedom (6DOF) loading in the absence of elastic fibres, which would present a challenging task. The selective digestion of elastic fibres in the disc and application of 6DOF loading to pre-herniate and herniate the disc would increase our knowledge about the role of elastic fibres in the mechanical properties of the disc.

9.5 Concluding statement

The findings from this thesis augment the understanding of the mechanical-structural relationship in the AF of the disc by using a multiscale approach. For the first time, a unique and novel method was developed for ultrastructural analysis of the elastic fibre network in the AF of the disc. The ultrastructural studies, further highlighted the mechanical role of the intact ILM and elastic fibres that have not been reported before. From a clinical point of view, for the first time, it was demonstrated that the ILM is weaker, and provides a pathway of least resistance than the lamella during the process of lumbar disc herniation. Based on the findings presented within this thesis, future work is required to elucidate the mechanism of herniation by presenting a 3D structural-based model and an effective strategy for AF regenerative closure.

References

1. Government, A. *Australia's health 2010*. Cat. no: AUS 122 2010; 2010:[Available from: https://www.aihw.gov.au/reports/australias-health/australias-health-2010/contents/table-of-contents.
2. Government, A. *Health expenditure for arthritis and musculoskeletal conditions, 2004-05*. 2009; Available from: https://www.aihw.gov.au/reports/health-welfare-expenditure/health-expenditure-for-arthritis-and-musculoskelet/contents/table-of-contents.
3. Ninomiya, M. and T. Muro, *Pathoanatomy of lumbar disc herniation as demonstrated by computed tomography/discography.* Spine (Phila Pa 1976), 1992. **17**(11): p. 1316-22.
4. Veres, S.P., P.A. Robertson, and N.D. Broom, *ISSLS prize winner: how loading rate influences disc failure mechanics: a microstructural assessment of internal disruption.* Spine, 2010. **35**(21): p. 1897-1908.
5. Adams, M.A., et al., *Mechanical initiation of intervertebral disc degeneration.* Spine (Phila Pa 1976), 2000. **25**(13): p. 1625-36.
6. Veres, S.P., P.A. Robertson, and N.D. Broom, *The morphology of acute disc herniation: a clinically relevant model defining the role of flexion.* Spine (Phila Pa 1976), 2009. **34**(21): p. 2288-96.
7. Vernon-Roberts, B., R.J. Moore, and R.D. Fraser, *The natural history of age-related disc degeneration: the pathology and sequelae of tears.* Spine (Phila Pa 1976), 2007. **32**(25): p. 2797-804.
8. Fazzalari, N.L., et al., *Mechanical and Pathologic Consequences of Induced Concentric Anular Tears in an Ovine Model.* Spine, 2001. **26**(23): p. 2575-2581.
9. Tavakoli, J., D.M. Elliott, and J.J. Costi, *Structure and mechanical function of the inter-lamellar matrix of the annulus fibrosus in the disc.* J Orthop Res, 2016. **34**(8): p. 1307-15.
10. Bruehlmann, S.B., et al., *Regional variations in the cellular matrix of the annulus fibrosus of the intervertebral disc.* J Anat, 2002. **201**(2): p. 159-71.
11. Smith, L.J. and N.L. Fazzalari, *The elastic fibre network of the human lumbar anulus fibrosus: architecture, mechanical function and potential role in the progression of intervertebral disc degeneration.* Eur Spine J, 2009. **18**(4): p. 439-48.
12. Melrose, J., et al., *Aggrecan, versican and type VI collagen are components of annular translamellar crossbridges in the intervertebral disc.* European Spine Journal, 2008. **17**(2): p. 314-324.
13. Yu, J., et al., *Microfibrils, elastin fibres and collagen fibres in the human intervertebral disc and bovine tail disc.* Journal of anatomy, 2007. **210**(4): p. 460-471.
14. Pezowicz, C.A., P.A. Robertson, and N.D. Broom, *Intralamellar relationships within the collagenous architecture of the annulus fibrosus imaged in its fully hydrated state.* Journal of Anatomy, 2005. **207**(4): p. 299-312.
15. Smith, L.J., et al., *Elastic fibers enhance the mechanical integrity of the human lumbar anulus fibrosus in the radial direction.* Annals of Biomedical Engineering, 2008. **36**(2): p. 214-223.
16. Smith, L.J. and N.L. Fazzalari, *Regional variations in the density and arrangement of elastic fibres in the anulus fibrosus of the human lumbar disc.* Journal of Anatomy, 2006. **209**(3): p. 359-367.
17. Veres, S.P., P.A. Robertson, and N.D. Broom, *ISSLS Prize Winner: Microstructure and Mechanical Disruption of the Lumbar Disc Annulus Part II: How the Annulus Fails Under Hydrostatic Pressure.* Spine, 2008. **33**(25): p. 2711-2720.
18. Gregory, D.E., et al., *Anular delamination strength of human lumbar intervertebral disc.* European Spine Journal, 2012. **21**(9): p. 1716-1723.

19. Lee, S.H., et al., *In vitro measurement of pressure in intervertebral discs and annulus fibrosus with and without annular tears during discography.* Spine J, 2004. **4**(6): p. 614-8.
20. Przybyla, A., et al., *Outer annulus tears have less effect than endplate fracture on stress distributions inside intervertebral discs: Relevance to disc degeneration.* Clinical Biomechanics, 2006. **21**(10): p. 1013-1019.
21. Osti, O.L., et al., *Annular tears and disc degeneration in the lumbar spine. A post-mortem study of 135 discs.* J Bone Joint Surg Br, 1992. **74**(5): p. 678-82.
22. Ciapetti, G., et al., *Ex vivo observation of human intervertebral disc tissue and cells isolated from degenerated intervertebral discs.* European Spine Journal, 2012. **21**: p. S10-S19.
23. Schollum, M.L., P.A. Robertson, and N.D. Broom, *ISSLS Prize Winner: Microstructure and Mechanical Disruption of the Lumbar Disc Annulus Part I: A Microscopic Investigation of the Translamellar Bridging Network.* Spine, 2008. **33**(25): p. 2702-2710.
24. Mengoni, M., et al., *Derivation of inter-lamellar behaviour of the intervertebral disc annulus.* Journal of the Mechanical Behavior of Biomedical Materials, 2015. **48**: p. 164-172.
25. Veres, S.P., P.A. Robertson, and N.D. Broom, *The influence of torsion on disc herniation when combined with flexion.* European Spine Journal, 2010. **19**(9): p. 1468-1478.
26. Pezowicz, C.A., et al., *Mechanisms of Anular Failure Resulting From Excessive Intradiscal Pressure: A Microstructural-Micromechanical Investigation.* Spine, 2006. **31**(25): p. 2891-2903.
27. Pezowicz, C.A., P.A. Robertson, and N.D. Broom, *The structural basis of interlamellar cohesion in the intervertebral disc wall.* Journal of Anatomy, 2006. **208**(3): p. 317-330.
28. Iatridis, J.C. and I. ap Gwynn, *Mechanisms for mechanical damage in the intervertebral disc annulus fibrosus.* Journal of Biomechanics, 2004. **37**(8): p. 1165-1175.
29. Sivan, S.S., et al., *Biochemical composition and turnover of the extracellular matrix of the normal and degenerate intervertebral disc.* Eur Spine J, 2014. **23 Suppl 3**: p. S344-53.
30. Ortolani, F., et al., *Localization of different alcian blue-proteoglycan particles in the intervertebral disc.* Basic Appl Histochem, 1988. **32**(4): p. 443-53.
31. Shine, K.M. and M. Spector, *The presence and distribution of lubricin in the caprine intervertebral disc.* Journal of Orthopaedic Research, 2008. **26**(10): p. 1398-1406.
32. Baldwin, A.K., et al., *Elastic fibres in health and disease.* Expert Reviews in Molecular Medicine, 2013. **15**.
33. Hayes, A.J., et al., *Comparative immunolocalization of the elastin fiber-associated proteins fibrillin-1, LTBP-2, and MAGP-1 with components of the collagenous and proteoglycan matrix of the fetal human intervertebral disc.* Spine (Phila Pa 1976), 2011. **36**(21): p. E1365-72.
34. Johnson, E.F., et al., *Elastic fibres in the anulus fibrosus of the adult human lumbar intervertebral disc. A preliminary report.* J Anat, 1985. **143**: p. 57-63.
35. Melrose, J., P. Ghosh, and T.K. Taylor, *A comparative analysis of the differential spatial and temporal distributions of the large (aggrecan, versican) and small (decorin, biglycan, fibromodulin) proteoglycans of the intervertebral disc.* J Anat, 2001. **198**(Pt 1): p. 3-15.
36. Urban, J.P., et al., *Swelling pressures of proteoglycans at the concentrations found in cartilaginous tissues.* Biorheology, 1979. **16**(6): p. 447-64.
37. Iatridis, J.C., et al., *Measurements of proteoglycan and water content distribution in human lumbar intervertebral discs.* Spine, 2007. **32**(14): p. 1493-1497.
38. Mikawa, Y., et al., *Elastin in the human intervertebral disk. A histological and biochemical study comparing it with elastin in the human yellow ligament.* Arch Orthop Trauma Surg, 1986. **105**(6): p. 343-9.

39. Kielty, C.M. and C.A. Shuttleworth, *Microfibrillar elements of the dermal matrix.* Microscopy Research and Technique, 1997. **38**(4): p. 413-427.
40. Han, S.K., et al., *Three dimensional mesoscale analysis of translamellar cross-bridge morphologies in the annulus fibrosus using optical coherence tomography.* Journal of Orthopaedic Research, 2015. **33**(3): p. 304-311.
41. Smith, L.J. and D.M. Elliott, *Formation of lamellar cross bridges in the annulus fibrosus of the intervertebral disc is a consequence of vascular regression.* Matrix Biology, 2011. **30**(4): p. 267-274.
42. Bruehlmann, S.B., P.A. Hulme, and N.A. Duncan, *In situ intercellular mechanics of the bovine outer annulus fibrosus subjected to biaxial strains.* Journal of biomechanics, 2004. **37**(2): p. 223-31.
43. Cassidy, J.J., A. Hiltner, and E. Baer, *Hierarchical structure of the intervertebral disc.* Connect Tissue Res, 1989. **23**(1): p. 75-88.
44. Marchand, F. and A.M. Ahmed, *Investigation of the laminate structure of lumbar disc anulus fibrosus.* Spine (Phila Pa 1976), 1990. **15**(5): p. 402-10.
45. Yu, J., et al., *Elastic fibre organization in the intervertebral discs of the bovine tail.* Journal of anatomy, 2002. **201**(6): p. 465-475.
46. Michalek, A.J., et al., *Measurement of local strains in intervertebral disc anulus fibrosus tissue under dynamic shear: contributions of matrix fiber orientation and elastin content.* J Biomech, 2009. **42**(14): p. 2279-85.
47. Schollum, M.L., P.A. Robertson, and N.D. Broom, *How age influences unravelling morphology of annular lamellae - a study of interfibre cohesivity in the lumbar disc.* Journal of Anatomy, 2010. **216**(3): p. 310-319.
48. Schollum, M.L., P.A. Robertson, and N.D. Broom, *A microstructural investigation of intervertebral disc lamellar connectivity: detailed analysis of the translamellar bridges.* Journal of Anatomy, 2009. **214**(6): p. 805-816.
49. Smith, L.J. and N.L. Fazzalari, *The elastic fibre network of the human lumbar anulus fibrosus: architecture, mechanical function and potential role in the progression of intervertebral disc degeneration.* European Spine Journal, 2009. **18**(4): p. 439-448.
50. Yu, J., et al., *Microfibrils, elastin fibres and collagen fibres in the human intervertebral disc and bovine tail disc.* Journal of Anatomy, 2007. **210**(4): p. 460-471.
51. Elliott, D.M. and L.A. Setton, *Anisotropic and inhomogeneous tensile behavior of the human anulus fibrosus: experimental measurement and material model predictions.* J Biomech Eng, 2001. **123**(3): p. 256-63.
52. Hsieh, A.H. and J.D. Twomey, *Cellular mechanobiology of the intervertebral disc: new directions and approaches.* Journal of biomechanics, 2010. **43**(1): p. 137-45.
53. Isaacs, J.L., et al., *Role of biomolecules on annulus fibrosus micromechanics: Effect of enzymatic digestion on elastic and failure properties.* Journal of the Mechanical Behavior of Biomedical Materials, 2014. **40**: p. 75-84.
54. Kirking, B., T. Hedman, and J. Criscione, *Changes in the interfacial shear resistance of disc annulus fibrosus from genipin crosslinking.* Journal of Biomechanics, 2014. **47**(1): p. 293-296.
55. Jacobs, N.T., et al., *Effect of orientation and targeted extracellular matrix degradation on the shear mechanical properties of the annulus fibrosus.* Journal of the Mechanical Behavior of Biomedical Materials, 2011. **4**(8): p. 1611-1619.
56. Roughley, P.J., *Biology of intervertebral disc aging and degeneration - Involvement of the extracellular matrix.* Spine, 2004. **29**(23): p. 2691-2699.
57. Gregory, D.E., et al., *Disc degeneration reduces the delamination strength of the annulus fibrosus in the rabbit annular disc puncture model.* The Spine Journal, 2014. **14**(7): p. 1265-1271.
58. Cloyd, J.M. and D.M. Elliott, *Elastin content correlates with human disc degeneration in the anulus fibrosus and nucleus pulposus.* Spine, 2007. **32**(17): p. 1826-1831.

59. Acaroglu, E.R., et al., *Degeneration and aging affect the tensile behavior of human lumbar anulus fibrosus.* Spine, 1995. **20**(24): p. 2690-2701.
60. Fujita, Y., N.A. Duncan, and J.C. Lotz, *Radial tensile properties of the lumbar annulus fibrosus are site and degeneration dependent.* Journal of Orthopaedic Research, 1997. **15**(6): p. 814-819.
61. Nerurkar, N.L., D.M. Elliott, and R.L. Mauck, *Mechanical design criteria for intervertebral disc tissue engineering.* Journal of Biomechanics, 2010. **43**(6): p. 1017-1030.
62. Gosline, J.M., *The physical properties of elastic tissue.* International review of connective tissue research, 1976. **7**: p. 211-49.
63. Lillie, M.A. and J.M. Gosline, *The effects of hydration on the dynamic mechanical properties of elastin.* Biopolymers, 1990. **29**(8-9): p. 1147-60.
64. Nerurkar, N.L., R.L. Mauck, and D.M. Elliott, *Modeling interlamellar interactions in angle-ply biologic laminates for annulus fibrosus tissue engineering.* Biomechanics and Modeling in Mechanobiology, 2011. **10**(6): p. 973-984.
65. Labus, K.M., et al., *A Computational Model to Describe the Regional Interlamellar Shear of the Annulus Fibrosus.* Journal of Biomechanical Engineering-Transactions of the Asme, 2014. **136**(5).
66. Goel, V.K., et al., *Interlaminar Shear Stresses and Laminae Separation in a Disc - Finite-Element Analysis of the L3-L4 Motion Segment Subjected to Axial Compressive Loads.* Spine, 1995. **20**(6): p. 689-698.
67. Costi, J.J., et al., *Direct measurement of intervertebral disc maximum shear strain in six degrees of freedom: motions that place disc tissue at risk of injury.* Journal of biomechanics, 2007. **40**(11): p. 2457-66.
68. O'Connell, G.D., et al., *Axial creep loading and unloaded recovery of the human intervertebral disc and the effect of degeneration.* Journal of the Mechanical Behavior of Biomedical Materials, 2011. **4**(7): p. 933-942.
69. Ushiki, T., *Collagen fibers, reticular fibers and elastic fibers. A comprehensive understanding from a morphological viewpoint.* Archives of Histology and Cytology, 2002. **65**(2): p. 109-126.
70. Yu, J., *Elastic tissues of the intervertebral disc.* Biochem Soc Trans, 2002. **30**(Pt 6): p. 848-52.
71. Guo, Z., et al., *Fibre–matrix interaction in the human annulus fibrosus.* Journal of the Mechanical Behavior of Biomedical Materials, 2012. **5**(1): p. 193-205.
72. Wade, K.R., P.A. Robertson, and N.D. Broom, *On how nucleus-endplate integration is achieved at the fibrillar level in the ovine lumbar disc.* Journal of Anatomy, 2012. **221**(1): p. 39-46.
73. Green, E.M., et al., *The structure and micromechanics of elastic tissue.* Interface Focus, 2014. **4**(2): p. 20130058.
74. Crissman, R.S., *SEM observations of the elastic networks in canine femoral artery.* Am J Anat, 1986. **175**(4): p. 481-92.
75. Crissman, R.S. and W. Guilford, *The three-dimensional architecture of the elastic-fiber network in canine hepatic portal system.* Am J Anat, 1984. **171**(4): p. 401-13.
76. Crissman, R.S. and L.A. Pakulski, *A Rapid Digestive Technique to Expose Networks of Vascular Elastic Fibers for Sem Observation.* Stain Technology, 1984. **59**(3): p. 171-180.
77. Richards, A.N. and W.J. Gies, *CHEMICAL STUDIES OF ELASTIN, MUCOID, AND OTHER PROTEIDS IN ELASTIC TISSUE, WITH SOME NOTES ON LIGAMENT EXTRACTIVES.* American Journal of Physiology -- Legacy Content, 1902. **7**(1): p. 93-134.
78. Samouillan, V., et al., *Characterisation of elastin and collagen in aortic bioprostheses.* Medical and Biological Engineering and Computing, 2000. **38**(2): p. 226-231.
79. Rezakhaniha, R., et al., *Experimental investigation of collagen waviness and orientation in the arterial adventitia using confocal laser scanning microscopy.* Biomech Model Mechanobiol, 2012. **11**(3-4): p. 461-73.

80. Tavakoli, J. and J.J. Costi, *A method for visualization and isolation of elastic fibres in annulus fibrosus of the disc.* Materials Science and Engineering: C, 2018. **93**: p. 299-304.
81. Kewley, M.A., F.S. Steven, and G. Williams, *The presence of fine elastin fibrils within the elastin fibre observed by scanning electron microscopy.* Journal of anatomy, 1977. **123**(Pt 1): p. 129-34.
82. Hickey, D.S. and D.W. Hukins, *Collagen fibril diameters and elastic fibres in the annulus fibrosus of human fetal intervertebral disc.* J Anat, 1981. **133**(Pt 3): p. 351-7.
83. Long, R.G., et al., *Mechanical restoration and failure analyses of a hydrogel and scaffold composite strategy for annulus fibrosus repair.* Acta Biomaterialia, 2016. **30**: p. 116-125.
84. Humzah, M.D. and R.W. Soames, *Human intervertebral disc: Structure and function.* The Anatomical Record, 1988. **220**(4): p. 337-356.
85. Vergari, C., et al., *Lamellar and fibre bundle mechanics of the annulus fibrosus in bovine intervertebral disc.* Acta Biomaterialia, 2016. **37**: p. 14-20.
86. Ushiki, T., *Collagen fibers, reticular fibers and elastic fibers. A comprehensive understanding from a morphological viewpoint.* Arch Histol Cytol, 2002. **65**(2): p. 109-26.
87. Montes, G.S., *Structural biology of the fibres of the collagenous and elastic systems.* Cell Biology International, 1996. **20**(1): p. 15-27.
88. Yu, J., et al., *ISSLS Prize Winner: A Detailed Examination of the Elastic Network Leads to a New Understanding of Annulus Fibrosus Organization.* Spine (Phila Pa 1976), 2015. **40**(15): p. 1149-57.
89. Buckwalter, J.A., R.R. Cooper, and J.A. Maynard, *Elastic fibers in human intervertebral discs.* The Journal of Bone & Joint Surgery, 1976. **58**(1): p. 73.
90. Johnson, E.F., et al., *The distribution and arrangement of elastic fibres in the intervertebral disc of the adult human.* J Anat, 1982. **135**(Pt 2): p. 301-9.
91. Akhtar, S., J.R. Davies, and B. Caterson, *Ultrastructural immunolocalization of alpha-elastin and keratan sulfate proteoglycan in normal and scoliotic lumbar disc.* Spine, 2005. **30**(15): p. 1762-1769.
92. Graham, H.K., et al., *Tissue section AFM: In situ ultrastructural imaging of native biomolecules.* Matrix Biology, 2010. **29**(4): p. 254-260.
93. Han, W.M., et al., *Multi-scale structural and tensile mechanical response of annulus fibrosus to osmotic loading.* Annals of biomedical engineering, 2012. **40**(7): p. 1610-21.
94. Inoue, H. and T. Takeda, *Three-dimensional observation of collagen framework of lumbar intervertebral discs.* Acta Orthop Scand, 1975. **46**(6): p. 949-56.
95. Inoue, H., *Three-dimensional observation of collagen framework of intervertebral discs in rats, dogs and humans.* Arch Histol Jpn, 1973. **36**(1): p. 39-56.
96. Inoue, H., *Three-dimensional architecture of lumbar intervertebral discs.* Spine (Phila Pa 1976), 1981. **6**(2): p. 139-46.
97. Tavakoli, J. and J.J. Costi, *Development of a rapid matrix digestion technique for ultrastructural analysis of elastic fibers in the intervertebral disc.* Journal of the Mechanical Behavior of Biomedical Materials, 2017. **71**: p. 175-183.
98. Crissman, R.S. and F.N. Low, *A study of fine structural changes in the cartilage-to-bone transition within the developing chick vertebra.* Am J Anat, 1974. **140**(4): p. 451-69.
99. Crissman, R.S., J.N. Ross, Jr., and T. Davis, *Scanning electron microscopy of an elastic fiber network which forms the internal elastic lamina in canine saphenous vein.* Anat Rec, 1980. **198**(4): p. 581-93.
100. Hossler, F.E. and F.C. Monson, *Microvasculature of the Rabbit Urinary-Bladder.* Anatomical Record, 1995. **243**(4): p. 438-448.
101. Nadasy, G.L., et al., *Passive geometric and elastic properties of human cadaver common carotid artery segments after intraluminal enzyme digestion with the aid of a four-way double balloon catheter.* Cor Vasa, 1991. **33**(1): p. 58-67.

102. Crissman, R.S., *The three-dimensional configuration of the elastic fiber network in canine saphenous vein. A stereo scanning electron microscopic study.* Blood Vessels, 1984. **21**(4): p. 156-70.
103. Crissman, R.S., *Comparison of Two Digestive Techniques for Preparation of Vascular Elastic Networks for SEM Observation.* Journal of Electron Microscopy Technique, 1987. **6**(4): p. 335-348.
104. Speakman, J.R., *Body composition analysis of animals: a handbook of non-destructive methods*. 2001: Cambridge University Press.
105. Steven, F.S., R.J. Minns, and H. Thomas, *The Isolation of Chemically Pure Elastins in a Form Suitable for Mechanical Testing.* Connective Tissue Research, 1974. **2**(2): p. 85-90.
106. Tseng, H. and K.J. Grande-Allen, *Elastic fibers in the aortic valve spongiosa: a fresh perspective on its structure and role in overall tissue function.* Acta biomaterialia, 2011. **7**(5): p. 2101-2108.
107. Yu, J., et al., *The elastic fiber network of the anulus fibrosus of the normal and scoliotic human intervertebral disc.* Spine (Phila Pa 1976), 2005. **30**(16): p. 1815-20.
108. Urban, J.P. and S. Roberts, *Degeneration of the intervertebral disc.* Arthritis Res Ther, 2003. **5**(3): p. 120-30.
109. Crean, J.K., et al., *Matrix metalloproteinases in the human intervertebral disc: role in disc degeneration and scoliosis.* Spine (Phila Pa 1976), 1997. **22**(24): p. 2877-84.
110. Mecham, R.P., et al., *Elastin degradation by matrix metalloproteinases. Cleavage site specificity and mechanisms of elastolysis.* J Biol Chem, 1997. **272**(29): p. 18071-6.
111. Fujita, K., et al., *Neutral proteinases in human intervertebral disc. Role in degeneration and probable origin.* Spine (Phila Pa 1976), 1993. **18**(13): p. 1766-73.
112. Saunders, J.M. and V.T. Inman, *PAthology of the intervertebral disk.* Archives of Surgery, 1940. **40**(3): p. 389-416.
113. Hirsch, C. and F. Schajowicz, *Studies on structural changes in the lumbar annulus fibrosus.* Acta Orthop Scand, 1952. **22**(1-4): p. 184-231.
114. Sylvest, J., B. Hentzer, and T. Kobayasi, *Ultrastructure of prolapsed disc.* Acta Orthopaedica Scandinavica, 1977. **48**(1): p. 32-40.
115. Postacchini, F., et al., *An ultrastructural study of recurrent disc herniation: a preliminary report.* Spine (Phila Pa 1976), 1982. **7**(5): p. 492-7.
116. Olczyk, K., *Age-Related-Changes of Elastin Content in Human Intervertebral Disks.* Folia Histochemica Et Cytobiologica, 1994. **32**(1): p. 41-44.
117. Kielty, C.M., M.J. Sherratt, and C.A. Shuttleworth, *Elastic fibres.* J Cell Sci, 2002. **115**(Pt 14): p. 2817-28.
118. Martin, J.T., et al., *Translation of an engineered nanofibrous disc-like angle-ply structure for intervertebral disc replacement in a small animal model.* Acta Biomaterialia, 2014. **10**(6): p. 2473-2481.
119. Johnson, E.F., et al., *Elastic fibers in the anulus fibrosus of the dog intervertebral disc.* Acta Anat (Basel), 1984. **118**(4): p. 238-42.
120. Tavakoli, J., D.M. Elliott, and J.J. Costi, *The ultra-structural organization of the elastic network in the intra- and inter-lamellar matrix of the intervertebral disc.* Acta Biomater, 2017. **58**: p. 269-277.
121. Fonck, E., et al., *Effect of aging on elastin functionality in human cerebral arteries.* Stroke, 2009. **40**(7): p. 2552-6.
122. Koo, T.K. and M.Y. Li, *A Guideline of Selecting and Reporting Intraclass Correlation Coefficients for Reliability Research.* Journal of Chiropractic Medicine, 2016. **15**(2): p. 155-163.
123. Osti, O.L., et al., *Annular Tears and Disk Degeneration in the Lumbar Spine - a Postmortem Study of 135 Disks.* Journal of Bone and Joint Surgery-British Volume, 1992. **74**(5): p. 678-682.

124. Gregory, D.E., et al., *Novel lap test determines the mechanics of delamination between annular lamellae of the intervertebral disc.* J Biomech, 2011. **44**(1): p. 97-102.
125. Hollingsworth, N.T. and D.R. Wagner, *Modeling shear behavior of the annulus fibrosus.* J Mech Behav Biomed Mater, 2011. **4**(7): p. 1103-14.
126. Tavakoli, J. and J. Costi, *Ultrastructural organization of elastic fibres in the partition boundaries of the annulus fibrosus within the intervertebral disc* Acta Biomaterialia, 2017. **(Accepted)**.
127. Iatridis, J.C., et al., *Shear mechanical properties of human lumbar annulus fibrosus.* Journal of Orthopaedic Research, 1999. **17**(5): p. 732-737.
128. Wilke, H.J., et al., *New in vivo measurements of pressures in the intervertebral disc in daily life.* Spine (Phila Pa 1976), 1999. **24**(8): p. 755-62.
129. Nachemson, A. and J.M. Morris, *IN VIVO MEASUREMENTS OF INTRADISCAL PRESSURE. DISCOMETRY, A METHOD FOR THE DETERMINATION OF PRESSURE IN THE LOWER LUMBAR DISCS.* J Bone Joint Surg Am, 1964. **46**: p. 1077-92.
130. Amin, D.B., et al., *Effect of degeneration on the six degree of freedom mechanical properties of human lumbar spine segments.* Journal of Orthopaedic Research, 2016. **34**(8): p. 1399-1409.
131. Costi, J.J., et al., *Frequency-Dependent Behavior of the Intervertebral Disc in Response to Each of Six Degree of Freedom Dynamic Loading: Solid Phase and Fluid Phase Contributions.* Spine, 2008. **33**(16): p. 1731-1738.
132. Pham, D.T., J.G. Shapter, and J.J. Costi, *Tensile behaviour of individual fibre bundles in the human lumbar anulus fibrosus.* J Biomech, 2018. **67**: p. 24-31.
133. Tavakoli, J. and J.J. Costi, *Ultrastructural organization of elastic fibres in the partition boundaries of the annulus fibrosus within the intervertebral disc.* Acta Biomaterialia, 2018. **68**: p. 67-77.
134. Yue, B., *Biology of the Extracellular Matrix: An Overview.* Journal of glaucoma, 2014: p. S20-S23.
135. Han, W.M., et al., *Macro- to Microscale Strain Transfer in Fibrous Tissues is Heterogeneous and Tissue-Specific.* Biophysical Journal, 2013. **105**(3): p. 807-817.
136. Gregory, D.E. and J.P. Callaghan, *Does Vibration Influence the Initiation of Intervertebral Disc Herniation?: An Examination of Herniation Occurrence Using a Porcine Cervical Disc Model.* Spine, 2011. **36**(4): p. E225-E231.
137. Wilke, H.-J., A. Kettler, and L.E. Claes, *Are sheep spines a valid biomechanical model for human spines?* Spine, 1997. **22**(20): p. 2365-2374.
138. O'connell, G.D., E.J. Vresilovic, and D.M. Elliott, *Comparison of animals used in disc research to human lumbar disc geometry.* Spine, 2007. **32**(3): p. 328-333.
139. Faury, G., et al., *Nuclear and cytoplasmic free calcium level changes induced by elastin peptides in human endothelial cells.* Proceedings of the National Academy of Sciences, 1998. **95**(6): p. 2967-2972.
140. Brassart, B., et al., *Conformational Dependence of Collagenase (Matrix Metalloproteinase-1) Up-regulation by Elastin Peptides in Cultured Fibroblasts.* Journal of Biological Chemistry, 2001. **276**(7): p. 5222-5227.
141. Jung, S., J.T. Rutka, and A. Hinek, *Tropoelastin and elastin degradation products promote proliferation of human astrocytoma cell lines.* J Neuropathol Exp Neurol, 1998. **57**(5): p. 439-48.
142. Vesely, I., *The role of elastin in aortic valve mechanics.* Journal of Biomechanics. **31**(2): p. 115-123.
143. Schmitz, N., et al., *Basic methods in histopathology of joint tissues.* Osteoarthritis and Cartilage, 2010. **18**: p. S113-S116.
144. Tavakoli, J. and J.J. Costi, *New findings confirm the viscoelastic behaviour of the inter-lamellar matrix of the disc annulus fibrosus in radial and circumferential directions of loading.* Acta Biomater, 2018. **71**: p. 411-419.

145. Schroeder, Y., et al., *Osmoviscoelastic finite element model of the intervertebral disc.* European Spine Journal, 2006. **15**(Suppl 3): p. 361-371.
146. Tavakoli, J. and J. Costi, *New findings confirm the viscoelastic behaviour of the inter-lamellar matrix of the disc annulus fibrosus in radial and circumferential directions of loading.* Acta Biomaterialia, 2018: p. (accepted).
147. Roach, M.R. and A.C. Burton, *The reason for the shape of the distensibility curves of arteries.* Can J Biochem Physiol, 1957. **35**(8): p. 681-90.
148. Tarulli, A.W. and E.M. Raynor, *Lumbosacral radiculopathy.* Neurol Clin, 2007. **25**(2): p. 387-405.
149. Hart, L.G., R.A. Deyo, and D.C. Cherkin, *Physician office visits for low back pain. Frequency, clinical evaluation, and treatment patterns from a U.S. national survey.* Spine (Phila Pa 1976), 1995. **20**(1): p. 11-9.
150. Bruske-Hohlfeld, I., et al., *Incidence of lumbar disc surgery. A population-based study in Olmsted County, Minnesota, 1950-1979.* Spine (Phila Pa 1976), 1990. **15**(1): p. 31-5.
151. Koebbe, C.J., et al., *Lumbar microdiscectomy: a historical perspective and current technical considerations.* Neurosurg Focus, 2002. **13**(2): p. E3.
152. Adams, M.A. and P. Dolan, *Intervertebral disc degeneration: evidence for two distinct phenotypes.* Journal of Anatomy, 2012. **221**(6): p. 497-506.
153. Jones, R.M., *Mechanics of composite materials*. 1998: CRC press.
154. Swanson, S.R., *Introduction to design and analysis with advanced composite materials*. 1997, Prentice Hall: Upper Saddle River, N.J. :.
155. van Heeswijk, V.M., et al., *Posterolateral Disc Prolapse in Flexion Initiated by Lateral Inner Annular Failure: An Investigation of the Herniation Pathway.* Spine, 2017. **42**(21): p. 1604-1613.
156. Wade, K.R., et al., *A more realistic disc herniation model incorporating compression, flexion and facet-constrained shear: a mechanical and microstructural analysis. Part I: Low rate loading.* European Spine Journal, 2017. **26**(10): p. 2616-2628.
157. Wade, K.R., et al., *"Surprise" Loading in Flexion Increases the Risk of Disc Herniation Due to Annulus-Endplate Junction Failure: A Mechanical and Microstructural Investigation.* Spine (Phila Pa 1976), 2015. **40**(12): p. 891-901.
158. Wade, K.R., et al., *How healthy discs herniate: a biomechanical and microstructural study investigating the combined effects of compression rate and flexion.* Spine (Phila Pa 1976), 2014. **39**(13): p. 1018-28.
159. Lawless, I.M., et al., *Adaptive velocity-based six degree of freedom load control for real-time unconstrained biomechanical testing.* J Biomech, 2014. **47**(12): p. 3241-7.
160. Schindelin, J., et al., *The ImageJ ecosystem: An open platform for biomedical image analysis.* Molecular Reproduction and Development, 2015. **82**(7-8): p. 518-529.
161. Holzapfel, G.A., et al., *Single lamellar mechanics of the human lumbar anulus fibrosus.* Biomechanics and Modeling in Mechanobiology, 2005. **3**(3): p. 125-140.
162. Ebara, S., et al., *Tensile Properties of Nondegenerate Human Lumbar Anulus Fibrosus.* Spine, 1996. **21**(4): p. 452-461.
163. Skaggs, D.L., et al., *Regional variation in tensile properties and biochemical composition of the human lumbar anulus fibrosus.* Spine (Phila Pa 1976), 1994. **19**(12): p. 1310-9.
164. Guthold, M., et al., *A Comparison of the Mechanical and Structural Properties of Fibrin Fibers with Other Protein Fibers.* Cell biochemistry and biophysics, 2007. **49**(3): p. 165-181.
165. Walter, B.A., et al., *Complex loading affects intervertebral disc mechanics and biology.* Osteoarthritis Cartilage, 2011. **19**(8): p. 1011-8.
166. Adams, M.A. and W.C. Hutton, *Prolapsed intervertebral disc. A hyperflexion injury 1981 Volvo Award in Basic Science.* Spine (Phila Pa 1976), 1982. **7**(3): p. 184-91.
167. Henry, J.L., et al., *Lumbar Facet Joint Compressive Injury Induces Lasting Changes in Local Structure, Nociceptive Scores, and Inflammatory Mediators in a Novel Rat Model.* Pain Research and Treatment, 2012. **2012**: p. 127636.

168. Dreischarf, M., et al., *Comparison of eight published static finite element models of the intact lumbar spine: predictive power of models improves when combined together.* Journal of biomechanics, 2014. **47**(8): p. 1757-1766.
169. Rohlmann, A., et al., *Analysis of the influence of disc degeneration on the mechanical behaviour of a lumbar motion segment using the finite element method.* Journal of biomechanics, 2006. **39**(13): p. 2484-2490.

Appendix A: SEM images of elastic fibre network in the disc

The unpublished SEM images that identify the ultrastructural organization of the elastic fibre network in different species (human, bovine and porcine) are available at:

https://researchdata.ands.org.au/ultra-structural-organization-intervertebral-disc/1306246

http://doi.org/10.4226/86/5a680f212c4f1

This dataset contains 30 image files (30 TIFF files) and a PDF with a description of each image. The total size of the dataset is 140 MB.

Appendix B: Database for the mechanical properties of the ILM and elastic fibre network in the disc

While the viscoelastic and failure properties of the ILM and elastic fibre network haven't been reported before, the following database was established to share the raw data that was obtained during mechanical characterization of the ILM.

http://researchdata.ands.org.au/view/?key=http%3A%2F%2Fhdl.handle.net%2F2328.1%2F1209

http://dx.doi.org/10.4226/86/5a79395794c45

This database contains the following folders:

1- The "ILM data" folder including:
    - Elastic fibre in shear
    - Elastic fibre in tension
    - ILM in shear
    - ILM in tension

The "ILM data folder" represents raw data for biomechanical characterization of the ILM (Studies 4 and 5). Each sub-folder contains CSV files presenting force-displacement data at different strain rates (slow- medium and fast) and failure for at least 10 samples.

2- The "ILM-LAM data" folder including:
    - Control group
    - pre-herniation group
    - Herniation group

The "ILM-LAM data folder" represents raw data for biomechanical characterization of the ILM (ILM) compared to the lamellae (LAM) during progression of herniation (Study 6). Each sub-folder contains excel files presenting failure properties (force-displacement data) for 7 samples at two different regions of anterior (AN) and posterolateral (PL).